
Methods¹

Expedition 309/312 Scientists²

Chapter contents

Introduction	1
Igneous petrology	3
Alteration	10
Structural geology	11
Geochemistry	13
Paleomagnetism	16
Physical properties	18
Digital imaging	21
Downhole measurements	22
Underway geophysics	27
References	28
Figures	31
Tables	56

Introduction

This chapter documents the procedures and methods employed in the various shipboard laboratories during Expedition 309/312 of the Integrated Ocean Drilling Program (IODP). This information applies only to shipboard work described in the “Expedition reports” section of the Expedition 309/312 *Proceedings* volume. Methods for shore-based analysis of Expedition 309/312 samples and data will be described in the individual scientific contributions to be published in the “Research results” section of the Expedition 309/312 *Proceedings* volume and elsewhere.

Authorship

All shipboard scientists contributed to the completion of this volume. The separate sections of the chapters were, however, written by groups of scientists as listed below (in order of contribution where appropriate and alphabetically otherwise):

Combined Expedition 309/312

Expedition 309/312 summary: Expedition 309/312 Scientists
Background and objectives: Teagle, Alt, Wilson, Umino,
Miyashita, Banerjee

Basement drilled in Hole 1256D during Expedition 309

Operations: Grigar, Banerjee
Geochemistry of basement fluid: Teagle, Gao, Lledo, Sakuyama,
Banerjee
Thermal state of Hole 1256D: Wilson, Teagle
Igneous petrology: Sano, Cordier, Durand, Geldmacher, Umino
Metamorphic/Alteration petrology: Laverne, Galli, Smith-
Duque, Banerjee, Coggon, Teagle
Structural geology: Tartarotti, Crispini, Galli
Igneous geochemistry: Lledo, Gao, Sakuyama, Teagle
Paleomagnetism: Wilson, Herrero-Bervera, Veloso, Tominaga
Physical properties: Gilbert, Tominaga
Digital imaging: Wilson, Holter
Downhole measurements: Einaudi, Belghoul
Underway geophysics: Wilson

¹Expedition 309/312 Scientists, 2006. Methods. In Teagle, D.A.H., Alt, J.C., Umino, S., Miyashita, S., Banerjee, N.R., Wilson, D.S., and the Expedition 309/312 Scientists. *Proc. IODP, 309/312*: Washington, DC (Integrated Ocean Drilling Program Management International, Inc.), 1–70. doi:10.2204/iodp.proc.309312.102.2006
²Expedition 309/312 Scientists' addresses.



Basement drilled in Hole 1256D during Expedition 312

Operations: Grout, Banerjee
 Igneous petrology: Christie, Maclennan, Koepke, Yamasaki, Park, Scheibner, Yamazaki, Miyashita
 Metamorphic/Alteration petrology: Teagle, Laverne, Morgan, Coggon, Alt
 Structural geology: Anma, Hayman, Veloso, Galli
 Igneous geochemistry: Ingle, Hirano, Neo, Maclennan
 Paleomagnetism: Wilson, Carlut
 Physical properties: Swift, Tikku
 Digital imaging: Tominaga, Wilson
 Downhole measurements: Reichow, Tominaga

Numbering of sites, holes, cores, and samples

Drilling sites are numbered consecutively from the first site drilled by the *Glomar Challenger* in 1968. Starting with IODP Expedition 301, the prefix “U” designates sites occupied by the U.S. Implementing Organization (USIO) vessel. Site 1256 does not follow this nomenclature because it was started during Ocean Drilling Program (ODP) Leg 206. At a site, multiple holes can be drilled by removing the drill pipe from the seafloor, moving the ship a short distance, and then drilling a new hole. For all IODP drill sites, a letter suffix distinguishes each hole drilled at the same site. The first hole drilled is assigned the site number modified by the suffix “A,” the second hole takes the site number and the suffix “B,” and so forth. The cored interval is measured in meters below seafloor (mbsf). Depth below seafloor is determined by subtracting the water depth estimated from the initial drill pipe measurement, which gives the length of pipe from the rig floor to the seafloor (measured in meters below rig floor [mbrf]), from the total drill pipe measurement. While on site, ship location over a hole is maintained with respect to a positioning beacon deployed on the seafloor and in active communication with the Nautrinix dynamic positioning system on the *JOIDES Resolution*. In general, the primary reference for dynamic positioning was the Global Positioning System (GPS); the beacon reference acts as a backup in the event that GPS is unreliable.

During most IODP expeditions, each cored interval is generally 9.5–9.8 m long, which is the length of a core barrel. However, one potential cause of poor recovery in hard rock coring is core jamming in the bit or throat of the core barrel. Once the opening in the bit is jammed, core may be prevented from entering the core barrel. During ODP hard rock coring missions, a novel coring approach employed to improve

recovery was to extract the core barrel at shorter penetration intervals in order to mitigate loss of core when the bit was blocked. Following this strategy, several cored intervals during Expedition 309 and all cored intervals during Expedition 312 were reduced to 4.5–5 m (half cores).

Each recovered core is divided into 1.5 m sections that are numbered serially from the top. When full recovery is achieved, sections are numbered sequentially as recovered, starting with 1 at the top of the core; the last section may be shorter than 1.5 m (Fig. F1). When the recovered core is shorter than the cored interval, the top of the core is equated with the top of the cored interval (in meters below seafloor) by convention to achieve consistency in handling analytical data derived from cores. All pieces recovered are placed immediately adjacent to each other in the core tray. Samples and descriptions of cores are designated by distance, measured in centimeters from the top of the section to the top and bottom of each sample or interval. A full identifier for a sample consists of the following information: expedition, site, hole, core number, core type, section number, piece number (for hard rock), and interval in centimeters measured from the top of section. For example, a sample identification of “309-1256D-80R-1, 30–32 cm” represents a piece of core removed from the interval between 30 and 32 cm below the top of Section 1, Core 80 (R designates that this core was taken with the rotary core barrel) of Hole 1256D from Expedition 309 (Fig. F1).

Core handling

Some cores recovered during Expedition 309 were extracted from the core barrel in plastic liners. These liners were carried from the rig floor to the core processing area on the catwalk outside the core laboratory, where they were split into 1.5 m sections. Liner caps (blue = top; colorless = bottom) were glued with acetone onto liner sections on the catwalk. The 1.5 m sections were transferred to the core splitting room, where the plastic liners were split lengthwise to expose the core. Most cores during Expedition 309 and all cores during Expedition 312 were recovered without plastic liners. Core pieces were extracted from the core barrel and placed in consecutive order in a split plastic liner. In either case, pieces of core were pushed together and the length of the core in each core liner was measured to the nearest centimeter; this measurement was entered into the IODP curation data acquisition program as liner length (LL in the database), and cores were transferred to the core splitting room.

Most pieces of core were marked on the bottom with a red wax pencil to preserve orientation, either be-

fore they were extracted from the core barrel or when they were removed from the split core liner. In some cases, pieces were too small to be oriented with certainty. Therefore, the red wax mark does not universally indicate that the core piece was oriented.

Adjacent core pieces that could be fit together along fractures were curated as single pieces. A plastic spacer was secured to the split core liner with acetone between individual pieces and/or reconstructed contiguous groups of pieces. These spacers may represent a substantial interval of no recovery. The length of each section of core, including spacers, was entered into the curation database as the curated length. Curated length commonly differs by a few centimeters from the liner length measured on the catwalk. Subsequently, cores were marked to indicate a split line, ideally maximizing the expression of dipping structures on the cut face of the core while maintaining representative features in both archive and working halves.

Each section was scanned using the shipboard multi-sensor track (MST) (see “[Physical properties](#)”), and the outer cylindrical surfaces of the whole-round pieces were scanned with the Deutsche Montan Technologie (DMT) Digital Color CoreScan system, using the split line marking for registration (see “[Digital imaging](#)”). Each piece of core was then split into archive and working halves, with the positions of plastic spacers between pieces maintained in both halves. Pieces are numbered sequentially from the top of each section, beginning with number 1; reconstructed groups of pieces are assigned the same number but are lettered consecutively. Pieces are labeled only on the outer cylindrical surfaces of the core. If the piece is oriented with respect to the way up, an arrow was added to the label, pointing to the top of the section.

The archive half of each core was described, and observations were recorded on IODP templates and spreadsheets developed by the expedition scientists (for details, see individual disciplinary sections in this chapter). Digital images of the dry, cut faces of the archive halves were captured with the IODP digital imaging system (DIS). Archive-half sections were also passed through the cryogenic magnetometer for magnetic remanence measurements.

Finally, digital photographs of the archive half were taken. Digital color close-up images were taken of particular features for illustrations in the summary of each site, as requested by individual scientists. Working halves of cores were sampled for both shipboard characterization of cores and shore-based studies. Samples were routinely taken for shipboard physical properties (minicore or 8 cm³ cube), paleomagnetic (minicore or 8 cm³ cube), thin section (billet or slab),

and geochemical (billet or quarter-round) analyses, as described in the sections below. Each extracted sample was logged into the sampling database program by location and the name of the investigator receiving the sample or by type of shipboard sample. Records of all removed samples are kept by the IODP Marine Curatorial Specialist. Extracted samples were sealed in plastic vials, cubes, or bags and labeled.

Following shipboard initial scientific measurements and sampling, both halves of the cores were shrink-wrapped in plastic to prevent rock pieces from moving out of sequence during transit. Working and archive halves were then put into labeled plastic tubes, sealed, and transferred to an onboard cold-storage space. At the end of Expedition 312, cores from both Expeditions 309 and 312 were transferred from the ship for permanent storage at the IODP Gulf Coast Repository in College Station, Texas (USA).

Hard rock core description

Hard rock petrographic observations made during Expedition 309/312 are stored in both written and electronic media. All descriptions and measurements were made on the archive halves of the cores, except where otherwise noted. A summary of macroscopic features observed in the cores is presented in visual core description (VCD) forms (Fig. F2). In VCD forms, individual piece numbers are noted along the left-hand side of the core image. In the column labeled Orientation, arrows indicate pieces large enough to be oriented with respect to the top of the core. The location of shipboard samples are noted in the Shipboard Studies column. Complete macroscopic descriptions and measurements are available in spreadsheet form (see the HRVCD directory in “[Supplementary material](#)”). For details on observations recorded in the spreadsheets, the reader is referred to the disciplinary sections in this chapter. Complete microscopic descriptions on petrographic thin sections are available (see “[Thin sections](#)” in “Core descriptions”).

Igneous petrology

Core curation and shipboard sampling

To preserve important features and structures, all core was examined before being split. Each piece was numbered sequentially from the top of each core section and labeled on the outside surface. Broken core pieces that could be fitted together were assigned the same number and lettered consecutively from the top down (e.g., 1A, 1B, and 1C). Rarely, composite pieces may have occupied more than one section. Plastic spacers were placed between pieces with dif-

ferent numbers. The presence of a spacer may represent a substantial interval without recovery. If it was evident that an individual piece could not have rotated about a horizontal axis during drilling, an arrow was added to the label, pointing to the top of the section. Nondestructive physical property measurements, such as magnetic susceptibility, natural gamma ray (NGR) emission, and digital imaging of the exterior of whole-core pieces were made before the core was split (see “[Physical properties](#)”). Pieces were split with a diamond-impregnated saw in such a way that important compositional and structural features were preserved in both the archive and working halves. After splitting, digital images of the core were taken using the Geotek DIS before being described on VCD forms. To minimize contamination of the core with platinum group elements and gold, describers removed jewelry from their hands and wrists before handling. After the core was split and described, the working half was sampled for shipboard physical properties, paleomagnetic studies, thin sections, X-ray diffraction (XRD), inductively coupled plasma–atomic emission spectroscopy (ICP-AES), and shore-based studies. Each section of core was examined consecutively by three teams of describers, focusing first on igneous characteristics, then on alteration, and finally on structure. Each team described all sections of hard rock cores. The igneous team recorded the depth interval and length of each piece in a piece log (Table [T1](#)).

Igneous units and contact logs

The first step in describing cores was the selection of unit boundaries on the basis of the presence of contacts, chilled margins, changes in primary mineralogy, color, grain size, and structural or textural variations (see Tables [T13](#) and [T35](#) in the “Site 1256” chapter). Unit boundaries of volcanic rocks were generally chosen to reflect different volcanic cooling units, although we were forced by limited recovery in some cases to arbitrarily decide the exact location of a unit boundary within an interval where the lithology above and below the interval was different. In order to preserve important information about volcanology without defining an unreasonable number of units within a single core, subunits were designated in cases where there were common changes in texture without accompanying changes in mineralogy. Where narrow dikes occur, each dike is labeled as a subunit. Within a core, if there is no significant change in dike mineralogy, all dike pieces are labeled as a single subunit. For Expedition 309 only, lithologically similar pieces from consecutive cores are labeled as different subunits. Subunits are designated in the VCDs, and their descriptions are included

within the overall written description of the unit. Igneous units and contact logs (see Tables [T13](#) and [T35](#) in the “Site 1256” chapter) provide information about unit boundaries and a brief description of each unit. For each unit, the table lists unit number, core number, section number, interval location in the core, piece number(s), depth (in meters below seafloor) of the upper contact (calculated from the curated depth of the top of the core), physical type of upper contact, minimum thickness of the unit (calculated from piece lengths), and rock type of each unit. An additional table is used to record fresh or altered glass occurrence (see Table [T14](#) in the “Site 1256” chapter). Units were numbered continuously from the end of Leg 206, starting with Unit 1256D-27.

Visual core description

General description

VCD forms (Fig. [F3](#)) were used to describe each section of igneous rock cores. The procedure closely follows Leg 206 core descriptions to provide consistency. A key to symbols used on the VCDs is given in Figure [F4](#). On the VCDs, the following are displayed from left to right:

1. A scale from 0 to 150 cm,
2. Piece number,
3. Photograph of the archive half of the core,
4. Piece orientation,
5. Locations of samples selected for shipboard studies,
6. Boundaries and number of lithologic units,
7. Structures,
8. Structural measurements,
9. Presence of glass or altered glass,
10. Phenocrysts (for volcanic rocks),
11. Constituent minerals (for plutonic rocks) and constituent minerals of phenocrysts (for volcanic rocks),
12. Grain size (of groundmass for volcanic rocks and of constituent minerals for plutonic rocks), and
13. Alteration intensity.

Vertically oriented pieces are indicated on the form by an upward-pointing arrow to the right of the appropriate piece (column 4). Locations of samples selected for shipboard studies are indicated in the Shipboard Studies column (5), using the following notation:

- XRD = X-ray diffraction analysis.
- ICP = ICP-AES analysis.
- TSB = petrographic thin section.
- PP = physical property analysis.
- PMAG= paleomagnetic analysis.

The Lithologic Unit column (6) displays the locations of boundaries between units and subunits and the unit designator (consecutive downhole subunits are designated by letters after the unit number; e.g., 1, 2a, 2b, etc.). The Structure column (7) displays graphical representations of structural types from the key in Figure F4. The Structural Measurement column (8) highlights structures that have been measured. Boundaries of lithologic units and subunits were drawn on the VCDs across columns 4–13 with solid lines denoting unit boundaries.

Grain sizes are defined as follows:

- p = pegmatitic (>30 mm).
- cg = coarse grained (5–30 mm).
- mg = medium grained (1–5 mm).
- fg = fined grained (0.2–1 mm).
- μx = microcrystalline (0.1–0.2 mm).
- cx = cryptocrystalline (<0.1 mm).
- g = glassy.

Volcanic rocks

During Expedition 309, we defined igneous rocks with glassy to fine-grained (average groundmass grain size = <1 mm) characteristics as volcanic rocks and the root term “basalt” was used. During Expedition 309, for holocrystalline, relatively fine to medium-grained rocks (1–5 mm) with doleritic texture (textures transitional between intergranular and ophitic), the root word “dolerite” was used (Fig. F5).

During Expedition 312, we refined the lithologic nomenclature slightly. For the majority of Expedition 312 samples, this nomenclature is consistent with that used during Expedition 309. The only exceptions may be in the naming of basaltic rocks that are present within the gabbro section below 1406.6 mbsf. We have also refined the definition of the rarely used (during Expedition 309/312) term “dolerite.” We used the following terms:

- Basalt: All igneous rocks of basaltic composition in the size range glassy to fine grained.
- Dolerite: Holocrystalline, medium-grained rocks of basaltic composition with well-developed intersertal, subophitic, or ophitic textures. In English language usage, this term is European in origin and functionally equivalent to the North American usage of “diabase,” which is the IODP standard term. In Japanese, however, the term diabase has a distinctly different meaning, referring to strongly altered (green) basaltic rocks, and is expressed differently in Kanji script. This usage of diabase is also prevalent in Europe. We therefore agreed to use dolerite and recommend its adoption by IODP as a uniquely defined term that can be readily understood worldwide.

VCDs of volcanic rocks contain a text description of each unit in each section of core that includes

- Expedition, site, hole, core number, core type, and section number;
- Depth of the top of the section in meters below seafloor;
- Unit number;
- Rock name;
- Summary description of unit as it appears in the section, including rock name and rock type (e.g., pillow basalt or sheet flow);
- Piece numbers included in the unit;
- Type of contacts when recovered;
- Munsell color;
- Phenocryst mineral abundance and size;
- Groundmass grain size and texture;
- Vesicle abundance;
- Nature of alteration;
- Information about abundance and filling of veins;
- Description of structures in the rock; and
- Any additional comments.

Units and subunits were named on the basis of groundmass texture and abundance of primary minerals. In cryptocrystalline to microcrystalline rocks, there is a clear distinction between phenocrysts and groundmass crystals. These were described based on the identification of phenocrysts in hand sample following the criteria listed below:

- Aphyric (<1% phenocrysts)
- Sparsely phyrlic (1%–5% phenocrysts)
- Moderately phyrlic (5%–10% phenocrysts)
- Highly phyrlic (>10% phenocrysts)

Rock names were further classified by types of phenocrysts present (e.g., sparsely plagioclase-olivine phyrlic, in which the amount of olivine exceeds the amount of plagioclase). In coarser grained rocks, those with seriate to equigranular textures, phenocrysts are difficult to distinguish. Therefore, in cases where grain size was fine grained or larger, we did not use these modifiers unless there was a clear distinction between phenocrysts and groundmass crystals. Rock color was determined on a wet, cut surface of the rock using Munsell color charts.

An estimate of the percentage of vesicles and their average size was included in the VCDs. Vesicularity is described according to the abundance, size, and shape (sphericity and angularity) of the vesicles. The subdivision was made according to the following:

- Nonvesicular (<1% vesicles)
- Sparsely vesicular (1%–5% vesicles)
- Moderately vesicular (5%–20% vesicles)
- Highly vesicular (>20% vesicles)

Pillow lavas were identified by curved chilled margins oblique to the vertical axis of the core or, when these margins were absent, by variolitic textures, curved fractures, and microcrystalline or cryptocrystalline grain size. Sheet flows were defined as sections of core <3 m thick with the same rock type and grain size that increased toward the center of the flows. Massive units were defined as continuous intervals >3 m thick of similar lithology. Minor dikes were identified when intrusive contacts with the host rock were present. Below the last identifiable flow units (>1060.9 mbsf), all basaltic units were identified as sheeted dikes (see discussion in “**Igneous petrology**” in “Expedition 312” in the “Site 1256” chapter). For Expedition 309, sheeted dike units were identified as massive basalts. The term “massive” was not used for Expedition 312. Other rock types distinguished were volcanic breccias and hyaloclastites.

Igneous fabrics include layering, lamination, and lineation for rocks exhibiting a preferred orientation of mineral grains. The term “glomerocrysts” was used for mineral aggregates.

Plutonic rocks

Plutonic rock descriptions during Expedition 312 closely followed those used during IODP Expedition 304/305. These, in turn, were based on procedures from ODP Leg 209 and earlier “gabbro” legs, so there could be a relatively high degree of uniformity. Plutonic rock units were defined on the basis of primary igneous rock types and textures. Mineral modes were visually estimated, using a binocular microscope when necessary. In many cases, several subintervals with sharp to gradational changes in grain size and/or mode over a few centimeters were grouped into a single lithologic unit.

Rock classification

Plutonic rocks were classified on the basis of abundance, grain size, and texture of their primary minerals (as inferred prior to alteration), based on the International Union of Geological Sciences (IUGS) system (Streckeisen, 1974; Le Maitre, 1989) (Fig. F6). For pervasively altered rocks, the “primary assemblage” was estimated based on textural evidence, mostly in thin section.

Minor modifications to the IUGS system were made to subdivide the rock types more accurately on the basis of significant differences rather than arbitrary cutoffs based on the abundance of a single mineral. We have attempted to follow as closely as possible the descriptions from Leg 209 (Kelemen, Kikawa, Miller, et al., 2004) and Expedition 304/305 (Black-

man, Ildefonse, John, Ohara, Miller, MacLeod, et al., 2006) to facilitate intersite comparison.

For gabbros, the following modifiers based on modal mineralogy are commonly used (not all were used during Expedition 312):

- Disseminated oxide gabbro (Fe-Ti oxide 1%–2%)
- Oxide gabbro (Fe-Ti oxide > 2%)
- Olivine-bearing gabbro (olivine 1%–5%)
- Olivine gabbro (olivine > 5%)
- Orthopyroxene-bearing gabbro (orthopyroxene 1%–5%)
- Gabbronorite (orthopyroxene > 5%)
- Troctolitic gabbro (olivine 5%–15%)
- Troctolite (clinopyroxene < 5%)
- Olivine-rich troctolite (>70% olivine)

Additional descriptive modifiers include

- Leucocratic (light colored, high proportions of plagioclase)
- Anorthositic (>80% plagioclase)
- Micro (dominant grain size < 1 mm)
- Doleritic (fine- or medium-grained gabbroic rocks with dominant ophitic or subophitic textures)

Several additional rock names are also used in this classification:

- Trondhjemite: Leucocratic rocks with >20% quartz and <1% K-feldspar (a restricted part of the IUGS “tonalite” field of the system). This usage is in keeping with previous usage in the ocean crust literature.
- Tonalite: IUGS tonalitic rocks (as defined by Streckeisen, 1974) that contain >10% mafic and related minerals; in practice, tonalites commonly contained significantly >10% mafic minerals.
- Quartz diorite: Some thin dikes in which plagioclase is the dominant (or only) feldspar and quartz forms 5%–20% of (quartz + feldspar).
- Quartz-rich oxide diorite: Nonstandard term that we applied to an unusual lithology that occurs at the top of the gabbro section and in some small dikes in the sheeted dike section. Initially described as tonalites or oxide-tonalites, these rocks have ~49 wt% SiO₂, 18 wt% FeO (total), and 4 wt% TiO₂. They are compositionally identical to the most evolved FeTi basalt compositions.

On hard rock VCDs, the rock names as described above are given at the top of each interval description; the IUGS names calculated from the mode are given in the text. Symbol swatches used in the VCDs are shown in Figure F4. If the assemblage consists of secondary minerals that completely obliterate the primary mineralogy and texture, or if the rock is made up of recrystallized primary minerals such that

the original igneous protolith cannot be recognized, the appropriate metamorphic rock names are used. The methods for describing the metamorphic and structural petrology of the core are outlined in subsequent sections of this chapter.

Primary minerals

The primary rock-forming minerals recovered are olivine, orthopyroxene, clinopyroxene, Fe-Ti oxide, plagioclase, quartz, and amphibole. The following data are recorded on the VCDs (see “**Core descriptions**”):

- Visually estimated modal percent of the primary minerals;
- Grain size;
- Average crystal size for each mineral phase;
- Mineral shape: equant, subequant, tabular, and elongated; and
- Mineral habit: euhedral, subhedral, anhedral, and interstitial.

Accessory phases are also noted, and the above five classes of observations are collected. Modal percentage of each mineral includes both fresh and altered parts of the rocks interpreted to represent that mineral.

Igneous textures

Textures are defined on the basis of grain size, grain shape and habit, preferred mineral orientation, and mineral proportions. We use the following textural terms: equigranular, inequigranular, and intergranular (only visible in thin sections). Inequigranular textures may be further described as seriate (continuous range of crystal sizes) or poikilitic (oikocrysts are relatively large crystals of one mineral, and chadacrysts enclose smaller crystals of one or more other minerals).

The terms euhedral, subhedral, anhedral, and interstitial are used to describe the shapes of crystals interpreted to preserve their igneous morphology. Crystal shapes are divided into four classes:

- Equant (aspect ratio < 1:2)
- Subequant (aspect ratio 1:2–1:3)
- Tabular (aspect ratio 1:3–1:5)
- Elongate (aspect ratio > 1:5)

Igneous fabrics that are distinguished include lamination and lineation for rocks exhibiting a preferred orientation of mineral grains, clusters for mineral aggregates, and schleiren for lenses of igneous minerals.

Oxides and sulfides

The abundance of primary Fe-Ti oxide and sulfide in the core is visually estimated but usually confirmed in thin section.

Textures of oxide and sulfide minerals are described in terms of the habit of the mineral and its relationship with adjacent minerals. Oxide habits are divided into

- Disseminated (scattered grains or grain clusters)
- Interstitial (interstitial to silicates)

Oxide shapes are divided into euhedral, anhedral, angular aggregates, amoeboid aggregates, and interstitial lenses. Euhedral and anhedral are used when it appears that isolated individual grains are present.

Igneous structures

Igneous structures include layering, lineation, gradational grain size variations, gradational modal variations, gradational textural variations, and breccias. Layering describes planar changes in grain size, mode, or texture within a unit.

Dikes/Veins

The term dike refers to any crosscutting feature formed by injection of magma. Vein describes epigenetic mineralized fractures. Veins are described in “**Alteration**.” Thin dikes are often designated as subunits, as described above in “**Igneous units and contact logs**.”

Contacts between lithologic intervals

The most common types of contacts are those without chilled margins. These include planar, curved, irregular, interpenetrative, sutured, or gradational. Sutured refers to contacts where individual mineral grains interlock across the contact. Contacts obscured by subsolidus or subrigidus deformation and metamorphism are called sheared if an interval with deformation fabric is in contact with an undeformed interval, foliated if both intervals have deformation fabrics, or tectonic if the contact appears to be the result of faulting. Indistinct contacts are also described as diffuse in some cases.

Thin sections

Thin sections of igneous rocks were studied to complete and refine the hand specimen observations. An example of the thin section description form is given in Figure F7. Thin section descriptions are included in “**Core descriptions**” and are available from the IODP **Janus** database. Digital photomicrographs were taken to document features described in thin sections. A list of available images, any of which can be obtained from the IODP **Data Librarian**, is given in the photomicrograph log (see PHOTOLOG.XLS in “**Supplementary material**”).

Thin section descriptions include textural features; grain size of phenocrysts and groundmass (volcanic

rocks) or constituent minerals (plutonic rocks); mineralogy, abundance, and type of glomerocrysts; and descriptions of inclusions. For glassy to aphanitic lavas with cryptocrystalline to microcrystalline grain sizes, modal proportions are based on visual estimates. During Expedition 309, mineral modes were determined by point counting (1000 points per thin section). During Expedition 312, modal estimation was conducted for phenocrysts only in volcanic rocks and for some plutonic rocks using whole thin section scanned images and Adobe Photoshop software. Details of this method are described below in [“Estimating modal proportions in basaltic thin sections.”](#)

Volcanic rocks

Volcanic rocks are described as holohyaline (100% glass) to holocrystalline (100% crystals). The terms phyrlic and glomeroporphyritic indicate the presence of phenocrysts and clusters of phenocrysts, respectively. For a continuous range in grain size, the texture is seriate. In cases where there is no significant grain size difference between groundmass crystals and somewhat larger and more euhedral crystals, which do not adhere to the definition of phenocrysts, the term microphenocryst is used.

In holohyaline to hypohyaline rocks, glasses were divided into four distinct types:

- Fresh glass (amber in transmitted polarized light and isotropic in transmitted cross-polarized light, commonly found in the outermost parts of preserved chilled margins);
- Dark (due to abundant crystallites) interstitial volcanic glass of basaltic composition termed tachylytic;
- Glass that contains abundant fibrous spherulites; and
- Glass that has been altered to clay minerals.

Spherulites form a meshwork of spheroidally arranged aggregates of acicular microcrystals emanating from a nucleus. Spherulites may crystallize directly from the melt in response to a large amount of undercooling or can be formed through devitrification of the glass in wet conditions (Fowler et al., 2002). When microlites are present, the following terms were used to describe textures:

- Variolitic (fanlike arrangement of divergent microlites)
- Intergranular (olivine and pyroxene grains between plagioclase laths)
- Intersertal (glass between plagioclase laths)
- Subophitic (partial inclusion of plagioclase in clinopyroxene)

- Ophitic (total inclusion of plagioclase in clinopyroxene)

Flow textures were described as follows:

- Trachytic (subparallel arrangement of plagioclase laths in the groundmass)
- Pilotaxitic (aligned plagioclase microlites embedded in a matrix of granular and usually smaller clinopyroxene grains)
- Hyalopilitic (aligned plagioclase microlites with glassy matrix)

Description of habits for plagioclase and clinopyroxene groundmass crystals was adapted from the practice during Leg 206 (Wilson, Teagle, Acton, et al., 2003) and in ODP Hole 896A, Leg 148 (see fig. 11 in Shipboard Scientific Party, 1993c). Four types of habits were identified:

1. Cryptocrystalline aggregates of fibrous crystals,
2. Comb-shaped or sheaflike plumose crystals,
3. Granular-acicular subhedral to anhedral crystals, and
4. Prismatic to stubby euhedral to subhedral crystals.

During Expedition 309/312, we referred to Type 1 and Type 2 textures as fibrous.

Plutonic rocks

Thin section descriptions of plutonic rocks complement and refine hand specimen observations. Data are recorded in IODP-format thin section descriptions and summarized in the thin section spreadsheet (see [“Thin sections”](#) in [“Core descriptions”](#)). Crystal size measurements are calibrated against a micrometer scale. Inclusions, overgrowths, and mineral zonation are noted, and an apparent order of crystallization may be suggested in the comments section. Relative abundances of accessory minerals such as oxides, sulfides, apatite, and zircon are noted. Modal orthopyroxene not readily identified in hand samples was observed in the thin sections of many gabbroic rocks, causing their reclassification as orthopyroxene-bearing gabbro or gabbronorite.

The same general types of data are collected from thin sections as from hand specimens and the terminology used is mostly the same.

Additional textural terms include

- Equigranular (crystals in contact with each other and similar in size)
- Intergranular (coarser touching grains form a framework with interstices filled by crystalline material [or glass for volcanic rocks])
- Ophitic (characterized by systematic enclosure of plagioclase by optically continuous clinopyroxene)

- Doleritic (used during Expedition 309 for textures transitional between intergranular and ophitic) (Fig. F5)
- Seriate (having a continuously variable range of grain size)

Crystal shape terms include

- Equant (aspect ratio < 1:2)
- Subequant (aspect ratio 1:2–1:3)
- Tabular (aspect ratio 1:3–1:5)
- Elongate (aspect ratio > 1:5)

Estimating modal phenocryst proportions in basaltic thin sections

Rationale

More than 80% of phenocryst-bearing basaltic thin sections from Hole 1256D have <1% phenocrysts. At this level, visual estimates and even formal point counts of phenocryst abundances have high absolute errors. For example, for a mineral abundance of 1%, a 1000 point count has an absolute error close to $\pm 0.5\%$ (50% relative) (Howarth, 1998). During Expedition 312, we developed a simple, rapid (5–10 min per thin section) method of phenocryst modal estimation using scanned thin section images. This method is both less labor intensive and significantly more accurate and precise than point counting for phenocryst contents up to ~5%. As with any method based on a single thin section, the applicability of the method to larger volumes depends on an assumption of homogeneity that may or may not be valid.

Equipment

The following equipment was routinely used during Expedition 312:

- Thin section scanner (Epson Perfection 4870 photo);
- Networked computer with Adobe Photoshop CS and Microsoft Excel; and
- Overhead projector transparency film, which takes ink evenly and crisply.

Method

Preparing and scanning acetates

Preparation of full-page, whole thin section scanned images from standard thin sections by placing them on (or between, for crossed polars) polaroid sheets in a standard scanner is a standard procedure during IODP “hard rock” expeditions. For phenocryst abundances less than ~5%, phenocryst outlines can be rapidly traced onto standard acetate film using an appropriate high-density marker pen. Not all films or

pens work well for this procedure. We used Canon transparency type E film and black marker pens from the Mitsubishi Pencil Corporation, product code PA-121TEW.

Prepared acetates were then scanned and saved as native Adobe Photoshop files.

Separating phases from background

With the image open in Adobe Photoshop, initiate the threshold function: go to Image→Adjustments→Threshold. (These instructions are for Macintosh computers; the procedure for PC computers may differ slightly.) In the resulting threshold dialog box, adjust the threshold level until phenocrysts show up as solid black surrounded by a white background. For the scan in Figure F8A, in which polarizing film was seated between the scanner and thin section, the best threshold is usually just to the dark side (lower value) of the peak associated with the gray film. Click OK to return to a black-and-white image, and crop the image using the crop tool. This requires some care for irregular thin sections, as the standard tool will only crop to rectangular areas. Use the eraser tool to remove all unwanted black from the cropped area, including the line that marks the edge of the sample (Fig. F8A, F8C, F8D). Make sure that the only black that is left corresponds to the phenocrysts.

In some cases, the shape of the thin section is too irregular to crop simply without losing important phenocrysts. In such cases, draw the rectangular line around the irregular thin section boundary and fill the margin between the rectangle and thin section boundary with the black color (Fig. F8B). After that, follow the same procedure used with the normal thin section case.

Using Photoshop histogram window to perform point count

Go to Window→Histogram. Click the options button in the resulting window; this is a right-pointing squat arrow set in a small circle in the upper-right corner. Select the “Expanded View” and “Show Statistics” options. Select “Uncached Refresh.” It is important to do this before every count is taken from the image.

This procedure will create a histogram with large peaks at the extreme left and extreme right, representing black and white, respectively, and almost imperceptible against the edges of the window (Fig. F8D). If there are visible peaks in the center of the histogram, it is necessary to reselect “uncached refresh” or repeat the threshold operation from the original cropped image.

Once the histogram is ready, carefully move the crosshair across the histogram window. Note that the values of “level” and “count” should change, but “pixels” (the total number of pixels in the image) should not change. Move the crosshair to the extreme left of the histogram, where the level reads zero. Note the value of “counts” at level 0, which is the number of black pixels in the image, and calculate the total percentage of phenocrysts as the number of black pixels divided by total pixels.

In case of an irregular thin section, after erasing whole phenocrysts in the photoshop image get the number of black pixels of the margin with the procedure described above. Then, to calculate modal proportion of phenocrysts, subtract black pixels of the gap from total black pixels, which include pixels from both phenocrysts and the black margin.

Dealing with multiple phases

There are several ways to deal with the presence of more than one phenocryst phase. We experimented with color shading but were not able to find pens with sufficient color density. Separate acetate-filled sheets could be prepared for each phase of interest, but this approach is time consuming. For small numbers of phenocrysts, we found it simple to initially measure total phenocrysts for the original scan and then to remove phases one by one from the image using the Photoshop eraser tool.

If an oxide is present in a thin section, it is possible to evaluate the modal proportion of the oxide by directly applying the method described above to whole thin section scan images without additional drawing of phenocrysts on overhead transparency film and scanning (Fig. F9). This is possible because only oxides have the black color among minerals in a thin section.

Alteration

Alteration characteristics of the drill core were determined using visual inspection of the core, microscopic thin section descriptions, and XRD analyses.

Core description

All igneous rocks recovered during Expedition 309/312 have undergone alteration. On the hard rock VCD forms, rocks were graded according to alteration intensity as follows:

- Fresh (<2% by volume alteration products)
- Slight (2%–10%)
- Moderate (10%–50%)
- High (50%–90%)
- Complete (90%–100%)

The approximate frequency (rare = 0–5/m, several = 5–15/m, common = 15–30/m, and very common = >30/m) and the thickness of veins are recorded, and their minerals are given in order of abundance. The frequency (rare, several, common, and very common) and types of alteration halos are recorded on the VCD forms, and their volume percents are given in the alteration log.

Alteration and vein core description logs on a piece-by-piece scale were tabulated to provide a consistent characterization of the rocks and to quantify the different alteration types (see Tables T2, T3). Alteration of plutonic rocks was described using the plutonic rock alteration log (Table T4). Where both basalts and gabbros are found in the same section, the appropriate alteration log sheet was used for intervals of each rock type. A comment was added, noting which intervals are different, including any additional information required. Veins in plutonic rocks were recorded using the standard vein log (see 309VEIN.XLS and 312VEIN.XLS in “[Supplementary material](#)”). Descriptions are based mostly on hand specimen observations; specific secondary minerals are not generally distinguished except where crystal morphology allows unequivocal identification. Where additional mineralogical evidence is available from either thin section descriptions and/or X-ray diffractograms, these identifications are integrated into the alteration and vein logs and the VCDs.

We recorded the following information in logs:

- Alteration log (e.g., Table T2): This log was used to record bulk rock alteration, either piece by piece or for a given group of pieces. Each entry records identifiers for core, section, piece(s), and interval (centimeters); length of each piece or group of pieces; depth below seafloor (in meters) of the top; and igneous unit. Information on alteration type (as represented by rock color and calibrated by thin section observations) for background rock, alteration patches, and alteration halos is provided. Four additional entries are included: (1) percentages of amygdules with mineral composition, (2) percentages of vesicles with mineral composition, (3) percentages of fresh and altered glass, and (4) comments.
- Vein log (e.g., Table T3): This log was used to record the location, apparent area, and mineralogy of veins, vein nets, and breccias and the alteration halos observed on the cut surfaces of the cores. Each entry records identifiers for core, section, piece, and subpiece. For each vein, the location of the top and bottom of the feature is recorded, along with vein width (in millimeters), mineral fillings, presence of a related alteration halo, and width (in millimeters) of the halo on

one side of the vein. Veins that do not intersect both sides of the cores are indicated with a “V” in the Vertical? column. For breccia and vein nets, recorded data include centimeter interval, percentages of nonbasaltic material (veins and cement), and percentages of secondary minerals within the latter. One column indicates veins and breccias studied by XRD (with mineral composition). Two columns provide the width and type of alteration halos adjacent to the vein. A column for comments is included.

- Plutonic rock alteration log (e.g., Table T4): This log was used to record bulk rock alteration of gabbros and other coarse-grained holocrystalline rocks, either piece by piece or for a specified group of pieces. Each entry records identifiers for core, section, piece(s), and interval; length of each piece or group of pieces; and igneous unit. Total modal percentage of secondary minerals were estimated in hand specimen, as were proportions of major primary igneous minerals (olivine, clinopyroxene, plagioclase, orthopyroxene, and oxides) and the secondary minerals by which they are replaced. A column for comments is included.

Thin section description

Thin sections of basement rocks recovered during Expedition 309/312 were examined in order to

- Confirm macroscopic identifications of secondary minerals;
- Determine their mode of occurrence in terms of vesicle and void fillings, vein composition, and primary mineral replacement;
- Identify chronological relationships between different secondary minerals or parageneses;
- Establish distribution, occurrences, and abundance of secondary minerals downhole; and
- Quantify the amount of alteration.

Modal compositions were estimated for each thin section after calibration by point counting on a selection of sections. Digital photomicrographs were taken during the expeditions to document features described in thin sections.

Structural geology

This section outlines the techniques used for macroscopic and microscopic description of structural features observed in hard rock basement cores. Conventions for structural studies established during Leg 206 (Shipboard Scientific Party, 2003b) and other ODP hard rock drilling legs (Leg 118, Shipboard Scientific Party, 1989; Leg 131, Shipboard Scientific

Party, 1991; Leg 135, Shipboard Scientific Party, 1992c; Leg 140, Shipboard Scientific Party, 1992b; Leg 141, Shipboard Scientific Party, 1992a; Leg 147, Shipboard Scientific Party, 1993b; Leg 148, Shipboard Scientific Party, 1993a; Leg 153, Shipboard Scientific Party, 1995; Leg 176, Shipboard Scientific Party, 1999; Leg 209, Shipboard Scientific Party, 2004) were generally followed during Expedition 309/312. Minor differences in protocol between Expeditions 309 and 312 are noted.

Macroscopic core description and terminology

We examined all material from both working and archive halves, although sketches of structures and orientation measurements were made from the archive half. The most representative structural features in the cores recovered during Expedition 309/312 are summarized on the VCD forms (see “[Core descriptions](#)”). For each section, more detailed structural information is described and sketched on a separate handwritten barrel sheet and in a separate spreadsheet log (see STRUCTUR.XLS in “[Supplementary material](#)”). The structure log contains data on location, orientation, and types of structures. Structural descriptions of cores recovered during Leg 206 and Expedition 309 incorporated a breccia log and a breccia list. The breccia log also contains data on clast, matrix, and cement properties of breccias. The breccia list contains data on positions of and structures in faults, microfaults, and other cataclases. Separate breccia records were not kept during Expedition 312 because of the amount and nature of the recovered breccias. Observations of breccias were instead incorporated into the structure log.

We recorded structural data, with reference to a structures checklist (Table T5), on

- Brittle structures,
- Types of breccia, and
- Magmatic and crystal-plastic structures.

Short explanations for terms and abbreviations are given below, and several full definitions are listed in Table T6. We followed the terminology used during Leg 206 (Shipboard Scientific Party, 2003b), based mainly on Ramsay and Huber (1987), Twiss and Moores (1992), Davis (1984), and Passchier and Trouw (1996).

Brittle deformation identifiers include the following:

- Fracture (f) = brittle failure with or without displacement;
- Joint (J) = fracture with no shear displacement;
- Vein (V) = fracture filled with secondary minerals;
- Shear vein (Sv) = vein with shear displacement;

- Fault (F) = fracture with shear displacement;
- Microfault (mF) = faults with <1 mm of related width of deformation; and
- Breccia (B):
 - Magmatic (Bm) = breccias containing glass or quench textures such as hyaloclastites and pillow breccia, primary matrix minerals;
 - Hydrothermal (Bh) = breccias with secondary matrix or vein minerals; and
 - Tectonic (Bc) = cataclastites and fault-gouges in which the matrix consists of the same material as the host rock.

Note that some breccias were classified as a combination of different types.

Magmatic and crystal-plastic structural identifiers include

- Igneous contacts (Ic) = demonstrably extrusive or intrusive contacts;
- Chilled margins (CM) = sharp gradients in grain size near igneous contacts;
- Magmatic vein (Vm) = thin, discontinuous intrusions of igneous material;
- Dike = greater than centimeter-scale tabular intrusions of igneous material;
- Magmatic fabric (M) = lineations, foliations (referred to as Mf when recognized), defined by shape-preferred orientation of primary minerals with no evidence of crystal-plastic deformation;
- Magmatic shear zone (Ms) = zones wherein the lineation or foliation indicate shear with no accompanying crystal-plastic or cataclastic deformation;
- Compositional layering (Cl) = subplanar to planar layers of finite width of similar mineralogical assemblage;
- Composition banding (Cb) = zones of contrasting compositions that are not easily distinguished, subtle compositional layers;
- Textural banding (Tb) = bands of contrasting igneous textures;
- Patches (P) = irregular areas of contrasting composition/texture;
- Crystal-plastic fabric (Cpf) = lineations or foliations defined by grains exhibiting plastic strain; and
- Alteration patches (see “[Alteration](#)”) = spherical, irregular, or elongate domains of enhanced alteration, only elongate patches were measured for orientation.

Where the identifier was unclear, details specific to structural features were illustrated with comments

and sketches. Descriptions of all features were recorded using curated depths (note that the Expedition 309 breccia log is only pieces) so that “structural intervals” could be correlated with lithologic core descriptions. A designation for the color of secondary minerals found in veins or halos was included in the structure log.

The morphology of each feature (Fig. [F10](#)) was recorded in the structure log (see STRUCTUR.XLS in “[Supplementary material](#)”). Standard abbreviations are shown in Table [T5](#). Additional terminology is defined in “[Microstructure of plutonic rocks.](#)” In gabbroic rocks, the morphology of each feature was based on the nature of its boundaries. Patches, shear zones, bands, and layers all have boundaries that are sharp, planar, irregular, or diffuse. Patches have distinctive morphologies classified as round, elongate, irregular, or amoeboid (shaped like an amoeba; a term used more widely to refer to the texture of olivine aggregates).

A semiquantitative scale of fracturing and veining intensities was used during core description. We assigned specific values to intensity estimates according to spacing of veins, volumetric occurrence of veins, percentage of matrix in cataclastic zones, and partitioning of deformation structures:

- Slight (5%–10%; = 1)
- Moderate (10%–40%; = 2)
- High (40%–70%; = 3)
- Complete (= 4)
- Evenly (E) or heterogeneously (H) distributed or localized (L)

Intensity values were assigned to section of each core and recorded in the deformation intensity log (see DEFINT.XLS in “[Supplementary material](#)”).

In the structure and breccia logs, additional comments were recorded for each structure, including the identifications of slickensides, slickenlines, vein-components, and additional morphologies that help characterize the structures.

Structural measurements

Structural features were recorded in centimeters from the top of each section. Depth of the structures was recorded as the distance from the top of the section to the top and bottom of the feature.

We measured structures on the archive half relative to the IODP core reference frame used during Leg 206. The plane normal to the axis of the borehole is referred to as the horizontal plane. On this plane, a 360° net is used with a pseudo-south (180°) pointing into the archive half and a pseudo-north (0°) pointing out of the archive half and perpendicular to the cut surface of the core (Fig. [F11](#)). The cut surface of

the core, therefore, is a vertical plane striking 90°–270°.

Apparent dip angles of planar features were measured on the cut face of the archive half of the core. To obtain a true dip value, a second apparent dip reading was obtained where possible in a section perpendicular to the core face (second apparent orientation). Dip and dip direction with respect to the archive half of the core are recorded on the spreadsheet together with second plane measurements. The two apparent dips and dip directions (or one apparent direction combined with the strike) measured for each planar feature are used to calculate the true orientation. If the feature intersected the upper or lower surface of the core piece, measurements of the strike were made directly in the core reference frame and combined with the apparent dip measurements to calculate the true dip values. The “LinesToPlane” Macintosh program by S.D. Hurst was used during Expedition 309. During Expedition 312, true dip was calculated within the structure log using trigonometric functions.

For structures with shear displacements, the assignment of sinistral, dextral, normal, and reverse sense of shear is independent of any reference frame. In shear veins and faults where the direction of slip is not indicated by structural indicators, we recorded the apparent sense of shear as it appears on the cut face of the core and/or on the top or bottom side of pieces.

Microstructure of volcanic rocks

In order to better characterize different types of deformation, we studied the microstructural features of some relevant mesoscopic structures. Thin sections of basement rocks recovered during Expedition 309/312 were examined in order to

- Confirm macroscopic descriptions of brittle structures,
- Characterize the microstructure of the rocks,
- Provide information on the kinematics of brittle and brittle-ductile deformation,
- Identify time relationships between magmatic deformation and alteration processes, and
- Document major structural zones and downhole variations.

Microstructural notes were entered into a thin section description form spreadsheet (see TSECT-LOG.XLS in “[Supplementary material](#)”), following the nomenclature and procedure adopted during Leg 206 for volcanic rocks. For descriptions of microstructures, we mostly used the terminology of Passchier and Trouw (1996). Shipboard thin sections

were oriented; the orientation is given relative to the core reference frame and was marked on each thin section by an arrow pointing upward and a short tick pointing toward “west” from the base of the arrow. Marking two directions is necessary in order to achieve complete orientation of thin sections cut parallel to the cut surface of the core. Digital photomicrographs were taken during Expedition 309/312 to document features described in thin sections.

Microstructure of plutonic rocks

Plutonic rocks were characterized with the goal of understanding the physical processes involved in their intrusion and crystallization. The lack of distinctive magmatic or deformational structures led us to introduce several terms in the descriptions such as “bands” and “patches.” These terms are nongenetic and meant to describe inhomogeneous distributions of phases and aggregates of phases. Otherwise, descriptions of structure and microstructure of plutonic rocks used identifiers and descriptions outlined in “[Macroscopic core description and terminology](#),” and some are tabulated in [Table T7](#). Additional classifications and terminology were incorporated from Legs 153, 176, and 209 and Expeditions 304 and 305. These terms were used for entering data into spreadsheets of thin section descriptions (see “[Thin sections](#)” in “[Core descriptions](#)”).

Geochemistry

Analysis of basement fluid

Water samples collected with the water-sampling temperature probe were double-filtered through 0.45 µm sterile Acrodisc filters. Aliquots for future shore-based analyses were treated following established protocols ([Table T8](#)). Full geochemical characterization was undertaken on the overflow sample, whereas a more limited suite of analyses was performed on the Ti-coil sample ([Table T8](#)). Salinity and total dissolved solids were determined with an optical handheld refractometer (Reichert), and pH and alkalinity were measured by Gran titration with a Brinkmann pH electrode and a Metrohm autotitrator. Chloride concentrations were determined by titration with AgNO₃. Silica, phosphate, and ammonium measurements were carried out by colorimetry using a Milton Roy Spectronic spectrophotometer, following the analytical techniques described by Gieskes et al. (1991).

Sulfate, potassium, calcium, and magnesium concentrations were analyzed by ion chromatography using the Dionex DX 120 ion chromatograph. Major and minor cation concentrations (Li, B, Sr, Ba, Mn, and

Fe) were determined using the Jobin-Yvon Ultrace ICP-AES following the procedure outlined by Murray et al. (2000). In preparation for analysis by ICP-AES, 0.5 mL aliquots of borehole fluid were acidified with 9.5 mL of nitric acid (HNO₃) and diluted 10-fold with a matrix solution (2.25% HNO₃ containing 9 ppm Y) for minor elements and diluted 50-fold for major elements. Analytical blanks were prepared in an identical manner by analyzing nanopure water acidified and diluted with a matrix solution to ensure a matrix match with the borehole fluid. Sodium was determined using a charge balance calculation, where $\Sigma_{\text{cations}} = \Sigma_{\text{anions}}$.

Dissolved organic carbon concentrations were measured using a TOC-5000A analyzer. Approximately 1.5 mL of the borehole fluid was removed from the overflow sample and quickly frozen to preserve the sample until an analysis could be made. Samples were diluted sixfold (1 mL of sample to 5 mL of nanopure water) and acidified to a pH of ~2 using 53 mL of 2N hydrochloric acid (HCl). Samples were then purged with purified air for 3 min (50 mL/min) and analyzed by triple injections of 25 μ L of sample.

International Association of Physical Sciences of Organization (IAPSO) standard seawater was used for calibrating most techniques. The reproducibility of these analyses, expressed as a percent of the standard deviation (1 σ) divided by the average of several IAPSO values, is summarized in Table T9. Accuracy of individual analyses is within the standard deviation range accepted for IAPSO values.

Hard rock sampling and geochemical analyses

Sample preparation

Representative samples of igneous rocks were analyzed for major and trace elements during Expedition 309/312 using ICP-AES. Approximately 20 cm³ samples for cryptocrystalline to fine-grained rocks and as much as 50 cm³ samples for medium- to coarse-grained rocks were cut from the core with a diamond saw blade, and when possible, a thin section billet was also taken. All outer surfaces were ground on a diamond-impregnated disk to remove surface contamination by saw marks and altered rinds resulting from drilling. Each cleaned sample was placed in a beaker containing trace metal-grade methanol and ultrasonicated for 15 min. The methanol was decanted, the samples were ultrasonicated twice in deionized water for 10 min and ultrasonicated for 10 min in nanopure deionized water. The cleaned pieces were then dried for 10–12 h at 110°C.

The clean, dry whole-rock samples were crushed to <1 cm chips between two disks of Delrin plastic in a

hydraulic press. The rock chips were then ground to a fine powder in a tungsten carbide mill in a SPEX 8510 shatterbox. After grinding, a 1.0000 \pm 0.0005 g aliquot of the sample powder was weighed on a Mettler Toledo balance and ignited at 1025°C for 4 h to determine weight loss on ignition (LOI) with an estimated precision of 0.02 g (2 wt%).

ODP *Technical Note 29* (Murray et al., 2000) describes in detail the shipboard procedure for digestion of rocks and ICP-AES analysis of samples. The following protocol is an abbreviated form of this with minor changes and additions. After determination of LOI, 100.0 \pm 0.2 mg aliquots of the ignited whole-rock powders were weighed and mixed with 400.0 \pm 0.5 mg of LiBO₂ flux that had been preweighed on shore. Standard rock powders and full procedural blanks were included with unknowns in each ICP-AES run. A check on grinding contamination contributed by the tungsten carbide mills (Table T10) was performed during Leg 206 and was found to be negligible (Shipboard Scientific Party, 2003b). All samples and standards were weighed on the Cahn C-31 microbalance (designed to measure on board) with weighing errors conservatively estimated to be \pm 0.02 mg.

A 10 mL aliquot of 0.172 mM aqueous LiBr solution was added to the flux and rock powder mixture as a nonwetting agent to prevent the cooled bead from sticking to the crucible. Samples were then individually fused in Pt-Au (95:5) crucibles for ~12 min at a maximum temperature of 1050°C in a Bead Sampler NT-2100 (internal rotating induction furnace). After cooling, beads were transferred to 125 mL high-density polypropylene bottles and dissolved in 50 mL 10% HNO₃, aided by shaking with a Burrell wrist-action bottle shaker for 1 h. Samples were ultrasonicated for ~1 h after shaking to ensure complete dissolution of the glass bead. After digestion of the glass bead, the solution was passed through a 0.45 μ m filter into a clean 60 mL wide-mouth high-density polypropylene bottle. Next, 2.5 mL of this solution was transferred to a plastic vial and diluted with 17.5 mL of 10% HNO₃ to bring the total volume to 20 mL. The final solution-to-sample dilution factor for this procedure was ~4000. During Expedition 312, stock standard solutions were ultrasonicated for 1 h prior to their final dilution and analysis to ensure a homogeneous solution.

Analyses

Major (Si, Ti, Al, Fe, Mn, Mg, Ca, Na, K, and P) and trace (Sc, V, Zn, Cr, Co, Ni, Cu, Sr, Y, Zr, Nb, and Ba) element concentrations of standards and samples were determined with the JY2000 Ultrace ICP-AES, which routinely measures wavelengths between

~100 and 800 nm. Specific analytical conditions for sample runs during Expedition 309/312 are provided in Table T11.

The JY2000 plasma was ignited at least 30 min before each sample run to allow the instrument to warm up and stabilize. After the warm-up period, a zero-order search was performed to check the mechanical zero of the diffraction grating. After the zero-order search, the mechanical step positions of emission lines were tuned by automatically searching with a 0.002 nm window across each emission peak using the BAS-140 standard (basalt interlaboratory standard created during Leg 140 in Hole 504B; Bach et al., 1996), or the BAS-206 standard (basalt interlaboratory standard created during Leg 206) prepared in 10% HNO₃. During the initial setup, an emission profile was selected for each peak, using BAS-140, to determine peak-to-background intensities and set the locations of background levels for each element. The JY2000 software uses these background locations to calculate the net intensity for each emission line. The photomultiplier voltage was optimized by automatically adjusting the gain for each element using BAS-140.

ICP-AES data presented in “**Geochemistry**” in “Expedition 309” and “**Geochemistry**” in “Expedition 312” (both in the “Site 1256” chapter) were acquired using either the Gaussian or Maximum mode of the Windows 5 JY2000 software. Gaussian mode fits a curve to points across a peak and integrates the area under the curve to determine element intensity; it was used for Si, Ti, Al, Fe, Ca, Na, K, Sc, V, Zn, Sr, Zr, Cu, and Nb. Maximum mode was used for elements with asymmetric emission peaks (Mn, Mg, P, Y, Cr, Ni, and Ba), and intensity was integrated using the maximum intensity detected. Each unknown sample was run at least twice (from the same dilute solution; i.e., in replicate), nonsequentially, within a given sample run. For Si and Nb, measurements were made at two wavelengths (Si = 251.611 and 288.158 nm; Nb = 269.706 and 309.418 nm) and for each analysis the peak with the better precision was used. Net intensities of the working blank for Nb were almost identical to the peak intensities of the standards and unknowns. Because a calibration line could not be established, Nb was excluded after Run 3 for Expedition 309 and measured but not reported for Expedition 312.

A typical hard rock ICP-AES run (Table T12) during Expedition 309 included

- A set of six certified rock standards (JA-3, JB-3, BHVO-2, AGV-1, BIR-1, and JGb-1) analyzed twice during each sample run;
- Up to 20 unknown samples run in replicate;

- A drift-correcting sample (BCR-2) spiked with Ni and Cr and analyzed every fourth sample position and at the beginning and end of each run;
- Blank solutions run near the beginning and end of each run; and
- A check standard (i.e., standard run as an unknown), typically BAS-140 or BAS-206.

A 10% HNO₃ wash solution was run for 90 s between each analysis.

Hard rock ICP-AES runs were slightly modified during Expedition 312 to include

- A set of three certified rock standards (BIR-1, JB-3, and JGb-1) having major and trace element compositions similar to the rock types recovered during Expedition 309 and those anticipated during Expedition 312;
- A set of four unknown samples run in replicate;
- A drift-correcting sample (BHVO-2) in every fourth sample position beginning with the first position of each run; and
- Interlaboratory standards run as unknowns that included, beginning with Run 3, BAS-140, BAS-148, BAS-206, and BAS-312.

The first two runs did not use the above running protocol and so were reanalyzed; only the data obtained during reanalysis are reported for these samples.

Data reduction

Following each sample run, raw intensities were transferred to a data file and all analyses were corrected first for drift and then for the full procedural blank. Drift correction was applied to each element by linear interpolation between drift-monitoring solutions run every fourth analysis. Following drift correction and blank subtraction, calibration curves were constructed based on six certified rock standards (JA-3, JB-3, BHVO-2, BIR-1, JGb-1, and BCR-2 run as the drift monitor) during Expedition 309. Expedition 312 calibration curves were constructed based on four certified rock standards (BIR-1, JB-3, JGb-1, and BHVO-2 run as the drift monitor). Unknown concentrations were then calculated from the calibration line.

Estimates of accuracy and precision of major and trace element analyses during Expedition 309 were based on replicate analyses of check standards (usually BAS-140 and BAS-206), the results of which are presented in Table T13. Run-to-run relative standard deviation by ICP-AES was generally $\pm 3\%$ for major elements and $\pm 10\%$ for trace elements. Exceptions typically occurred when the element in question was near background levels. Estimates of reproducibility

during Expedition 312 were based on replicate analyses of interlaboratory rock standards (BAS-140, BAS-148, BAS-206, and BAS-312), the results of which are presented in Table T14. Relative standard deviation (i.e., precision) for the major elements is $\pm 2\%$ and for most trace elements is $\pm 5\%$. Details regarding the precision for individual elements can be found in Table T14.

Paleomagnetism

Paleomagnetic investigations during Expedition 309/312 consisted mainly of routine remanent magnetization measurements of archive-half sections and discrete samples from the working-half sections. Magnetization measurements were carried out before and after alternating-field demagnetization and, in some cases, after thermal demagnetization. Although it was reported after Leg 206 (Shipboard Scientific Party, 2003b) that most of the archive-half samples were strongly remagnetized because of a drilling-induced overprint, we measured some of the oriented specimens from the archive half. This was done to determine which portions of the recovered cores were not strongly influenced by the induced drilling overprint and to identify the possible portion suitable for future analyses.

Instruments and measurements

Remanent magnetization

Measurements of remanent magnetization were made using an automated pass-through cryogenic magnetometer with direct-current superconducting quantum interference devices (DC-SQUIDs) (2G Enterprises model 760-R). The magnetometer is equipped with an inline alternating-field demagnetizer (2G Enterprises model 2G600) capable of producing peak fields of 80 mT with 200 Hz frequency. The magnetometer is run and data are acquired by a program called LongCore (version 207.3) written by W.G. Mills (IODP) in LabView (version 6.1) programming language. This version of LongCore was last updated during ODP Leg 207. Key parameters used within the program, including calibration constants for the SQUIDs and coil response functions, are given in Table T15.

Natural remanent magnetization was routinely measured on most of the oriented pieces from the archive-half sections before demagnetization. Most of these sections were also progressively alternating-field demagnetized up to 40 mT. The remaining remanent magnetization, including orientation and intensity, was measured after each step.

Repeated tuning of the magnetometer is necessary, which often entails heating the SQUID coils to re-

lease trapped magnetic flux. If not constantly monitored and tuned, the additional magnetometer noise that results from measuring the strong intensity split-core samples can lead to erratic results. We did, however, experiment with several continuous pieces that had few or no fractures or gaps over their entire 1.5 m section length. For these sections and for the routine experiments, the sensor velocity on the magnetometer was set at 1 cm/s in order to avoid saturation of the magnetometer electronics that causes flux-jumps.

Discrete samples from working-half sections were also measured with the cryogenic magnetometer. Typically, samples were demagnetized in steps of 5 to 40–80 mT. A total of 12 samples during Expedition 309 and 8 samples during Expedition 312 from the working-half sections were also progressively demagnetized using a Schonstedt Thermal Demagnetizer (model TSD-1) in steps of 50°C from room temperature (typically 26°C) to 500°C and in steps of 25°C from 500° to 600°C. After each demagnetization step, samples were cooled down in a low-magnetic field environment (<10 nT) and the remaining magnetic intensity and orientation were measured in the SQUID magnetometer.

Calibration and instrument sensitivity

Even though results from the shipboard cryogenic magnetometer have been compared with many other laboratories and are shown to give consistent results, it is useful to check the calibration of the magnetometer against a known standard at the beginning of each expedition. We used a standard purchased from Geofyzika that is an 8 cm³ cube with an intensity of 7.62 A/m (moment = 6.096×10^{-5} Am²). All three axes gave results that differ $<2\%$ from the standard certified results. In addition, automated tray positioning was checked by putting the standard at known positions and measuring the tray. The position indicated by the software was found to be accurate to better than ± 1 cm, which is reasonable given the stretch in the pulley system used to move the sample boat.

Based on tests conducted during ODP Legs 186, 200, and 206, the background noise level of the magnetometer in the shipboard environment is $\sim 2 \times 10^{-9}$ Am² (Shipboard Scientific Party, 2000, 2003a, 2003b). During Expedition 309, the background noise level was frequently measured on an empty split-core tray (also referred to as the sample boat). Results were similar in that the x-, y-, and z-axis moments measured on the sample boat before cleaning were less than $\pm 2 \times 10^{-9}$ Am² (Fig. F12A). After cleaning the sample boat and demagnetization at 80 mT, the moments are all less than $\pm 1 \times 10^{-9}$ Am² (Fig.

F12B). These results include the drift correction, which only marginally changes the results (Fig. **F12**). During Expedition 309, tray corrections to the split-core and discrete samples were applied for every measurement sequence. The tray-corrected data are the measured magnetic moments for a sample minus those measured at the same position for the empty sample boat. The relative size of these values, however, should always be comparable to those shown in Figure **F12** for the clean, empty sample boat. When the tray correction is applied to measurements made on a clean, empty sample boat, the moments drop to less than $\pm 2 \times 10^{-10}$ Am² (Fig. **F13**).

To test the noise in the sample boat after cleaning and alternating-field demagnetization at 80 mT, the empty sample boat was measured every 5 cm in continuous mode. When measured in discrete mode and when tray corrected, four sample positions were used (20, 60, 100, and 140 cm tray slots) to ensure that samples were not influenced by the magnetizations of adjacent samples (Fig. **F14**).

The noise level of the magnetometer is sufficiently low that it is of minor significance for most samples measured. As was apparent when the sample boat was not clean, a small amount of dirt on the tray induces noise level in the 10^{-9} Am² range. Noise related to dirt on the sample boat and to the magnetization will at least be in this range. We conclude that under favorable conditions the noise level will be approximately $\pm 2 \times 10^{-9}$ Am². For discrete samples, which typically have volumes of 1 or 9 cm³, the minimum measurable remanent intensities are greater than $\sim 10^{-4}$ A/m.

Core orientation

The standard IODP paleomagnetic coordinate system was used. In this system, +x is perpendicular to the split core surface and into the working half, +z is downcore, and +y is orthogonal to x and z in a right-hand sense (i.e., it points left along the split-core surface when looking upcore at the archive half) (Fig. **F15**).

For hard rocks, it is possible to correlate images of the exterior of the core with images of the borehole wall from the Formation MicroScanner (FMS) logging tool (see “**Downhole measurements**”). To allow for this possibility, the outside surface of all cylindrical core pieces were scanned with the DMT CoreScanner (see “**Digital imaging**”). Postcruise analysis of FMS and digital images will allow reorientation of some distinctive pieces of core to true geographical north, and, by extension, absolute orientation data for magnetic declinations should be obtained.

Sampling methods and orientations for discrete samples

During both expeditions, oriented discrete samples were taken from the working halves of selected sections. Samples with ~ 2 cm \times ~ 2 cm \times ~ 2 cm exterior dimensions (volume = ~ 9 cm³) were typically collected per core for shipboard magnetic analysis and physical properties studies. In most of the intervals, we drew an arrow on the split-core face pointing upcore and used the rock saw to cut the sample. We also collected 1 cm \times 1 cm \times 1 cm (volume = 1 cm³) pieces for alternating-field and thermal demagnetization analyses. This was done in order to avoid the drilling-induced overprint, which has been reported to be stronger away from the center of the core. When measuring the samples (i.e., working half), we placed the side with the arrow down in the tray with the arrow pointing along the $-z$ axis, or uphole, which makes the orientation the same as that of the archive half.

Magnetic overprints

Several types of secondary magnetization were acquired during coring, which sometimes hampered interpretation. The most common was a steep downward-pointing overprint attributed to the drill string, which was also observed in Leg 206 cores (Shipboard Scientific Party, 2003b). This was also seen as a bias for 0° declinations in archive-half sections, which has been shown during many previous cruises and has been interpreted as a radially inward overprint (Fig. **F15**).

Data reduction and analysis

During Expedition 312, characteristic remanent magnetization (ChRM) was estimated in two ways:

1. When only the highest demagnetization step was needed to remove the drilling overprint, results from the remanence measured after this single demagnetization step were interpreted as the best estimate of the ChRM. This technique was rarely used during Expedition 309.
2. When multiple demagnetization steps were measured at fields above that needed to remove the drilling overprint, the ChRM was estimated by principal component analysis (PCA) (Kirschvink, 1980) of three or more of the stable endpoint directions.

PCA analysis was conducted using a program that iteratively searches for the demagnetization steps that minimize the size of the maximum angular deviation (MAD). This angle is a measure of how well the vector demagnetization data fit a line, formally a quality index for the calculated ChRM. MAD values

>15° were typically considered ill defined, and therefore such samples were rejected from the analysis (e.g., Butler, 1992). Because drilling overprint persisted beyond 15 mT demagnetization in most of the intervals, we only used results from 15 mT or higher in the PCA, and usually above 25 mT.

During some Expedition 312 alternating-field demagnetizations, a significant anhysteretic remanent magnetization was noted, especially as a tendency for multiple samples to converge toward steep positive inclinations. In some cases, we tried to correct this effect by repeating the demagnetization with the sample in a different orientation, generally rotated 180° about the x-axis. These rotated samples were distinguished in the database by adding 0.5 cm to the depth and were averaged offline.

Expedition 312 thermal demagnetizations were preceded by alternating-field demagnetization at 10 mT to partly remove the drilling overprint. Prior to measurement at each temperature step, the alternating-field demagnetization was repeated to remove the effects of laboratory fields. Because the LongCore software does not support labeling a demagnetization as both alternating-field and thermal, repeat measurements were taken with the alternating-field run labeled as such and the repeat run labeled as a thermal run with the temperature offset by 1°C from the oven temperature. Because the measurement immediately after alternating-field demagnetization should be least affected by exposure to laboratory fields, the label for this measurement was edited to indicate thermal demagnetization at the oven temperature. All measurements were saved for completeness, but temperatures at multiples of 5° are most meaningful.

Physical properties

Shipboard measurements of physical properties were undertaken to provide preliminary information on variations in the recovered core material. After equilibrating to room temperature, measurements of physical properties were made on whole-round sections, undisturbed parts of split cores, and discrete samples. Nondestructive measurements of bulk density, magnetic susceptibility, and NGR were made on whole-round sections using the MST. Thermal conductivity measurements were made on split cores. Measurements of *P*-wave velocity and moisture and density properties were made on discrete sample cubes (~9 cm³). A comprehensive discussion of all methodologies and calculations used in the *JOIDES Resolution* physical properties laboratory can be found in Blum (1997).

Multisensor track measurements

The MST consists of four physical property sensors on an automated track that measure, in order, magnetic susceptibility, gamma ray attenuation (GRA) bulk density, compressional *P*-wave velocity, and NGR emissions on whole-round core sections. During Expedition 309/312, only magnetic susceptibility, GRA bulk density, and NGR were measured on cores. The *P*-wave logger, which requires full-diameter core and adequate coupling to the liner for velocity to be measured effectively, was not used.

Magnetic susceptibility

The degree to which a sample can be magnetized by an external magnetic field is magnetic susceptibility. Whole-core magnetic susceptibility was measured using a Bartington MS2 meter coupled to a MS2C sensor coil with a diameter of 8.8 cm operating at 565 Hz. The measurement resolution of the MS2C sensor is 4 cm, with a minimum statistically significant count time of 1 s. During Expedition 309/312, magnetic susceptibility was measured every 2.5 cm along cores, with five data acquisitions at each interval. Magnetic susceptibility data were archived as raw instrument units (SI). Raw susceptibility measurements can be converted to SI volume units by multiplying by 10⁻⁵ and then multiplying by a correction factor to account for the volume of material that passed through the susceptibility coils. This factor is typically ~0.7 for IODP cores (Blum, 1997); however, none of these data were corrected for volume.

Typically, the center of a long piece will have higher magnetic susceptibility than the ends because of the incomplete volume of rock on the ends. However, anomalously low values of magnetic susceptibility were observed in long sections of intact core for which GRA bulk density values were high. For example, both Cores 312-1256D-187R and 189R consist of long rock pieces with high density, but only the former exhibits anomalously low values (Fig. F16). These low values are interpreted as a simple truncation of the digit in the ten-thousand position. Any value which exceeds 10,000 SI is reported as the value minus 10,000. When we ran the archive half of one of the problem cores through the MS2C loop, we received values that were greater than the values for the whole core and about half of the sum of the reported number plus 10,000 SI. Technical services at Bartington Instruments confirmed our interpretation. We plotted and reviewed all magnetic susceptibility values recorded during Expedition 309/312 using graphs similar to Figure F16. However, it is possible that in some cores the data truncation prob-

lem was missed in our visual review of magnetic susceptibility plots. Further examination of magnetic susceptibility or magnetic mineralogy is necessary to confirm the validity of other low values. For observations that we judged to be in error, we altered the values in the Janus database by adding 10,000. The green line in Figure F16 shows the new interpretation. Altered magnetic susceptibility data can be identified easily as the only values >10,000 SI.

GRA bulk density

Measurement of bulk density by the GRA densiometer is based on the principle that the attenuation, mainly by Compton scattering, of a collimated beam of gamma rays produced by a ^{137}Ce source passing through a known volume is related to material density (Evans, 1965). Calibration of the GRA densiometer was completed using known seawater/aluminum density standards. A freshwater control standard was run with each section to measure instrument drift.

The measurement width of the GRA sensor is ~5 mm, with sample spacing set at 2.5 cm for Expedition 309/312. The minimum integration time for a statistically significant GRA measurement is 1 s, and routine Expedition 309/312 GRA measurements used a 5 s integration time.

GRA density output is based on the assumption that core is 66 mm in diameter. However, the average diameter of intact cores is ~58 mm. Thus, GRA density values would be more accurate if scaled by a factor of 66/58. Further corrections to data would need to be made to account for irregular shapes and broken pieces. GRA density values in the Janus database and those reported here have not been volume corrected, unless otherwise indicated.

Natural gamma radiation

NGR emissions of rocks are a function of the random and discrete decay of radioactive isotopes, predominantly those of uranium, thorium, and potassium, and are measured through scintillation detectors arranged at 90° to each other and perpendicular to the core. The installation and operating principles of the NGR system used on the *JOIDES Resolution* are discussed in Hoppie et al. (1994). Data from 256 energy channels were collected and archived. For presentation purposes, the counts were summed over the range of 200–3000 keV, so as to be comparable with data collected during previous cruises. This integration range also allows direct comparison with down-hole logging data, which are collected over a similar integration range (Hoppie et al., 1994). Over the 200–3000 keV integration range, background counts, measured using a core liner filled with distilled water, averaged 30 during a 1 h measurement period.

Before taking measurements, each of the four NGR amplifiers was adjusted so that the thorium peak was at the highest resolution possible when the other three amplifiers were disabled. The multichannel analyzer was then calibrated by assigning certain channels to the characteristic energies of ^{40}K and the main peak of ^{232}Th (Blum, 1997).

The measurement width of the NGR is ~15 cm, with a minimum statistically significant count time of 5 s, depending on lithology. During Expedition 309/312, NGR measurements were made every 5 cm along cores for 20 s each. NGR values were recorded in units of gAPI (Blum, 1997). No corrections were made to NGR data to account for core diameters of <66 mm.

Thermal conductivity

Thermal conductivity is the rate at which heat flows through a material and is dependent on composition, porosity, and structure. Thermal conductivity was measured by transient heating of the core with a known heating power and a known geometry and recording the change in temperature with time using the TK04 system (Blum, 1997). The temperature of the superconductive probe has a linear relationship with the natural logarithm of the time after the initiation of heat:

$$T(t) = (q/4k) \ln(t) + C,$$

where

- T = temperature,
- q = heat input per unit length per unit time,
- k = thermal conductivity,
- t = time after the initiation of heat, and
- C = a constant.

Thermal conductivity was measured on the archive half of the split core, with the probe in half-space mode (Vacquier, 1985). These half-space determinations were made with a needle probe embedded in the surface of an epoxy block with a low thermal conductivity (Vacquier, 1985). Samples needed to be quite smooth to ensure adequate contact with the heating needle. Visible saw marks were removed by grinding and polishing the split face using 120 gauge silicon carbide powder.

Samples were allowed to equilibrate to room temperature for at least 4 h, and then a sample and the sensor needle were equilibrated together in a room-temperature seawater bath enclosed within a cooler for at least 15 min prior to measurement. Isolation of the samples and sensor needle eliminated the effect of rapid but small temperature changes introduced by air currents in the laboratory. The instrument internally measures drift and does not begin a heating run until sufficient thermal equilibrium is attained.

Cores were measured at irregular intervals (at least one sample every other core), depending on the availability of pieces long enough to be measured without edge effects (>7 cm) and on the degree of lithologic variability. Measurements were made at room pressure and temperature and were not corrected for in situ conditions. Results were reported in units of watts per meter degree Kelvin.

Compressional wave velocity

Compressional wave velocity was measured using *P*-wave sensor 3 (PWS3), a modified and updated version of the classic Hamilton Frame velocimeter designed with one transducer fixed and the other mounted on an adjustable screw. The compressional wave velocity calculation is based on the accurate measurement of the delay time of a 500 kHz square wave signal traveling between the pair of transducers. Transducer separation was measured by a digital caliper attached to the transducers.

Samples of ~ 9 cm³ were collected at a frequency of one every other section, depending on the availability of relatively homogeneous pieces without cracks. The PWS3 is used to measure velocity in each direction (*x*, *y*, and *z*) of the cubes, which are marked during sampling with an arrow pointing upcore in the *z*-direction on the *x*-direction face (Fig. F17). The PWS3 is mounted vertically, and samples were manually rotated to measure each direction. Deionized water was added to the contact between the transducers and sample to improve acoustic coupling. The sample was placed on the lower transducer, and the upper transducer was slowly adjusted until direct contact with the upper surface transducer pair was made with the sample.

Core temperature is recorded at the time velocity is measured; however, velocity data stored in the Janus database are uncorrected for in situ temperature and pressure. These corrections can be made using the relationships outlined in Wyllie et al. (1956), Wilson (1960), and Mackenzie (1981).

A significant offset occurs at ~ 1255 mbsf between compressional velocities measured on minicubes during Expedition 309/312 (see Fig. F330 in the “Site 1256” chapter). We attribute the jump to a change in instrumentation calibration. To verify this, both physical properties specialists on Expedition 312 measured three axes of velocity on six samples obtained during Expedition 309 after rehydrating the samples in a vacuum for 36 h (see Table T48 in the “Site 1256” chapter). The mean difference between all Expedition 309 measurements and all Expedition 312 measurements is 0.42 km/s with a standard deviation of 0.07 km/s ($N = 28$), whereas the mean difference between the two observers on Expedition 312 is

<0.01 km/s \pm 0.04 km/s ($N = 14$) (see Fig. F330 in the “Site 1256” chapter). Removal of water from sample porosity can reduce velocity, so we also tested the possibility that drying and storage of the Expedition 309 samples decreased their velocity. After Expedition 312, the Hamilton Frame was moved from the *JOIDES Resolution* to the IODP core repository in Bremen, Germany. In March 2006, the velocities of five samples from Expedition 312 were measured after rehydration for 36 h (see Table T49 in the “Site 1256” chapter). There is no significant difference between velocities of Expedition 312 samples measured during Expedition 312 and those measured after the expedition (see Fig. F330 in the “Site 1256” chapter), indicating that the drying process used during measurement of density did not affect velocity. These results convince us that the offset does not reflect a change in rock properties. Velocities of most Expedition 309 samples tested exceed sonic log velocities, consistent with the occurrence of crack porosity on length scales greater than a few centimeters. In contrast, Expedition 312 minicube velocities are lower than sonic log velocities, so the figures in this section use Expedition 312 V_p to which 0.42 km/s has been added, but the results in the Janus database remain unchanged.

Moisture and density properties

Samples used for velocity measurements were also used to calculate bulk density, grain density, and porosity from wet weight, dry weight, and dry volume. First, samples were soaked in seawater, and then wet mass (M_w) was determined. Samples were then desiccated so that dry mass (M_d) and dry volume (V_d) could be measured. During Expedition 309, moisture and density properties were computed with a spreadsheet, whereas IODP computer programs were used during Expedition 312; both methods are based on the calculations below.

Mass and volume

To prepare samples for wet mass determination, they were placed in a vacuum within open vials of seawater for 24 h. Next, excess water was wiped from the samples and wet mass was determined to a precision of 0.01 g using two Scientech 202 electronic balances and a computer averaging system to compensate for the ship’s motion. Samples were lightly wiped with deionized water, placed in an oven at $105^\circ \pm 5^\circ\text{C}$ for 24 h, and then allowed to cool in a desiccator. Dry mass was determined using the Scientech 202 electronic balances, and dry volume was determined using a five-chambered Pentapycnometer, which is a helium-displacement pycnometer with a precision of 0.02 cm³. Calibration was maintained by

including a standard reference sphere in one of the operating cells for each run and cycling it sequentially between the cells for successive runs. The cell volumes were recalibrated if the measured volume of the standard was not within 0.02 cm³ of the known volume of the standard. During Expedition 309, measurements were repeated five times for each sample, whereas only one measurement was made on each sample during Expedition 312. All cells were calibrated after four sample runs to check for instrument drift and systematic error. A purge time of 1 min was used before each run.

Bulk density calculation

For density calculations, both mass and volume are first corrected for the salt content of the pore fluid:

$$M_s = (s[M_w - M_d]) / (1 - s),$$

where

- s = pore water salinity (0.0355, from the fluid sampled at ~713 m in the hole),
- M_s = mass of salt,
- M_d = dry mass of the sample, and
- M_w = wet mass of the sample.

Grain density (ρ_g) is determined from the dry mass and dry volume measurements:

$$\rho_g = (M_d - M_s) / (V_d - [M_s - \rho_s]),$$

where ρ_s = density of salt (2.257 g/cm³). The salt-corrected mass of the pore water (M_{pw}) is calculated as

$$M_{pw} = (M_w - M_d) / (1 - s).$$

Then, the volume of pore water (V_{pw}) is

$$V_{pw} = M_{pw} / \rho_{pw} = (M_w - M_d) / [(1 - s)\rho_{pw}],$$

where the density of the pore fluid (ρ_{pw}) = 1.024 g/cm³ (from calculations of fluid sampled at ~713 m in the hole). To calculate sample bulk density (ρ_b), first compute the bulk volume:

$$V_b = V_d + V_{pw},$$

and then

$$\rho_b = M_w / V_b.$$

Porosity calculation

Porosity (ϕ) is simply the ratio of pore water volume to the total sample volume and can be calculated from the two volume parameters above:

$$\phi = V_{pw} / V_b.$$

Digital imaging

During Expedition 309/312, external surfaces of whole-round basalt, dike, and gabbro cores were scanned using the DMT Digital Color CoreScan system after they had been run through the MST but

prior to splitting. In addition, all archive-half cores were imaged in slabbed mode with the Geotek DIS. Core imaging during this expedition had four main objectives:

1. To provide a comprehensive suite of digital core images, including both unrolled 360° and slabbed images, to aid petrological interpretation;
2. To identify and measure planar features on unrolled images for comparison with core structural analysis and integration with structures measured on geographically oriented FMS and Ultrasonic Borehole Imager (UBI) images (see “[High-resolution electrical images](#)” and “[Ultrasonic borehole images](#)”);
3. To correlate core images with FMS and UBI images of the borehole wall derived from downhole logging measurements to determine true core depth as opposed to curated depth in intervals with <100% recovery; and
4. To match structures observed on core images with FMS and UBI images, as well as to reorient core pieces and associated structural data to magnetic north obtained from the General Purpose Inclinerometer Tool (GPIT) on the FMS and UBI tool strings.

Core orientation is particularly important for Expedition 309/312 because Site 1256 has a low paleolatitude, which means the paleomagnetic inclination will be nearly horizontal and the magnetic polarity will be indeterminate from azimuthally unoriented cores. Similarly, without a known polarity, the paleomagnetic declination cannot be used to orient the core for structural analyses or for the determination of anisotropy of physical properties. Site 1256 is sufficiently close (<10 km) to the magnetic Anomaly 5Bn/5Br boundary that the polarity cannot simply be assumed. In order to determine the source of marine magnetic anomalies, which is one of the expedition objectives, estimating the true, rather than the relative, paleomagnetic direction is critical and can only be accomplished if the core is oriented.

DMT CoreScan system

The DMT Color CoreScan system (Fig. F18), developed by Deutsche Montan Technologie, is a portable core imaging device that was previously used on board the *JOIDES Resolution* during ODP Legs 173 (Whitmarsh, Beslier, Wallace, et al., 1998), 176 (Dick, Natland, Miller, et al., 1999), 197 (Tarduno, Duncan, Scholl, et al., 2002), and 206 (Wilson, Teagle, Acton, et al., 2003). Images are recorded on whole-round outer core surfaces using a 3 pixel × 1728 pixel, 24 bit/pixel, three-color (red, green, and blue) charge-coupled device line-scan camera that has a spectral response between 400 and 700 nm, positioned to

have a resolution of 5.0 pixel/mm (DMT GeoTec, 1996; DMT GmbH, 2000).

The whole-round core is rotated 360° around its cylindrical axis with the line-scan camera positioned parallel to the axis of rotation. The unrolled images, up to 1.5 m long, are recorded in 30–34 cm sections that are integrated and light calibrated using the DigiCore software provided with the DMT CoreScan system. Whole-round cores are scanned in the unrolled mode at a rate of ~1.2 min/m, creating a ~14 MB bitmap file per meter of core (DMT GeoTec, 1996). The scanned images were then integrated for each core using the Core Recovery Quality Control program (DMT GmbH, 2000). The images are plotted on a depth scale according to their IODP curated depths and then edited and saved in Adobe Illustrator format with a corresponding slab image of split archive-half cores obtained by Geotek DIS.

Methodology

During Expedition 309/312, all core pieces that could be rotated cleanly through 360° were scanned in unrolled mode. Conventional IODP core piece numbers, associated curated depths, and piece lengths were entered into a spreadsheet (see “**Digital imaging**” in “Expedition 309” and “**Digital imaging**” in “Expedition 312” in the “Site 1256” chapter and SCANLOG.XLS in “**Supplementary material**”). The lengths of intervals of unscanned pieces were measured and recorded in the spreadsheet so that allowance could be made for them when integrated into core barrel lengths using the DMT CoreLog software (DMT GeoTec, 1996; DMT GmbH, 2000). During Expedition 312, some pieces that were not fully cylindrical or oriented were scanned because subparallel horizontal fractures and vein features on the core surface may prove to help finalize depth-matching between whole core images and FMS logs.

On each core piece, a vertical red line was drawn with a red grease pencil to define the core split. Convention is such that, with the core upright, the archive half is to the left of this line and the working half is to the right. When the core images are unrolled, nonhorizontal planar structures (e.g., veins, faults, or fractures) produce sinusoidal-shaped curves. These can be matched to similar-shaped features imaged along the borehole wall by the four pads of the FMS or by the UBI logging tools (see “**Ultrasonic borehole images**”). Other distinct petrological features or structures that are imaged on the outer surface of the core and the borehole wall can be similarly matched to determine the depth of the core in the borehole and reorient the core azimuth (Haggas et al., 2001). Initial comparisons with FMS and UBI images and structural analyses were per-

formed onboard, but detailed structural analysis, core-log integration, and core reorientation work will be done postcruise.

Funding for the DMT 360° core scanner on Expedition 309/312 was provided by Natural Environment Research Council (U.K.) Integrated Ocean Drilling Program Directed Science Programme Urgency Grant (NE/D001277/1 to Teagle/Brewer) and the generous support of the School of Ocean and Earth Science, University of Southampton; the Department of Geology, University of Leicester; and the U.S. National Science Foundation, through the Integrated Ocean Drilling Program (Texas A&M University) and the United States Science Support Program (Joint Oceanographic Institutions, Inc.).

Downhole measurements

Downhole wireline logs are spatially continuous records of the in situ physical, chemical, and structural properties of the formation penetrated by a borehole. They provide information on a scale that is intermediate between laboratory measurements on core samples and geophysical surveys. The logs are recorded rapidly using a variety of probes or sondes combined into tool strings (Fig. F19). These tool strings are lowered downhole on a heave-compensated electrical wireline and raised at a constant speed (typically 250–400 m/h) to provide continuous simultaneous measurements of the various properties as a function of depth, with a vertical sampling interval ranging from 2.5 mm to 15 cm. During Expedition 309/312, wireline logging provided continuous, in situ measurements of geophysical properties of drilled basalts, dikes, and gabbros. A main objective of the wireline logging program was to orient faults, fractures, deformation features, and any obvious petrologic boundaries using borehole imaging techniques. Downhole measurements will be used in conjunction with whole-core images from the DMT Core Scanner to reorient veins, fractures, and other features back into the geographic reference frame. Borehole images then help orient core pieces or sections where core recovery is sufficiently high. Core recovery during drilling of igneous basement is often incomplete and biased, with weaker rock types preferentially lost. In contrast, wireline logging provides continuous data across all intervals, including those with low recovery. In addition to defining structural features, the logging program will also attempt to establish lithologic or physical property boundaries, as interpreted from logging tool response characteristics as a function of depth; determine alteration patterns in basalts, sheeted dikes, and the upper plutonic section; and produce direct correlations with discrete laboratory measurements on recovered core.

Tool string configurations

Individual logging tools were joined together into tool strings so that several measurements could be made during each logging run (Table T16). Tool strings were lowered to the bottom of the borehole on a wireline cable, and data were logged as the tool string was pulled back up the hole. Repeat runs were made to improve coverage and document the accuracy of log data. Several different tool strings were deployed during Expedition 309/312, and their principal configurations are demonstrated in Figures F19 and F20:

- The triple combination (triple combo) tool string, which consists of the Hostile Environment Spectral Gamma Ray Sonde (HNGS), the Dual Latero-Log (DLL) tool, the Hostile Environment Litho-Density Sonde (HLDS), the Accelerator Porosity Sonde (APS), and the Lamont-Doherty Earth Observatory (LDEO) Temperature/Acceleration/Pressure (TAP) tool. During Expedition 312, the Environment Measurement Sonde (EMS) was also included to the tool string;
- The FMS-sonic tool string, which consists of the FMS, the GPIT, the Scintillation Gamma Ray Tool (SGT), and the Dipole Sonic Imager (DSI) tool;
- The UBI tool string, which also includes the GPIT and the SGT; and
- The Well Seismic Tool (WST) and Versatile Seismic Imager (VSI).

Explanations of tool name acronyms and their measurement units are summarized in Table T16. Parameters measured by each tool, sample intervals used, and vertical resolution are summarized in Table T17. More detailed descriptions of individual logging tools and their geological applications can be found in Ellis (1987), Goldberg (1997), Rider (1996), Schlumberger (1989, 1994), Serra (1984, 1986, 1989), and the LDEO-Borehole Research Group (BRG) Wireline Logging Services Guide (1994).

Natural gamma radiation

Two gamma ray tools were used to measure and characterize natural radioactivity in the formation: the HNGS and the SGT. The HNGS measures natural gamma radiation from isotopes of potassium, thorium, and uranium using five-window spectroscopy to determine concentrations of radioactive potassium (in weight percent), thorium (in parts per million), and uranium (in parts per million). The HNGS uses two bismuth germanate scintillation detectors for gamma ray detection with full spectral processing. Corrections are made to account for variability in borehole size and borehole potassium concentrations during processing of HNGS data at LDEO-BRG.

The HNGS also measures total gamma ray emission (in gAPI units) and the uranium-free or computed gamma ray (in gAPI units). The SGT uses a sodium iodide (NaI) scintillation detector to measure the total NGR emission, combining the spectral contributions of potassium, uranium, and thorium concentrations in the formation. The SGT is not a spectral tool but provides high-resolution total gamma ray data for depth correlation between logging strings. It is included in the FMS-sonic, UBI, and VSI tool strings to provide a reference log to correlate depth between different logging runs.

Density

Density was measured with the HLDS, which consists of a radioactive cesium (^{137}Cs) gamma ray source (622 keV) and far and near gamma ray detectors mounted on a shielded skid, which is pressed against the borehole wall by a hydraulically activated eccentricizing arm (Fig. F19). Gamma rays emitted by the source experience both Compton scattering and photoelectric absorption. Compton scattering involves the transfer of energy from gamma rays to electrons in the formation via elastic collision. The number of scattered gamma rays that reach the detectors is directly related to the number of electrons in the formation, which is a function of the bulk density. The HLDS measures the photoelectric effect factor (PEF) caused by absorption of low-energy gamma rays. Photoelectric absorption occurs when gamma ray energies drop to <150 keV after being repeatedly scattered by electrons in the formation. As the PEF depends on the atomic number of the elements in the formation, it is essentially independent of porosity (Gardener and Dumanoir, 1980). Thus, the PEF varies according to the chemical composition of the formation. Some examples of PEF values are: pure pyrite = 16.97, calcite = 5.08, potassium feldspar = 2.86, and quartz = 1.81 b/e⁻²⁴ (barn = 10⁻²⁴ cm²). Coupling between the tool and borehole wall is essential for good HLDS logs. Poor contact results in underestimation of density values. Both density correction and caliper measurement of the hole are used to check contact quality.

Neutron porosity

The APS consists of a minitron neutron generator that produces fast neutrons (14.4 MeV) and five neutron detectors (four epithermal and one thermal) positioned at different spacings along the tool. The tool is pressed against the borehole wall by an eccentricizing bow-spring (Fig. F19). Emitted high-energy (fast) neutrons are slowed by collisions with other atoms, and the amount of energy lost per collision depends on the relative mass of the nucleus with

which the neutron collides. Significant energy loss occurs when the neutron strikes a hydrogen nucleus of equal mass, which is mainly present in pore water. Degrading to thermal energies (0.025 eV), the neutrons are captured by the nuclei of silicon, chlorine, boron, and other elements, resulting in a gamma ray emission. The neutron detectors record both the numbers of neutrons arriving at various distances from the source and the neutron arrival times, which act as a measure of formation porosity. Hydrogen bonds in minerals such as clays, however, also contribute to the measurement, so the raw porosity value is often an overestimate. In sediments, hydrogen is mainly present in pore water, so the neutron log is essentially a measure of porosity, assuming pore fluid saturation. In igneous and hydrothermally altered rocks, hydrogen may also be present in alteration minerals such as clays; therefore, neutron logs may not give accurate estimates of porosity in these rocks. The pulsing of the neutron source provides the measurement of the thermal neutron cross section in capture units. This is a useful indicator for the presence of elements of high thermal neutron capture cross section such as boron, chloride, and rare earth elements.

Electrical resistivity

The DLL tool provides two resistivity measurements with different depths of investigation: deep and shallow. In both devices, a 61 cm thick current beam is forced horizontally into the formation by using focusing (also called bucking) currents. Two monitoring electrodes are part of the loop that adjusts the focusing currents so that there is no current flow in the borehole between the two electrodes. For the deep laterolog (LLD) measurement, both measuring and focusing currents return to a remote electrode on the surface; this configuration greatly improves the depth of investigations and reduces the effect of borehole and adjacent formation conductivity. In the shallow laterolog (LLS) measurement, the return electrodes that measure the focusing currents are located on the sonde, and therefore the current sheet retains focus over a shorter distance than the LLD. Fracture porosity can be estimated from the separation between the LLD and LLS measurements, based on the observation that the former is sensitive to the presence of horizontal conductive fractures only whereas the latter responds to both horizontal and vertical conductive structures. Because the solid constituents of rocks are essentially infinitely resistive relative to the pore fluids, resistivity is controlled mainly by the nature of the pore fluids, porosity, and permeability. In most rocks, electrical conduction occurs primarily by ion transport through pore fluids and is strongly dependent on porosity.

Temperature/Acceleration/Pressure

The TAP tool was deployed in low-resolution memory mode (4 Hz for accelerometry data and 1 Hz for temperature and pressure) with data being stored in the tool and then downloaded after the logging run was completed. The EMS tool, used during Expedition 312, uses a platinum resistor to measure the borehole fluid temperature. Temperatures determined using these tools are not necessarily in situ formation temperatures because water circulation during drilling will have disturbed temperature conditions in the borehole. From the spatial temperature gradient, however, abrupt temperature changes can be identified that may represent localized fluid flow into the borehole, indicating fluid pathways, fracturing, and/or changes in permeability at lithologic boundaries.

Acoustic velocities

The DSI tool employs a combination of monopole and dipole transducers to make accurate measurements of sonic wave propagation in a wide variety of formations. The omnidirectional source generates compressional, shear, and Stoneley waves in hard formations. The configuration of the DSI tool also allows recording of both inline and crossline dipole waveforms. In hard rocks, dipole sources can result in a better or equivalent estimate of shear wave velocity than that from a monopole source. These combined modes can be used to estimate shear wave splitting caused by preferred mineral and/or structural orientation in consolidated formations. A low-frequency (80 Hz) source enables Stoneley waveforms to be generated as well. The DSI tool measures transit times between sonic transmitters and an array of eight receiver groups with 15 cm spacing along the tool, each consisting of four orthogonal elements that are aligned with the dipole transmitters. During acquisition, the output from these 32 individual elements are differenced or summed appropriately to produce inline and crossline dipole signals or monopole-equivalent (compressional and Stoneley) waveforms, depending on the operation modes. Preliminary processing of DSI data estimates monopole and dipole mode velocities using waveform correlation of the digital signals recorded at each receiver.

High-resolution electrical images

The FMS provides high-resolution electrical-resistivity-based images of borehole walls (Fig. F21). The tool has four orthogonal arms (pads), each containing 16 microelectrodes, or “buttons,” which are pressed against the borehole wall during recording. The electrodes are arranged in two diagonally offset

rows of eight electrodes each, spaced ~2.5 mm apart. A focused current is emitted from the four pads into the formation, with a return electrode near the top of the tool. Array buttons on each of the pads measure the current intensity variations. The FMS image is sensitive to structure within ~25 cm of the borehole wall and has a vertical resolution of 5 mm with coverage of 22% of the borehole wall on a given pass where the borehole is in gauge. FMS logging commonly includes two passes, the images of which are merged to improve borehole wall coverage. The pads must be firmly pressed against the borehole wall to produce reliable FMS images. In holes with a diameter >38 cm (15 inches), the pad contact will be inconsistent and the FMS images can be blurred. The maximum borehole deviation where good data can be recorded with this tool is 10° from vertical. Irregular borehole walls will also adversely affect the images, as contact with the wall is poor. FMS images are oriented to magnetic north using the GPIT. Processing transforms these measurements of the micro-resistivity variations of the formation into continuous, spatially oriented, and high-resolution images that mimic geologic structures behind the borehole walls. This allows the dip and azimuth of geologic features intersecting the hole to be measured from the processed FMS image. FMS images can be used to visually compare logs with core to ascertain the orientations of lithologic boundaries and fracture patterns. FMS images are particularly useful for mapping structural features, dip determination, detailed core-log correlation, positioning of core sections with poor recovery, and stress distribution. FMS images have proved to be particularly valuable in the interpretation of volcanic stratigraphy (Ayadi et al., 1998; Lovell et al., 1998; Brewer et al., 1999; Barr et al., 2002) and gabbroic structure (Haggas et al., 2001; Miller et al., 2003) during ODP legs.

Further interpretation of FMS images in combination with other log data and core imaging will be carried out postcruise. Conventionally, structural analysis of FMS images is achieved by fitting sinusoidal curves on the unwrapped borehole image. Each planar structure intersecting the borehole wall corresponds to a sinusoid on the FMS images and is indicated by a color distinction. As the borehole image orientation is known, we can extract for each plane its azimuth and dip. The plane azimuth is determined by picking the inflexion point of the sinusoid where the amplitude is half the peak value (H). The dip is calculated as $\tan^{-1}(H/D)$, with D being the borehole diameter. FMS data processing and analysis were undertaken using Geoframe (version 4.0.4.2), a Schlumberger software program that al-

lows interactive display and analysis of the oriented images.

Ultrasonic borehole images

The UBI features a high-resolution transducer that provides acoustic images of the borehole wall. The transducer emits ultrasonic pulses at a frequency of 250 or 500 kHz (low and high resolution, respectively), which are reflected by the borehole wall and then received by the same transducer. Amplitude and traveltime of the reflected signal are then determined (Fig. F22). The continuous rotation of the transducer and the upward motion of the tool produce a complete map of the borehole wall. Amplitude depends on the reflection coefficient of the borehole fluid/rock interface, the position of the UBI tool in the borehole, the shape of the borehole, and the roughness of the borehole wall. Changes in borehole wall roughness (e.g., at fractures intersecting the borehole) are responsible for the modulation of the reflected signal; therefore, fractures or other variations in the character of drilled rocks can be recognized in the amplitude image. The recorded travel-time image gives detailed information about the shape of the borehole, which allows calculation of one caliper value of the borehole from each recorded traveltime. Amplitude and traveltime are recorded together with a reference to magnetic north by means of a magnetometer (GPIT), permitting the orientation of images. If features (e.g., fractures) recognized in the core are observed in the UBI images, orientation of the core is possible. UBI oriented images can also be used to measure stress in the borehole through identification of borehole breakouts and slip along fault surfaces penetrated by the borehole (i.e., Paillet and Kim, 1987). In an isotropic, linearly elastic rock subjected to an anisotropic stress field, drilling a subvertical borehole causes breakouts in the direction of the minimum principal horizontal stress (Bell and Gough, 1983).

Magnetic field

Downhole magnetic field measurements were made with the GPIT. The GPIT is included in the FMS and UBI tool strings to calculate tool acceleration and orientation during logging. Tool orientation is defined by three parameters: tool deviation, tool azimuth, and relative bearing. The GPIT utilizes a three-axis inclinometer and a three-axis fluxgate magnetometer to record the orientation of the FMS and UBI images as the magnetometer records the magnetic field components (Fx, Fy, and Fz). Corrections for cable stretching, tool sticking, and/or ship heave using acceleration data (Ax, Ay, and Az) allow precise determinations of log depths.

Well Seismic Tool and Versatile Seismic Imager

Borehole seismic tools are used in wells to detect the acoustic signal generated at the surface. The WST and VSI are used to determine the time–depth relation and to produce a zero-offset vertical seismic profile and/or check shots in the borehole. The WST consists of a single geophone (Fig. F19) used to record the full waveform of acoustic waves generated by a seismic source positioned just below the sea surface. The VSI (Fig. F20) uses three-axis single sensor seismic hardware and software and advanced wireline telemetry for efficient data delivery from the borehole to the surface. Each sensor package delivers high-fidelity wavefields through the use of a three-axis geophone accelerometer, which are acoustically isolated from the main body of the tool (Fig. F20). The geophone accelerometer detects particle motion and provides a linear and flat response from 3 to 200 Hz. The VSI maximal operational temperature is 177°C or 350°F.

A generator-injector air gun, positioned at a water depth of ~7 m with a borehole offset of 50 m on the port side of the *JOIDES Resolution*, was used as the seismic source. The VSI was used during Expedition 312 and clamped against the borehole in 22 m intervals. The generator-injector air gun mode during the Expedition 312 vertical seismic profile experiment was set to “harmonic mode” with a chamber configuration of 150 and 105 inch³, respectively (see “[Downhole measurements](#)” in “Expedition 312” in the “Site 1256” chapter for details). The recorded waveforms were stacked during each operation, and a one-way traveltime was determined from the median of the first breaks for each station, thus providing check shots for calibration of the integrated transit time calculated from sonic logs. Check shot calibration is required for the core-seismic correlation because *P*-wave velocities derived from the sonic log may differ significantly from true formation velocity because of (1) frequency dispersion (the sonic tool operates at 10–20 kHz, but seismic data are in the 50–200 Hz range), (2) differences in travel paths between well seismic and surface seismic surveys, and (3) borehole effects caused by formation alterations (Schlumberger, 1989). In addition, sonic logs cannot be measured through pipe, so traveltime down to the uppermost logging point has to be estimated by other means.

In situ temperature measurements

During Expedition 309, temperature measurements were taken before coring recommenced in Hole 1256D to determine the in situ temperature at the bottom of the borehole. Two discrete in situ measurements were made with the APCT tool run in iso-

lation into the borehole because borehole conditions exceeded the maximum range (60°C) of the temperature probe on the water-sampling temperature probe (WSTP) deployed during Expedition 309. The components of the APCT tool include a platinum temperature sensor and a battery-powered data logger. The platinum resistance-temperature device is calibrated for temperatures ranging from –20° to 100°C, with a resolution of 0.01°C (see Horai and Von Herzen, 1985). During operation, the APCT tool is mounted on a regular rotary core barrel and lowered down the pipe by wireline. The tool was held for 8 min at 4358 mbrf to equilibrate with near-bottom water temperatures and was then lowered to the bottom of the open hole (~4370 mbrf), where it was held for a further 5 min to measure the temperature. This provided a sufficiently long transient record to estimate steady-state temperature. The nominal accuracy of the temperature measurement is ±0.1°C.

Temperatures were also measured using the TAP tool (see “[Temperature/Acceleration/Pressure](#)”) that was run as part of the triple combo logging string following the second WSTP deployment. However, the TAP tool was run during Expedition 312 as part of the triple combo tool string and in combination with the EMS temperature and the DLL tools after drilling and coring ceased.

Logging operations

In preparation for logging, the borehole is flushed with fresh water. Tool strings are then lowered downhole during sequential runs. Tool strings are pulled uphole at constant speed (typically at 250–400 m/h). Each tool string also contains a telemetry cartridge, facilitating communication from the tools along a double-armored seven-conductor wireline cable to the Schlumberger Minimum Configuration Maxis (MCM) van on the drill ship. Data for each wireline-logging run are recorded, stored digitally, and monitored in real time using the Schlumberger MAXIS 500 system located in the Offshore Service Unit-F-model Modular Configuration MAXIS Electrical Capstan Capable (OSU-FMEC) winch unit. The logging cable connects the MCM to the tool string through the logging winch and LDEO-BRG wireline heave compensator (WHC). The WHC is employed to minimize the effect of ship’s heave on the tool position in the borehole. After the logs are acquired, data are transferred to the downhole measurements laboratory and also to LDEO-BRG.

Wireline log data quality

Logging data quality may be seriously degraded by changes in hole diameter and in sections where the borehole diameter greatly decreases or is washed out.

Deep-investigation measurements such as resistivity and sonic velocity are less sensitive to borehole conditions. Nuclear measurements (density, neutron porosity, and both natural induced spectral gamma rays) are more sensitive because of their shallower depth of investigation and the effect of drilling fluid volume on neutron and GRA. Corrections can be applied to the original data in order to reduce these effects. Very large washouts, however, cannot be corrected for. HNGS and SGT data provide a depth correlation between logging runs, but logs from different tool strings may still have minor depth mismatches caused by either cable stretch or ship heave during recording. To minimize such errors, hydraulic heave compensator adjusts for ship motion in real time. Downhole data cannot be precisely matched with core data in zones where core recovery is low because of the inherently ambiguous placement of the recovered section within the interval cored.

Logging data flow and processing

Data for each wireline logging run were recorded, stored digitally, and monitored in real time using the Schlumberger MAXIS 500 system. After each logging phase was completed in Hole 1256D, data were transferred to the shipboard downhole measurements laboratory for preliminary processing and interpretation. FMS and UBI image data were interpreted using Schlumberger's Geoframe (version 4.0.4.2) software package. Logging data were also transmitted to shore for processing. Onshore data processing consisted of (1) depth-shifting all logs relative to a common datum (i.e., in meters below seafloor), (2) corrections specific to individual tools, and (3) quality control and rejection of spurious values. Once processed onshore, data were transmitted back to the ship, providing final processed logging results during the expedition. Data in ASCII are available directly from the IODP-USIO Science Services, LDEO, Web site (iodp.ldeo.columbia.edu/DATA/IODP/index.html). A summary of "logging highlights" is also posted on this Web site at the end of each expedition.

Underway geophysics

While transiting between Panama and Site 1256 during Expedition 309, we collected 3.5 and 12 kHz echo sounder and magnetometer data. Because the exact location of Site 1256 is well established based on analysis of site survey data and drilling during Leg 206, no additional surveys were conducted.

Navigation data were acquired throughout the expedition on an Ashtech GG24 GPS receiver. The antenna was mounted on the starboard stack 46.33 m

aft of the moonpool (Fig. F23). The datum is the moonpool. GPS fixes were recorded by WinFrog navigation software every 60 s. Generic Mapping Tools software (Wessel and Smith, 1995) on Sun Sparc 10 Unix workstations was used to process and display the navigation data.

Time datum for all underway geophysics activities is Universal Time Coordinated (UTC) (similar to Greenwich Mean Time), as provided from the Ashtech receivers. If communication between the Ashtech receiver and the satellite is interrupted, the receiver uses its own internal clock to maintain the time base. The WinFrog navigation system displays UTC time many times per second, but the internal clock is not synchronized to UTC.

Magnetic data were acquired with an EG&G Geometrics Marine Proton Magnetometer (model G-886) towed 500 m behind the ship. Values of total field intensity were acquired every 60 s using the WinFrog navigation software on a Windows PC.

Underway 3.5 and 12 kHz echo sounder data were acquired using an EDO Model 515A-250 transceiver mounted in a sonar dome located 45.52 m forward of the moonpool. Data were processed in real time using a Raytheon CESP III (Correlator Echo Sounder Processor). Underway echo sounder data were not digitized but were recorded on an EPC 9802 analog linescan thermal paper recorder. The ship's speed, heading, and position were annotated on the EPC recorders and logged each minute on WinFrog. The paper recorder was set to a 1 s sweep, and uncorrected depths were logged at 5 min intervals by hand.

Uncorrected depths convert traveltime to nominal depth assuming a velocity of 1500 m/s. A corrected depth (using Matthews's tables to allow for varying sound speed with depth and location in the ocean [Carter, 1980]) was computed by hand upon arrival at the site.

Transducer elements are 0.9 m below the keel of the ship and 18.4 m below the dual elevator stool (the reference datum for drilling activities). Water depth relative to sea level was obtained by adding 0.9 m and the mean draft (typically 6.5 ± 0.6 m) to the corrected echo sounder depth. Figure F24 is a schematic of the ship that summarizes some key dimensions used in computing depth to various datums.

A program called U/W Watch was developed by ODP to configure acquisition sequences for the echo sounder and the magnetometer and to display and annotate echo sounder output on the EPC graphic recorders. This program is written in the National Instruments LabView language and runs on a Compaq Deskpro Workstation.

References

- Ayadi, M., Pezard, P.A., Laverne, C., and Bronner, G., 1998. Multi-scalar structure at DSDP/ODP Site 504, Costa Rica Rift, I: stratigraphy of eruptive products and accretion processes. In Harvey, P.K., and Lovell, M.A. (Eds.), *Core-Log Integration*. Geol. Soc. Spec. Publ., 136:297–310.
- Bach, W., Erzinger, J., Alt, J.C., and Teagle, D.A.H., 1996. Chemistry of the lower sheeted dike complex, Hole 504B (Leg 148): influence of magmatic differentiation and hydrothermal alteration. In Alt, J.C., Kinoshita, H., Stokking, L.B., and Michael, P.J. (Eds.), *Proc. ODP, Sci. Results*, 148: College Station, TX (Ocean Drilling Program), 39–55.
- Barr, S.R., Revillon, S., Brewer, T.S., Harvey, P.K., and Tarnay, J., 2002. Determining the inputs to the Mariana subduction factory: using core-log integration to reconstruct basement lithology at ODP Hole 801C. *Geochem., Geophys., Geosyst.*, 3. doi:10.1029/2001GC000255.
- Bell, J.S., and Gough, D.I., 1983. The use of borehole breakouts in the study of crustal stress. In Zoback, M.D., and Haimson, B.C. (Eds.), *Hydraulic Fracturing Stress Measurements*: Washington (National Academy Press), 201–209.
- Blackman, D.K., Ildefonse, B., John, B.E., Ohara, Y., Miller, D.J., MacLeod, C.J., and the Expedition 304/305 Scientists, 2006. *Proc IODP*, 304/305: College Station, TX (Integrated Ocean Drilling Program Management International, Inc.). doi:10.2204/iodp.proc.304305.2006
- Blum, P., 1997. Physical properties handbook: a guide to the shipboard measurement of physical properties of deep-sea cores. *ODP Tech. Note*, 26 [Online]. Available from World Wide Web: <http://www-odp.tamu.edu/publications/tnotes/tn26/INDEX.HTM>.
- Brewer, T.S., Harvey, P.K., Lovell, M.A., Haggas, S., Pezard, P.A., and Goldberg, D., 1999. Borehole images of the ocean crust: case histories from the Ocean Drilling Program. In Lovell, M.A., Williamson, and Harvey, P.K. (Eds.), *Borehole Images: Application and Case Histories*. Geol. Soc. Spec. Publ., 159:283–294.
- Butler, R.F., 1992. *Paleomagnetism: Magnetic Domains to Geologic Terranes*: Boston (Blackwell).
- Carter, D.J.T., 1980. *Echo-Sounding Correction Tables (Formerly Matthews' Tables)*: Taunton, Somerset, UK (Hydrographic Dept., Min. of Defence).
- Cordier, C., Clement, J.-P., Caroff, M., Hémond, C., Blais, S., Cotten, J., Bollinger, C., Launeau, P., and Guille, J., 2005. Petrogenesis of coarse-grained intrusives from Tahiti Nui and Raiatea (Society Islands, French Polynesia). *J. Petrol.*, 46(11):2281–2312. doi:10.1093/petrol-ogy/egi055
- Davis, G.H., 1984. *Structural Geology of Rocks and Regions*: New York (John Wiley & Sons, Inc.).
- Dick, H.J.B., Natland, J.H., Miller, D.J., et al., 1999. *Proc. ODP, Init. Repts.*, 176: College Station, TX (Ocean Drilling Program). doi:10.2973/odp.proc.ir.176.1988
- DMT GmbH, 2000. *DMT CoreScan Color Acquisition Software Digicore and Hardware Information*: Essen, Germany (Deutsche Montan Technologie GmbH).
- DMT GeoTec, 1996. *DMT CoreScan Color User's Manual: Acquisition and Evaluation Software*: Essen, Germany (Deutsche Montan Technologie GmbH).
- Ellis, D.V., 1987. *Well Logging for Earth Scientists*: New York (Elsevier).
- Evans, H.B., 1965. GRAPE—a device for continuous determination of material density and porosity. *Trans. SPWLA 6th Ann. Logging Symp.*: Dallas, 2:B1–B25.
- Fowler, A.D., Bergerb, B., Shore, M., Jonesa, M.I., and Ropchan, J., 2002. Supercooled rocks: development and significance of varioles, spherulites, dendrites and spinifex in Archaean volcanic rocks, Abitibi greenstone belt, Canada. *Precambrian Res.*, 115:311–328.
- Gardener, J.S., and Dumanoir, J.L., 1980. Litho-density log interpretation. *Trans. SPWLA Annu. Logging Symp.*, 21:1–23.
- Gieskes, J.M., Gamo, T., and Brumsack, H., 1991. Chemical methods for interstitial water analysis aboard *JOIDES Resolution*. *ODP Tech. Note*, 15 [Online]. Available from World Wide Web: http://www-odp.tamu.edu/publications/tnotes/tn15/f_chem1.htm.
- Goldberg, D., 1997. The role of downhole measurements in marine geology and geophysics. *Rev. Geophys.*, 35:315–342. doi:10.1029/97RG00221
- Haggas, S., Brewer, T.S., Harvey, P.K., and Iturrino, G., 2001. Relocating and orienting cores by the integration of electrical and optical images: a case study from Ocean Drilling Program Hole 735B. *J. Geol. Soc. (London, U. K.)*, 158:615–623.
- Hoppie, B.W., Blum, P., and the Shipboard Scientific Party, 1994. Natural gamma-ray measurements on ODP cores: introduction to procedures with examples from Leg 150. In Mountain, G.S., Miller, K.G., Blum, P., et al., *Proc. ODP, Init. Repts.*, 150: College Station, TX (Ocean Drilling Program), 51–59.
- Horai, K., and Von Herzen, R.P., 1985. Measurement of heat flow on Leg 86 of the Deep Sea Drilling Project. In Heath, G.R., Burckle, L.H., et al., *Init. Repts. DSDP*, 86: Washington (U.S. Govt. Printing Office), 759–777.
- Howarth, R.J., 1998. Improved estimators of uncertainty in proportions, point-counting, and pass-fail test results. *Am. J. Sci.*, 298:594–607.
- Kelemen, P.B., Kikawa, E., Miller, D.J., et al., 2004. *Proc. ODP, Init. Repts.*, 209: College Station, TX (Ocean Drilling Program). doi:10.2973/odp.proc.ir.209.2004
- Kirschvink, J.L., 1980. The least-squares line and plane and the analysis of palaeomagnetic data. *Geophys. J. R. Astron. Soc.*, 62(3):699–718.
- Lamont-Doherty Earth Observatory-Borehole Research Group, 1994. *Wireline Logging Services Guide* [Online]. Available from World Wide Web: <http://www.ldeo.columbia.edu/BRG/ODP/LOGGING/>.
- Le Maitre, R.W., 1989. *A Classification of Igneous Rocks and Glossary of Terms*: Oxford (UGS, Blackwell).
- Lovell, M.A., Harvey, P.K., Brewer, T.S., Williams, C., Jackson, P.D., and Williamson, G., 1998. Application of FMS images in the Ocean Drilling Program: an overview. In Cramp, A., MacLeod, C.J., Lee, S.V., and Jones, E.J.W. (Eds.), *Geological Evolution of Ocean Basins: Results from*

- the Ocean Drilling Program*. Geol. Soc. Spec. Publ., 131:287–303.
- Mackenzie, K.V., 1981. Nine-term equation for sound speed in the oceans. *J. Acoust. Soc. Am.*, 70:807–812. doi:10.1121/1.386920
- Miller, D.J., Iturrino, G.J., and McGuire, J.C., 2003. Core-log correlations in oceanic basement from Hole 1105A on the Southwest Indian Ridge. In Casey, J.F., and Miller, D.J. (Eds.), *Proc. ODP, Sci. Results*, 179: College Station, TX (Ocean Drilling Program), 1–29.
- Murray, R.W., Miller, D.J., and Kryc, K.A., 2000. Analysis of major and trace elements in rocks, sediments, and interstitial waters by inductively coupled plasma–atomic emission spectrometry (ICP-AES). *ODP Tech. Note*, 29 [Online]. Available from World Wide Web: <http://www-odp.tamu.edu/publications/tnotes/tn29/INDEX.HTM>.
- Paillet, F.L., and Kim, H., 1987. Character and distribution of borehole breakouts and their relationship to in situ stresses in deep Columbia River basalts. *J. Geophys. Res.*, 92:6223–6234.
- Passchier, C.W., and Trouw, R.A.J., 1996. *Microtectonics*: Berlin (Springer-Verlag).
- Ramsay, J.G., and Huber, M.I., 1987. *The Techniques of Modern Structural Geology* (Vol. 2): *Folds and Fractures*: New York (Acad. Press).
- Rider, M.H., 1996. *The Geological Interpretation of Well Logs* (2nd ed.): Caithness (Whittles Publishing).
- Schlumberger, 1989. *Log Interpretation Principles/Applications*: Houston (Schlumberger Educ. Services), SMP-7017.
- Schlumberger, 1994. *Log Interpretation Charts*: Sugarland, TX (Schlumberger Wireline and Testing), SMP-7006.
- Serra, O., 1984. *Fundamentals of Well-Log Interpretation* (Vol. 1): *The Acquisition of Logging Data*: Dev. Pet. Sci., 15A: Amsterdam (Elsevier).
- Serra, O., 1986. *Fundamentals of Well-Log Interpretation* (Vol. 2): *The Interpretation of Logging Data*. Dev. Pet. Sci., 15B: Amsterdam (Elsevier).
- Serra, O., 1989. *Formation MicroScanner Image Interpretation*: Houston (Schlumberger Educ. Services), SMP-7028.
- Shipboard Scientific Party, 1989. Introduction and explanatory notes. In Robinson, P.T., Von Herzen, R., et al., *Proc. ODP, Init. Repts.*, 118: College Station, TX (Ocean Drilling Program), 3–24. doi:10.2973/odp.proc.ir.118.101.1989
- Shipboard Scientific Party, 1991. Explanatory notes. In Taira, A., Hill, I., Firth, J.V., et al., *Proc. ODP, Init. Repts.*, 131: College Station, TX (Ocean Drilling Program), 25–60.
- Shipboard Scientific Party, 1992a. Explanatory notes. In Behrmann, J.H., Lewis, S.D., Musgrave, R.J., et al., *Proc. ODP, Init. Repts.*, 141: College Station, TX (Ocean Drilling Program), 37–71.
- Shipboard Scientific Party, 1992b. Explanatory notes. In Dick, H.J.B., Erzinger, J., Stokking, L.B., et al., *Proc. ODP, Init. Repts.*, 140: College Station, TX (Ocean Drilling Program), 5–33.
- Shipboard Scientific Party, 1992c. Explanatory notes. In Parson, L., Hawkins, J., Allan, J., et al., *Proc. ODP, Init. Repts.*, 135: College Station, TX (Ocean Drilling Program), 49–79.
- Shipboard Scientific Party, 1993a. Explanatory notes. In Alt, J.C., Kinoshita, H., Stokking, L.B., et al., *Proc. ODP, Init. Repts.*, 148: College Station, TX (Ocean Drilling Program), 5–24.
- Shipboard Scientific Party, 1993b. Explanatory notes. In Gillis, K., Mével, C., Allan, J., et al., *Proc. ODP, Init. Repts.*, 147: College Station, TX (Ocean Drilling Program), 15–42.
- Shipboard Scientific Party, 1993c. Site 896. In Alt, J.C., Kinoshita, H., Stokking, L.B., et al., *Proc. ODP, Init. Repts.*, 148: College Station, TX (Ocean Drilling Program), 123–192.
- Shipboard Scientific Party, 1995. Explanatory notes. In Cannat, M., Karson, J.A., Miller, D.J., et al., *Proc. ODP, Init. Repts.*, 153: College Station, TX (Ocean Drilling Program), 15–42.
- Shipboard Scientific Party, 1999. Explanatory notes. In Dick, H.J.B., Natland, J.H., Miller, D.J., et al., *Proc. ODP, Init. Repts.*, 176: College Station, TX (Ocean Drilling Program), 1–42. doi:10.2973/odp.proc.ir.176.102.1999
- Shipboard Scientific Party, 2000. Explanatory notes. In Sacks, I.S., Suyehiro, K., Acton, G.D., et al., *Proc. ODP, Init. Repts.*, 186: College Station, TX (Ocean Drilling Program), 1–51. doi:10.2973/odp.proc.ir.186.102.2000
- Shipboard Scientific Party, 2003a. Explanatory Notes. In Stephen, R.A., Kashara, J., Acton, G.D., et al., *Proc. ODP, Init. Repts.*, 200: College Station, TX (Ocean Drilling Program), 1–66. doi:10.2973/odp.proc.ir.200.102.2003
- Shipboard Scientific Party, 2003b. Explanatory notes. In Wilson, D.S., Teagle, D.A.H., Acton, G.D., *Proc. ODP, Init. Repts.*, 206: College Station, TX (Ocean Drilling Program), 1–94. doi:10.2973/odp.proc.ir.206.102.2003
- Shipboard Scientific Party, 2004. Explanatory notes. In Kelemen, P.B., Kikawa, E., Miller, D.J., et al., *Proc. ODP, Init. Repts.*, 209: College Station, TX (Ocean Drilling Program), 1–75. doi:10.2973/odp.proc.ir.209.102.2004
- Sparks, J.W., and Zuleger, E., 1995. Data report: chemical analyses of the Leg 140 reference sample. In Erzinger, J., Becker, K., Dick, H.J.B., Stokking, L.B. (Eds.), *Proc. ODP, Sci. Results*, 137/140: College Station, TX (Ocean Drilling Program), 353–355.
- Streckeisen, A., 1974. Classification and nomenclature of plutonic rocks recommendations of the IUGS subcommission on the systematics of igneous rocks. *Geol. Rundsch.*, 63:773–786. doi:10.1007/BF01820841
- Tarduno, J.A., Duncan, R.A., Scholl, D.W., et al., 2002. *Proc. ODP, Init. Repts.*, 197: College Station, TX (Ocean Drilling Program). doi:10.2973/odp.proc.ir.197.2002
- Twiss, R.J., and Moores, E.M., 1992. *Structural Geology*: New York (Freeman).
- Vacquier, V., 1985. The measurement of thermal conductivity of solids with a transient linear heat source on the plane surface of a poorly conducting body. *Earth Planet. Sci. Lett.*, 74:275–279. doi:10.1016/0012-821X(85)90027-5

- Wessel, P., and Smith, W.H.F., 1995. New version of the Generic Mapping Tools released. *Eos, Trans. Am. Geophys. Union*, 76:329.
- Whitmarsh, R.B., Beslier, M.-O., Wallace, P.J., et al., 1998. *Proc. ODP, Init. Repts.*, 173: College Station, TX (Ocean Drilling Program).
- Wilson, D.S., Teagle, D.A.H., Acton, G.D., 2003. *Proc. ODP, Init. Repts.*, 206: College Station, TX (Ocean Drilling Program). doi:10.2973/odp.proc.ir.206.2003
- Wilson, W.D., 1960. Speed of sound in seawater as a function of temperature, pressure and salinity. *J. Acoust. Soc. Am.*, 32(6):641–644. doi:10.1121/1.1908167
- Wyllie, M.R.J., Gregory, A.R., and Gardner, L.W., 1956. Elastic wave velocities in heterogeneous and porous media. *Geophysics*, 21(1):41–70. doi:10.1190/1.1438217

Publication: 28 December 2006
MS 309312-102

Figure F1. Integrated Ocean Drilling Program (IODP) labeling scheme used for holes, cores, and sections. mbsl = meters below sea level, mbsf = meters below seafloor.

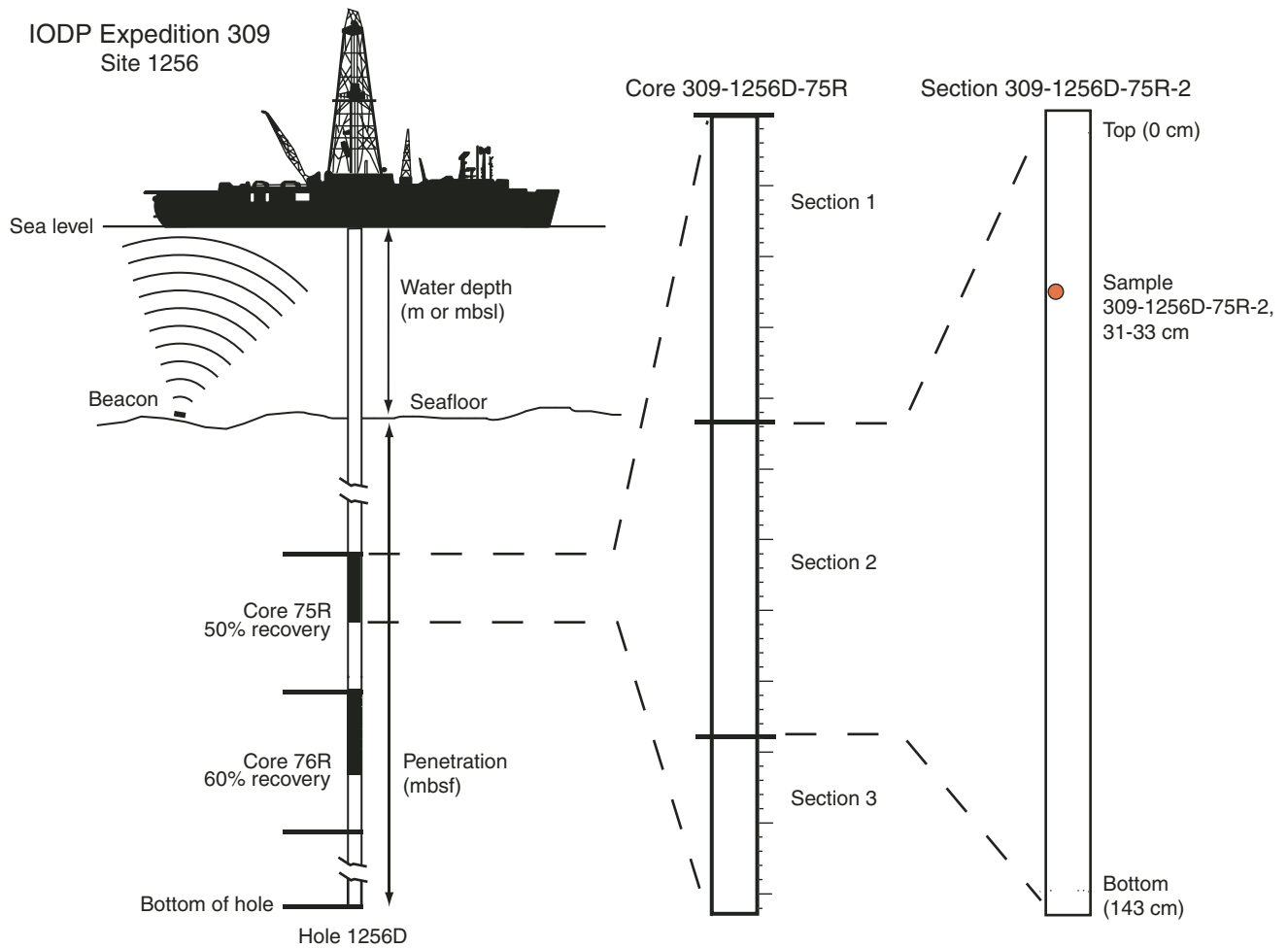


Figure F2. Example of a visual core description log sheet.

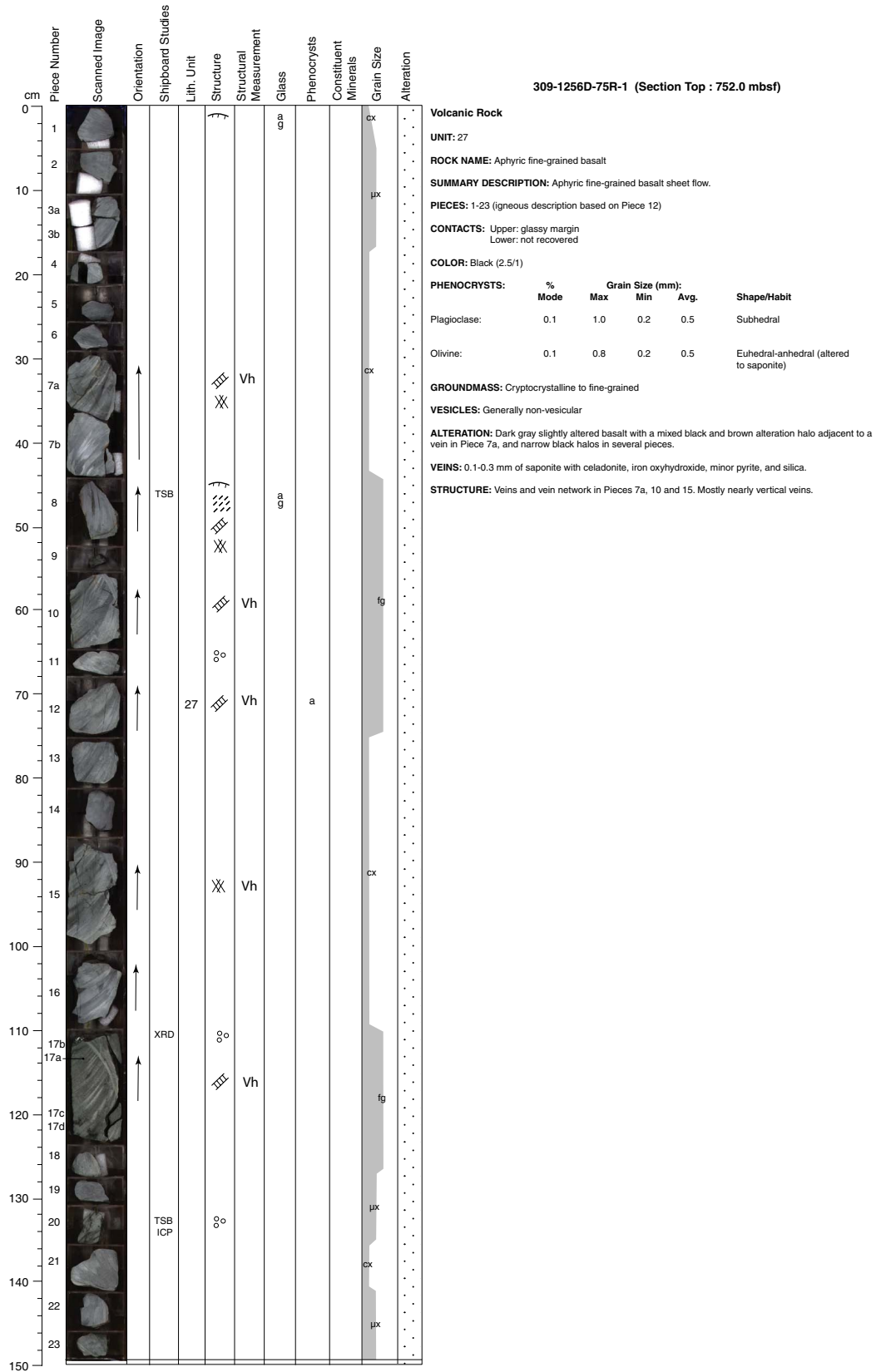


Figure F3. Examples of VCDs. A. Volcanic rock. (Continued on next page.)

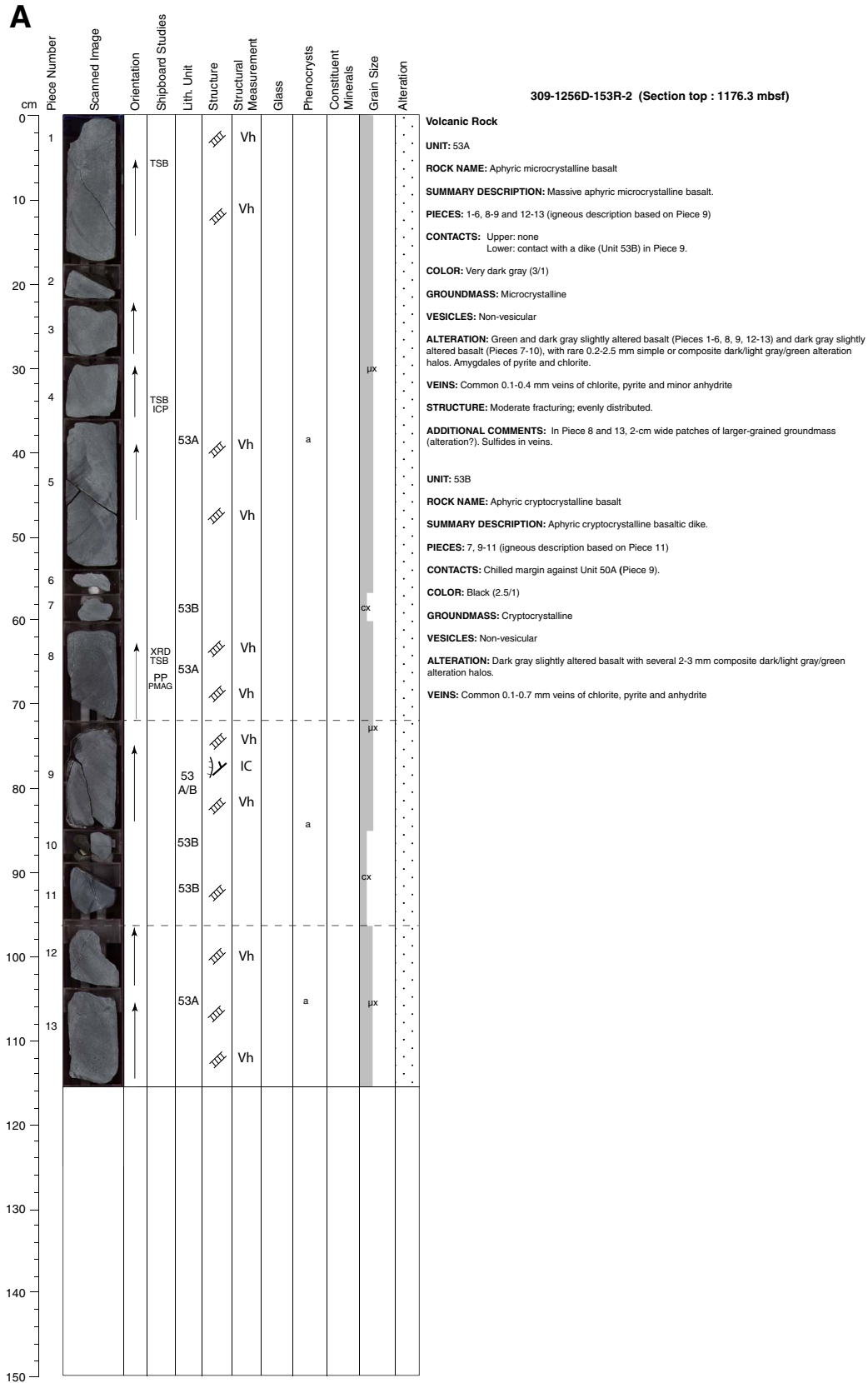


Figure F3 (continued). B. Plutonic rock.

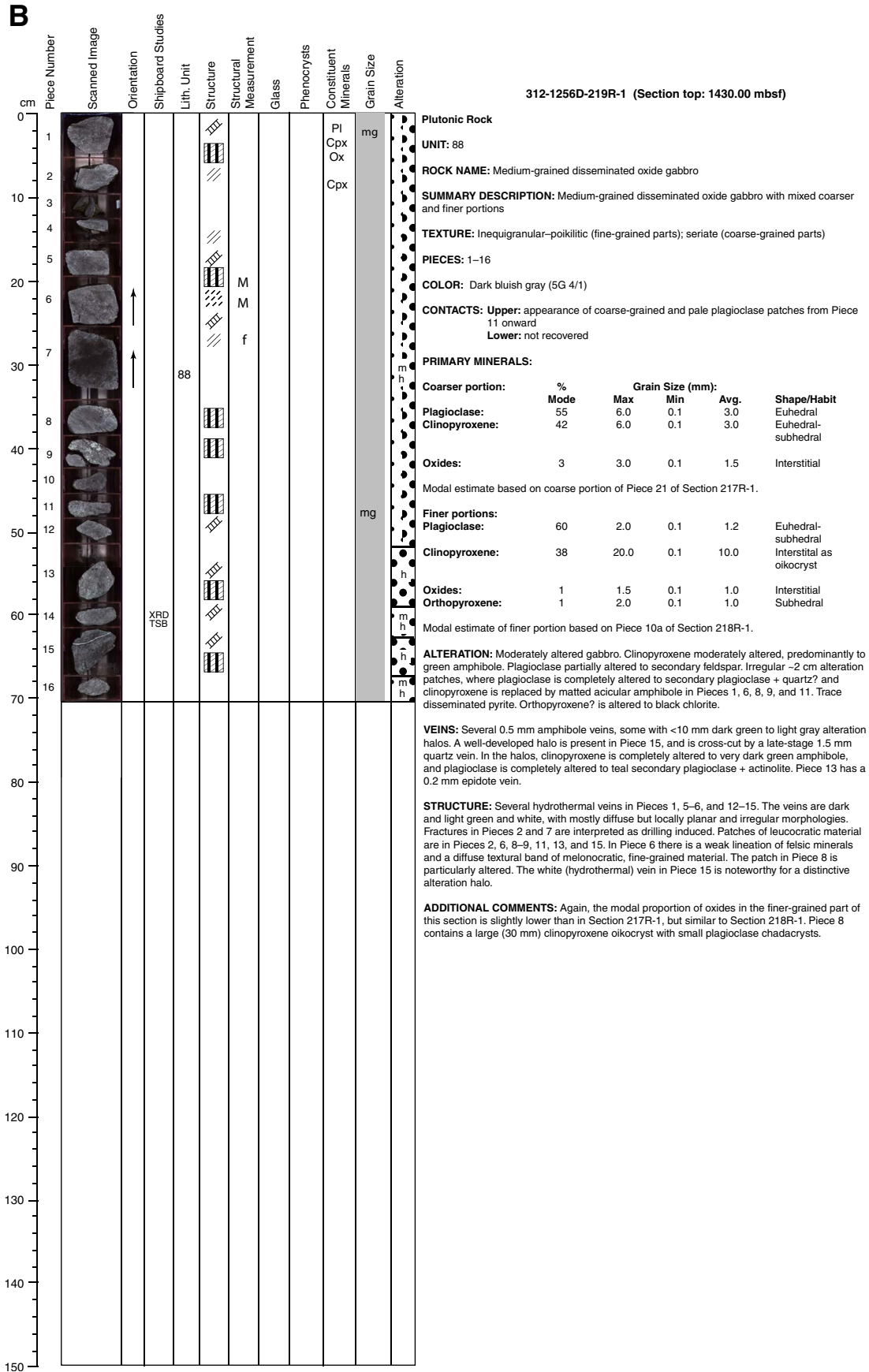


Figure F4. Key for VCDs. ICP-AES = inductively coupled plasma-atomic emission spectroscopy.

Shipboard studies	ICP	Ph	PMAG	PP	TSB	XRD				
	ICP-AES analysis	Close-up photo	Paleomagnetic analysis	Physical property analysis	Petrographic thin section	X-ray diffraction analysis				
Structure	Chilled margin (ticks on quenched side)		Metamorphic foliation	Conjugate veins		Cataclastic zone				
	Igneous contact		Breccia	Joint		Primary ductile deformation (e.g., folded flow tops or bottoms)				
	Dike contact		Magmatic vein	Conjugate joints		Magmatic and textural banding and patches				
	Vesicles		Vein	Microfault		Fractures				
	Pipe vesicles		Shear vein	Slickenline/Slickenfiber						
	Magmatic foliation		Vein network	Apparent sense of shear						
Structural measurement	IC	L	M	Mf	Sv	Vh	Vm	f	J	F
	Igneous contact	Lineation	Magmatic fabric	Magmatic foliation	Shear vein	Hydrothermal vein	Magmatic vein	Fractures	Joint	Fault
Glass		a								
	g	g								
	Fresh glass	Altered glass								
Phenocryst	a	s	m	h						
	Aphyric (<1%)	Sparsely phyric (1%-5%)	Moderately phyric (5%-10%)	Highly phyric (>10%)						
Constituent minerals	Ol = Olivine; Pl = Plagioclase; Cpx = Clinopyroxene; Opx = Orthopyroxene; Amp = Amphibole; Ox = Oxide; Sp = Spinel									
Grain size		G	CX	μX	fg	mg	cg	vc		
		Glassy	Cryptocrystalline (<0.1 mm)	Microcrystalline (0.1-0.2 mm)	Fine grained (0.2-1 mm)	Medium grained (1-2 mm)	Coarse grained (2-5 mm)	Very coarse grained (>5 mm)		
	Gray rectangles or triangles schematically indicate uniform grain size or gradual increase/decrease in grain size, respectively.									
Alteration										
	Fresh (<2%)	Slight (2%-10%)	Moderate (10%-50%)	High (50%-95%)	Complete (95%-100%)					

Figure F5. Classification of coarse-grained rocks (modified after Cordier et al., 2005).

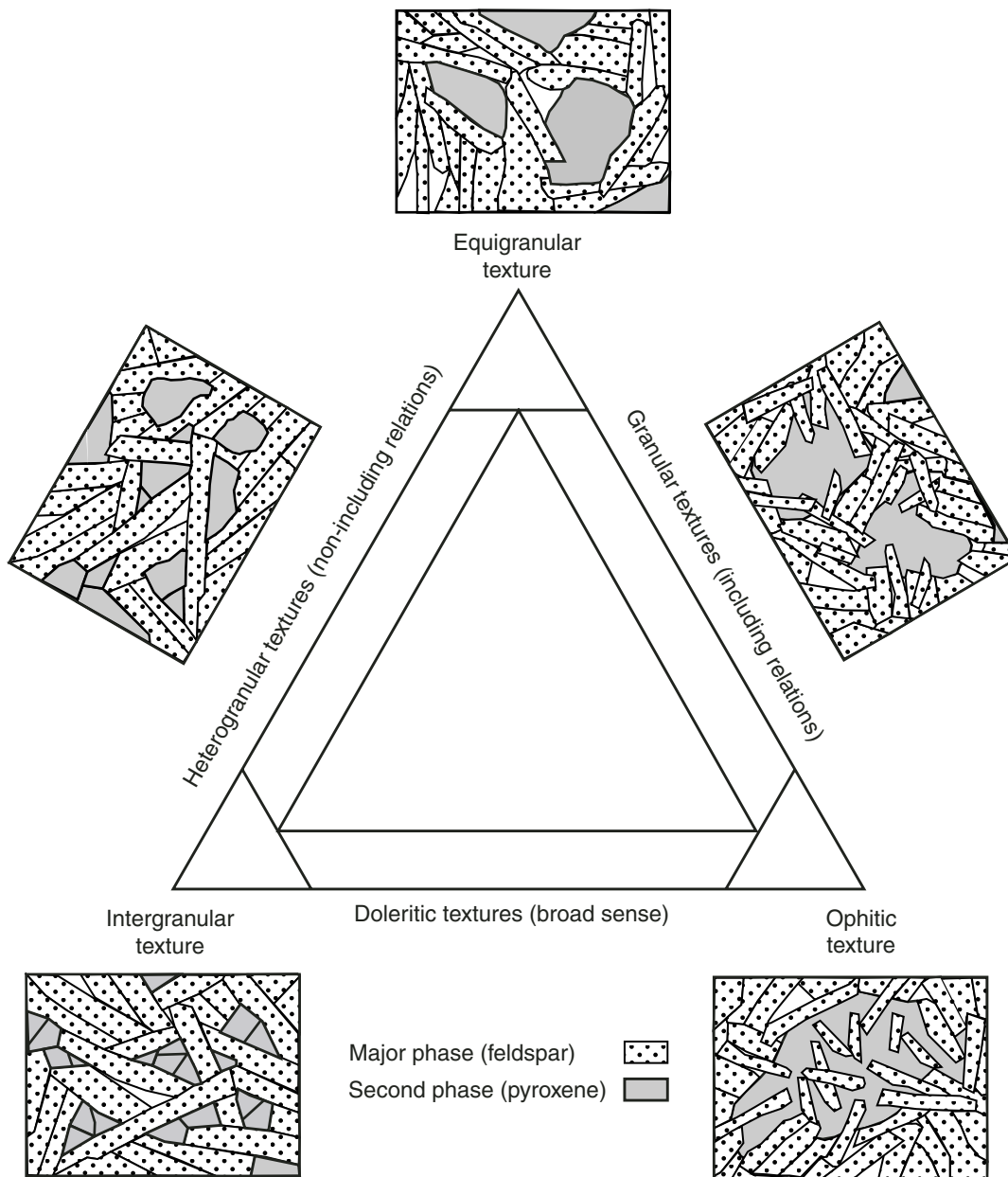


Figure F6. Modal classification scheme for plutonic igneous rocks (after Streckeisen, 1974).

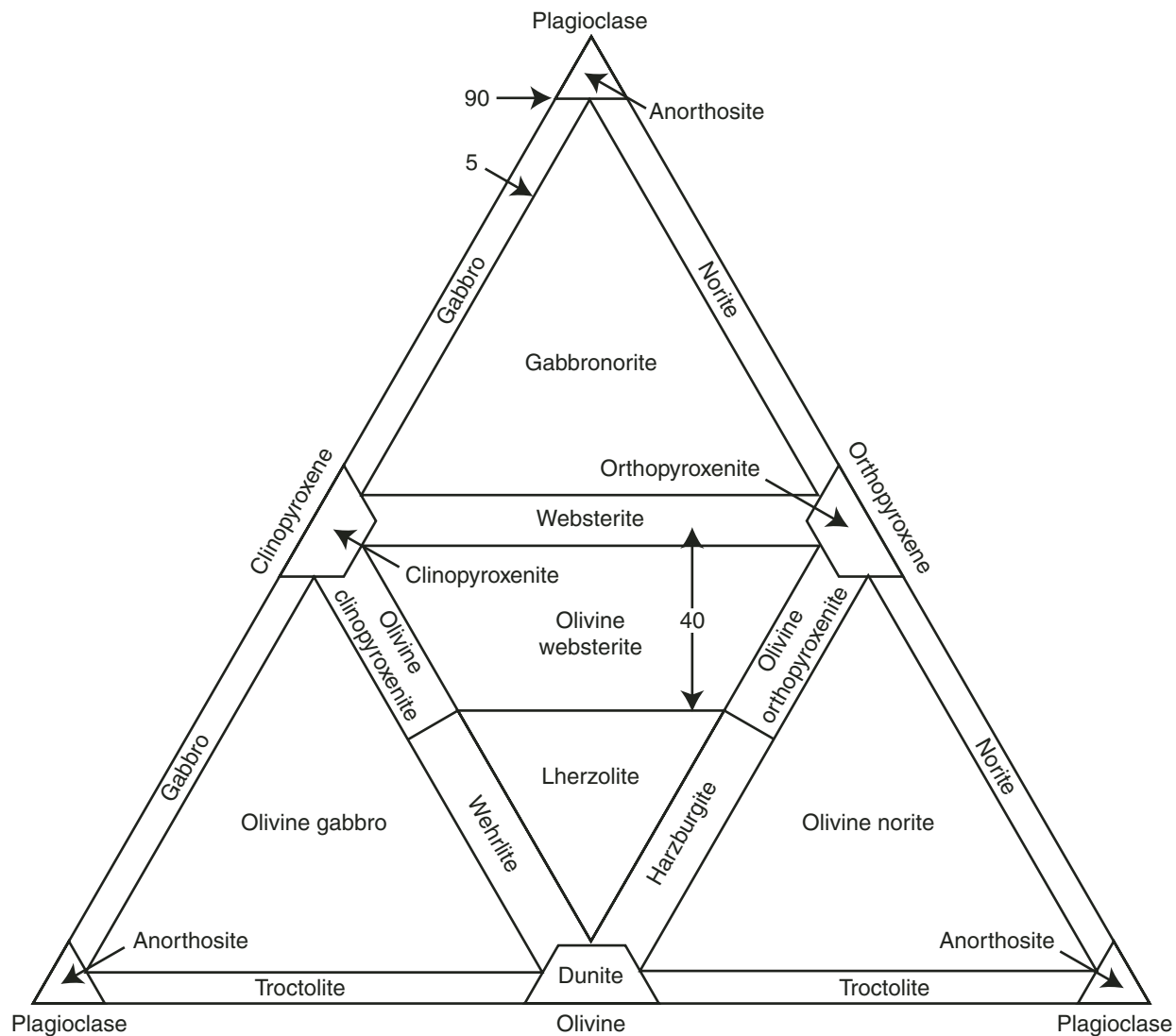




Figure F7. Example thin section form.

THIN SECTION DESCRIPTIONS

THIN SECTION:		Piece No.:		Unit:		OBSERVER:	
ROCK NAME:							
WHERE SAMPLED:							
GRAIN SIZE:							
TEXTURE:							
PRIMARY MINERALOGY	PERCENT PRESENT	PERCENT ORIGINAL	SIZE (mm)			MORPHOLOGY	COMMENTS
			min.	max.	av.		
PHENOCRYSTS							
GROUNDMASS							
SECONDARY MINERALOGY	PERCENT		SIZE (mm)			REPLACING / FILLING	COMMENTS
			min.	max.	av.		
STRUCTURE :							
COMMENTS :							

Figure F8. Procedure of modal count using Photoshop. A. Scanned image. B. Cropping of image. C. Irregular thin section. D. After threshold, counting pixels.

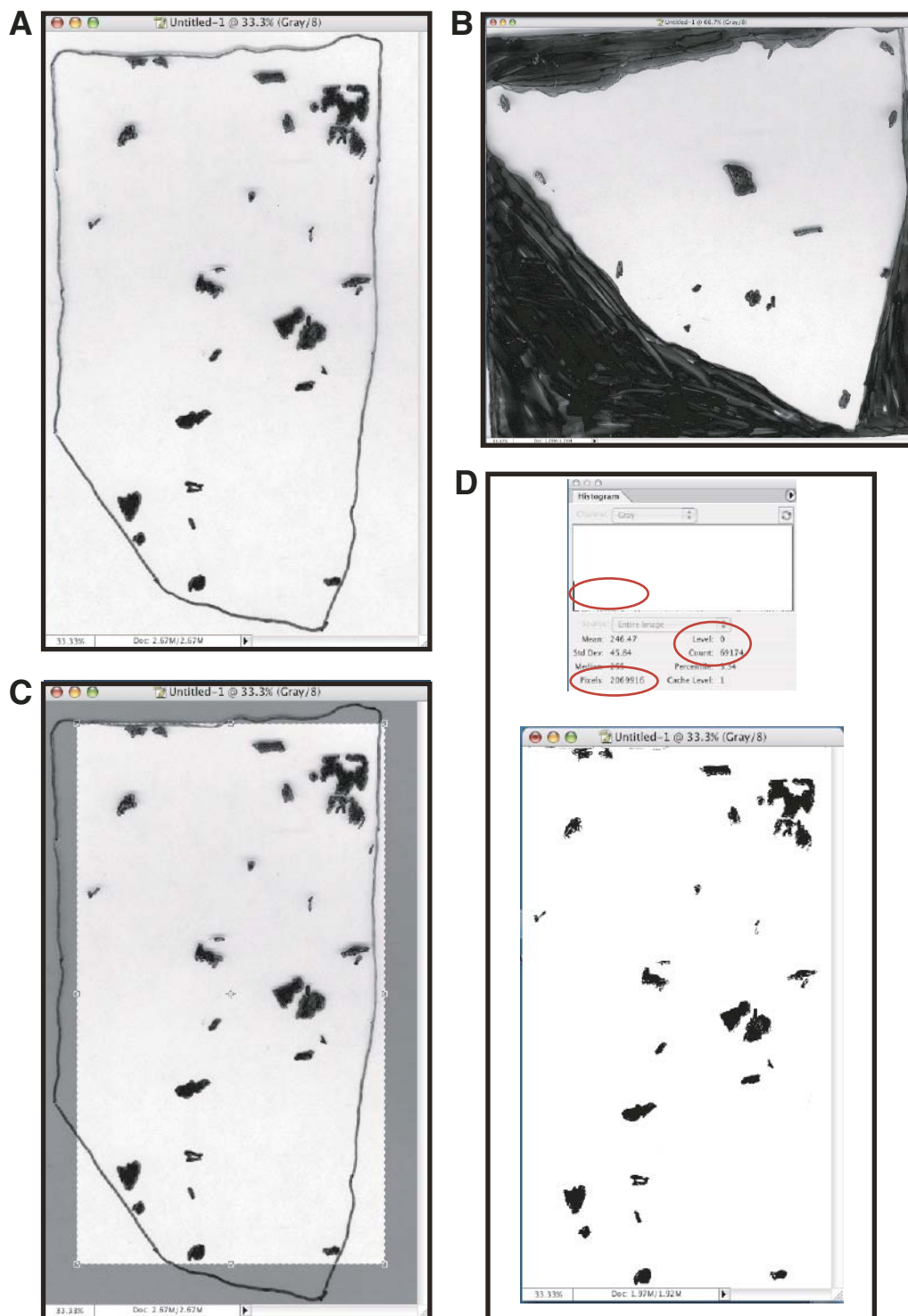


Figure F9. Oxide modal count using Photoshop. A. Whole thin section scan. B. Image after threshold.

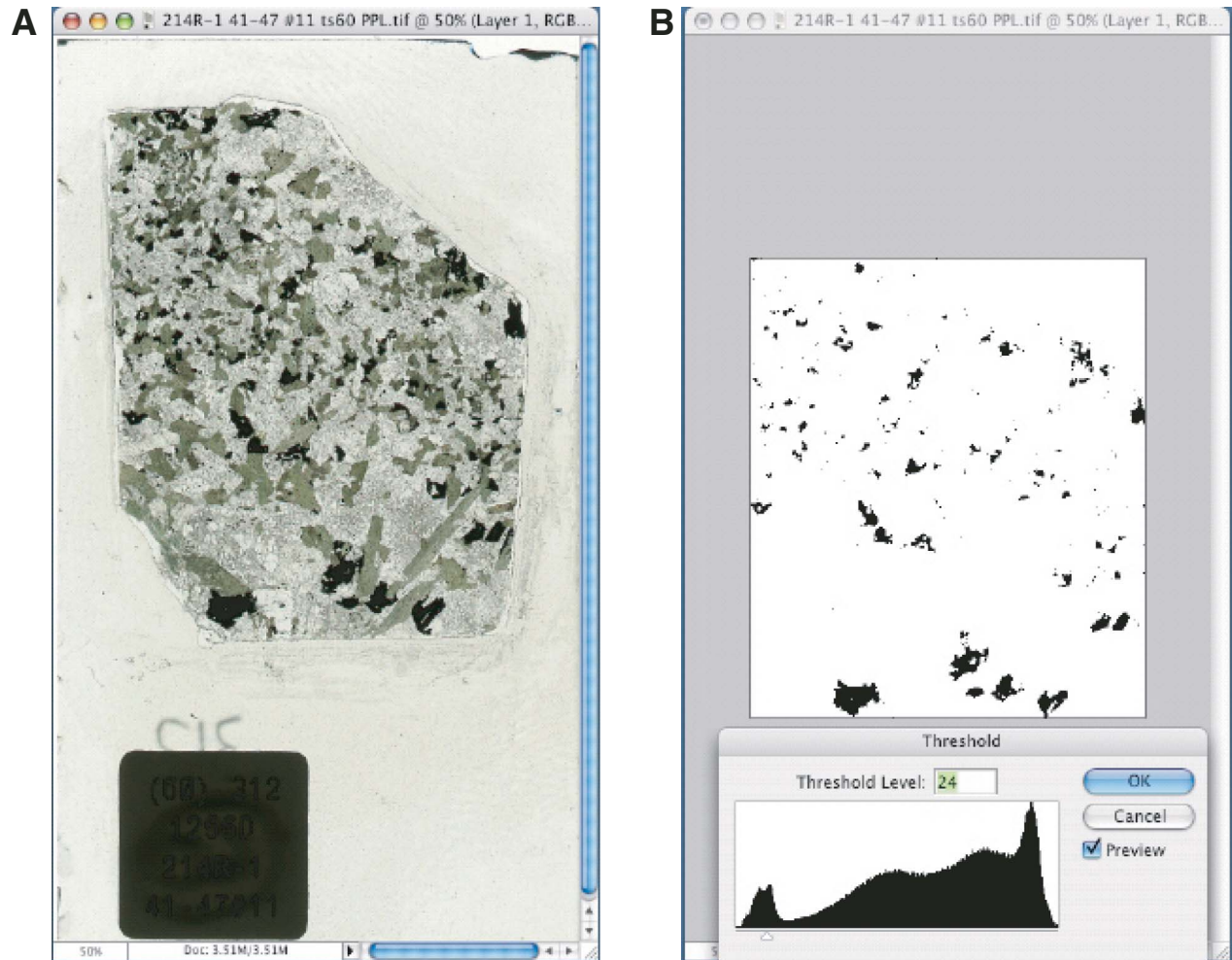


Figure F10. Structures commonly found during Expedition 309/312 (redrawn from Leg 206).

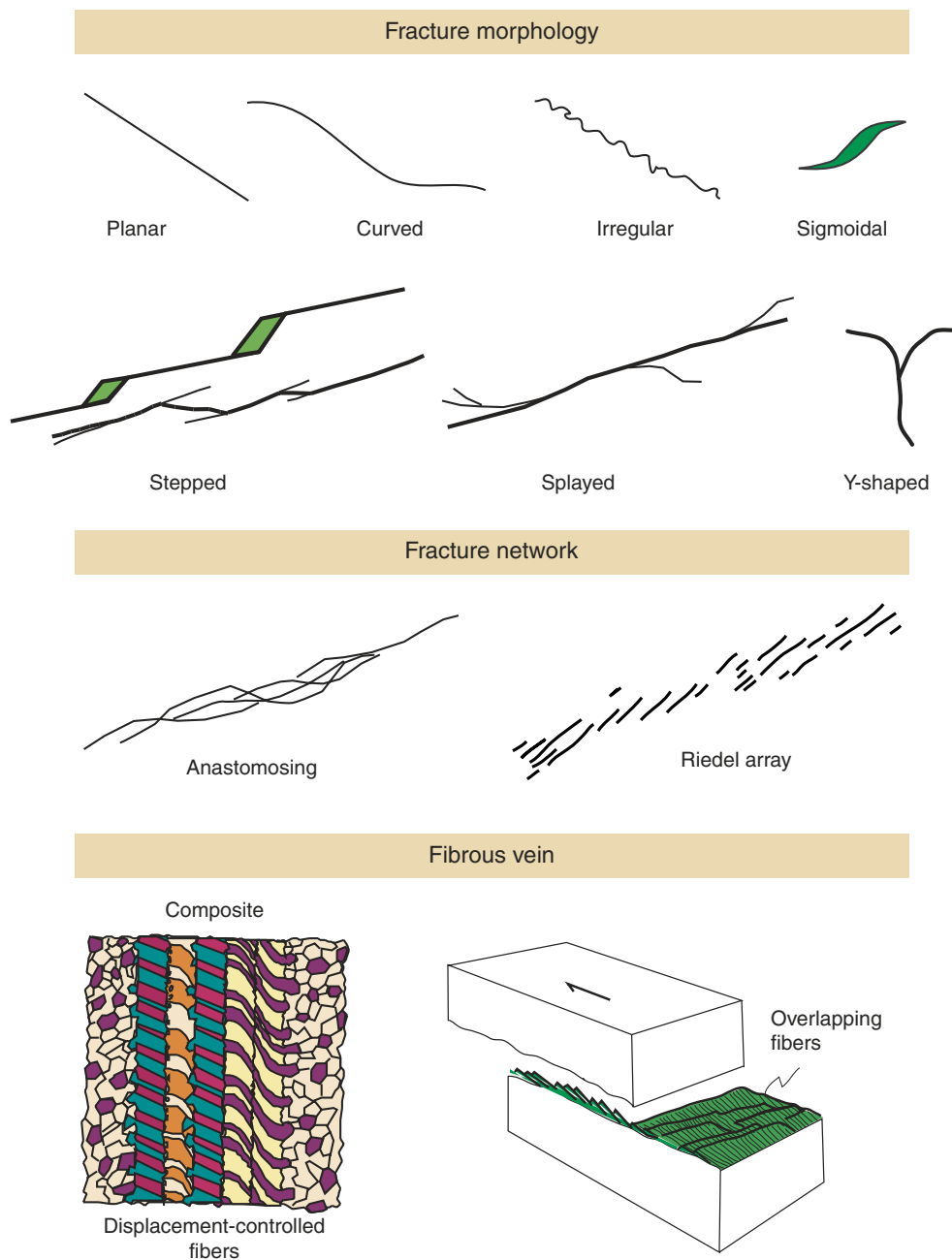


Figure F11. Conventions used for measuring orientation of structural features shown on the archive half of the core. Examples of orientation measurements with protractor-based device are shown.

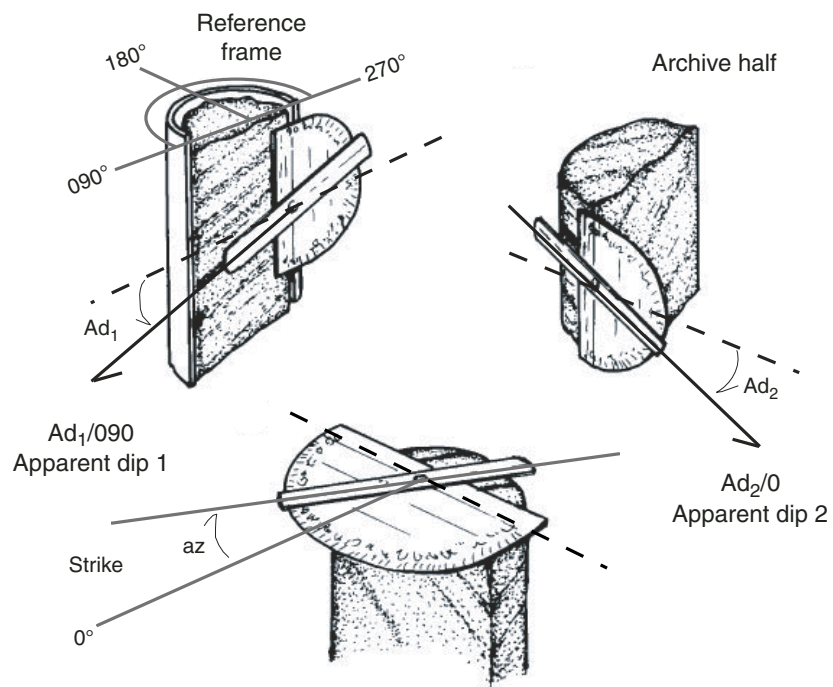


Figure F12. Magnetic moments for x-, y-, and z-axis measured on an empty sample boat at the beginning of Expedition 309 (A) prior to cleaning the sample boat and (B) after the sample boat was cleaned with window cleaner and alternating-field demagnetized at 80 mT.

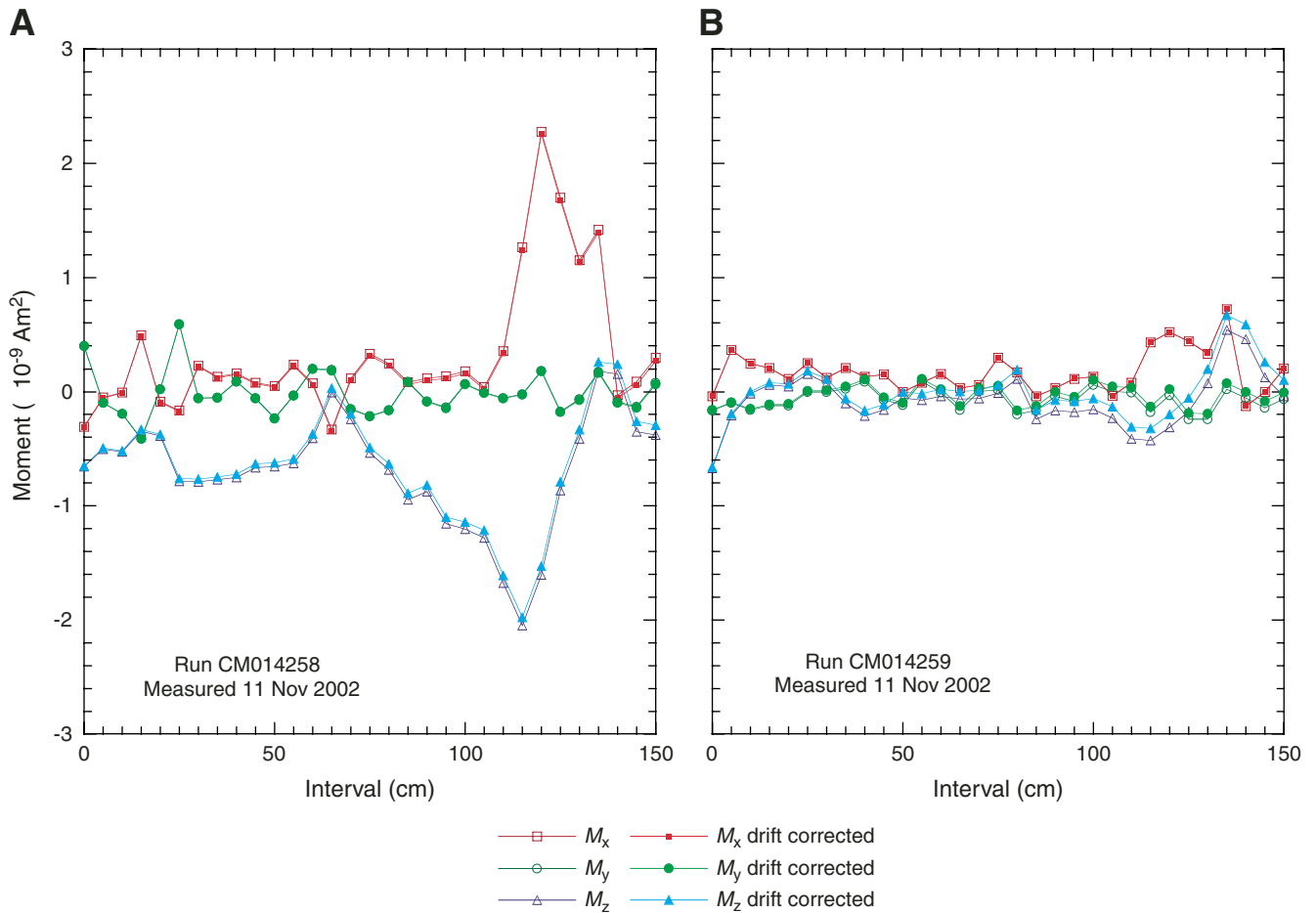


Figure F13. Magnetic moments for x-, y-, and z-axis measured for a clean empty sample boat before and after drift and tray correction.

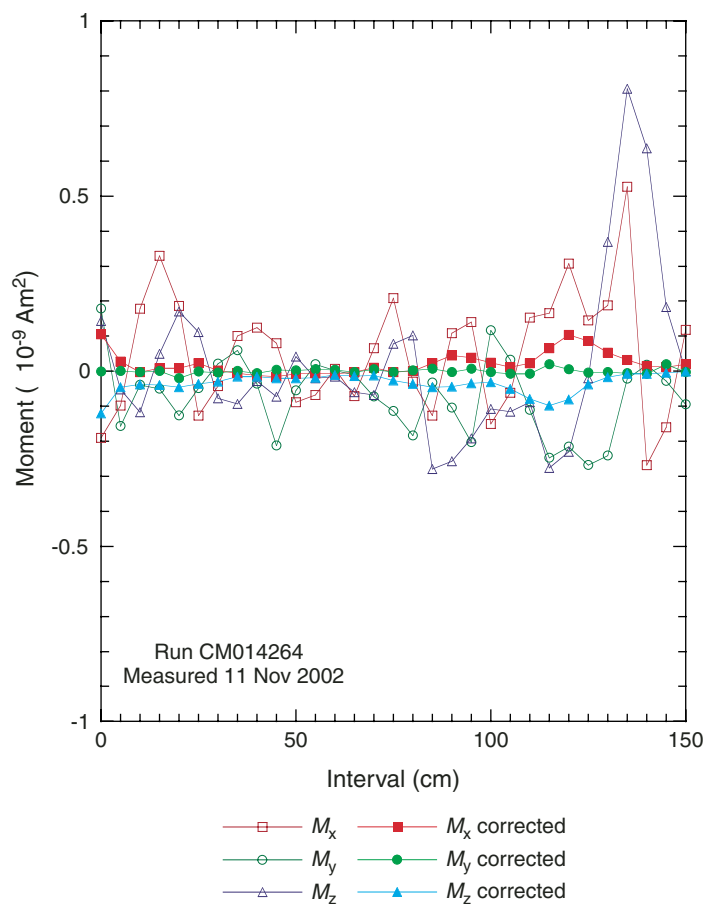


Figure F14. Magnetic moments for x-, y-, and z-axis measured for an empty discrete sample tray on the sample boat. Moment was measured after the tray was cleaned with window cleaner and alternating-field demagnetized at 80 mT. Drift correction has been applied, as well as tray correction that removes magnetization related to the sample boat but not the discrete sample tray.

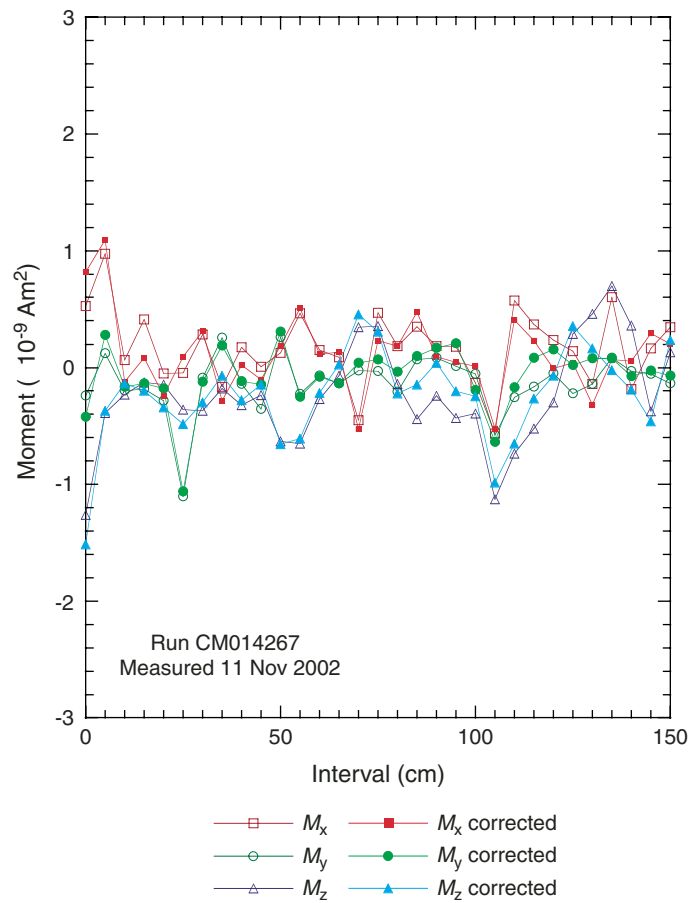


Figure F15. IODP paleomagnetic coordinate system for archive and working halves with radial and vertical overprints shown.

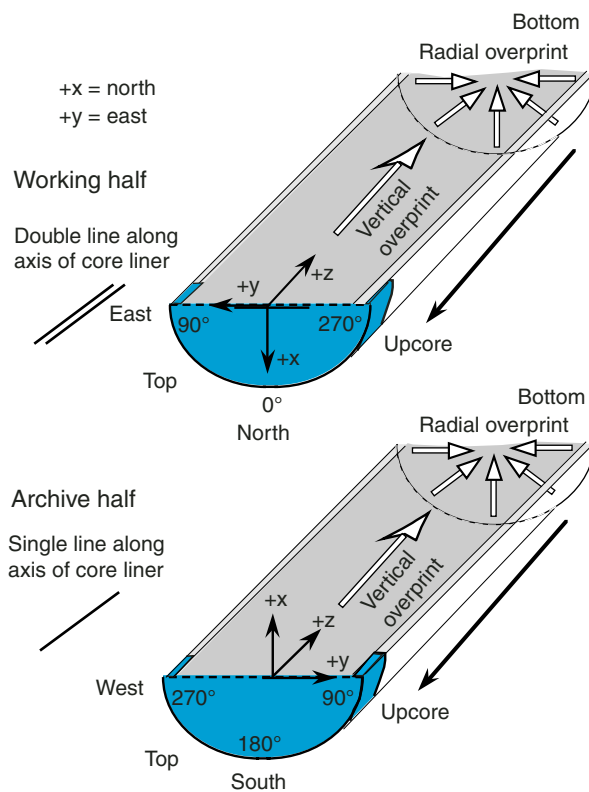


Figure F16. Example of MST logs of a core (Core 312-1256D-187R) for which magnetic susceptibility values reported by the Bartington MS2C loop (red line) were truncated and a core (Core 312-1256D-189R) for which magnetic susceptibility values appear valid. Gamma ray attenuation density values are high in both cores. Broken vertical black line shows the position and length of each rock piece logged; pieces at least 20 cm long are present in both cores. Green line indicates the correct magnetic susceptibility values after addition of 10,000 SI.

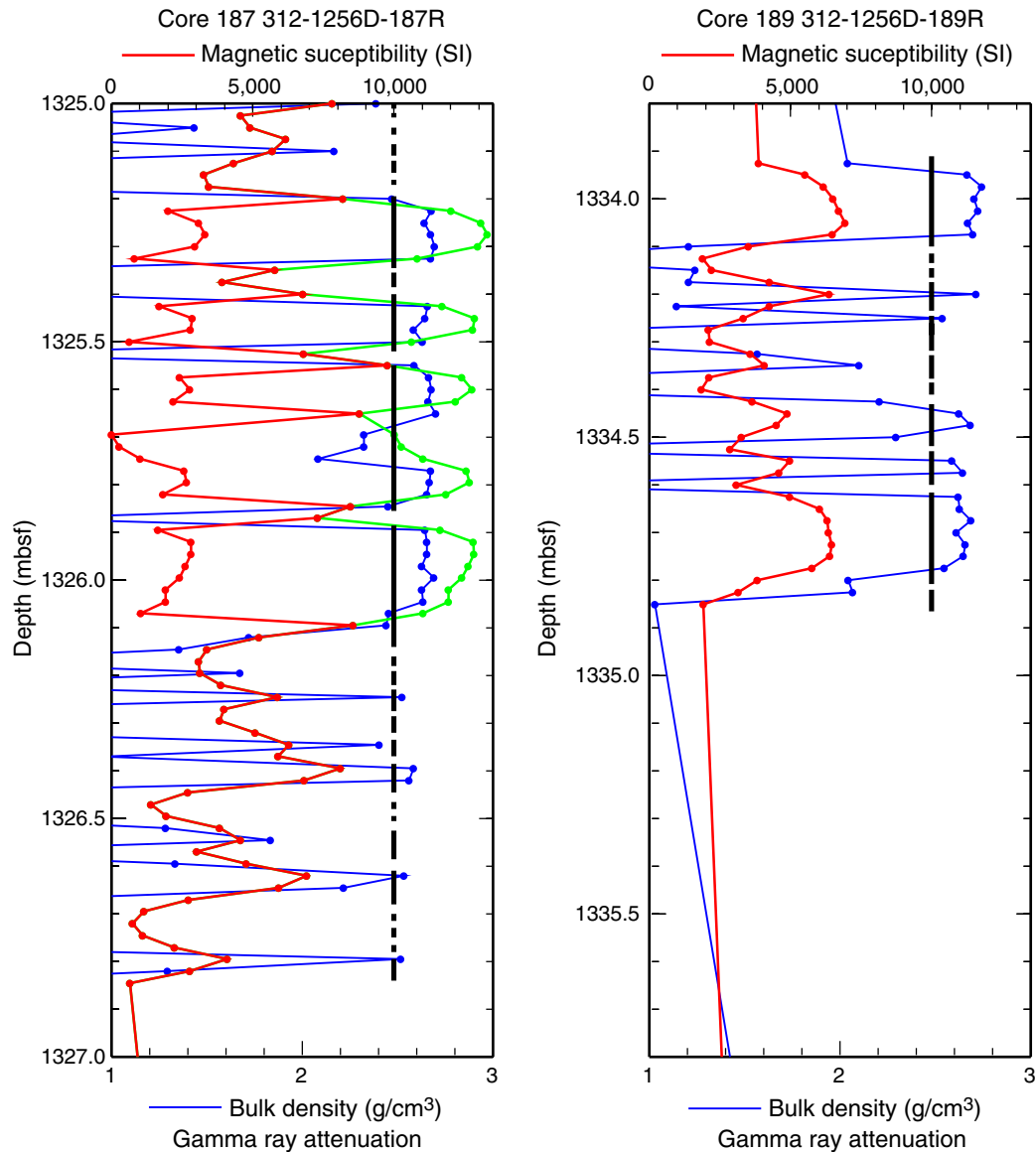


Figure F17. Directions for manual rotation of samples for V_p measurements in x, y, and z directions. Arrow is marked pointing up on the split face of the core. During V_p (x) measurement, arrow points directly at the PWS3 operator. Note that x and y directions are horizontal, but not oriented geographically.

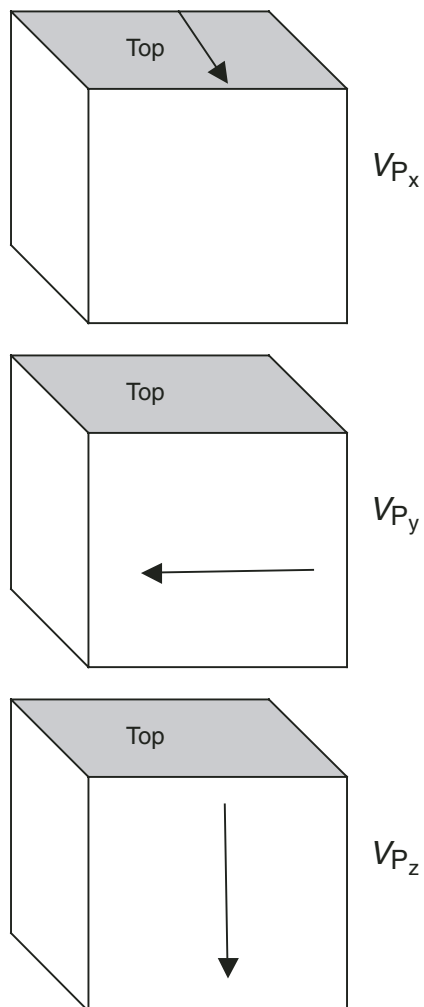


Figure F18. DMT Digital Color CoreScan system similar to that used during Expedition 309/312.

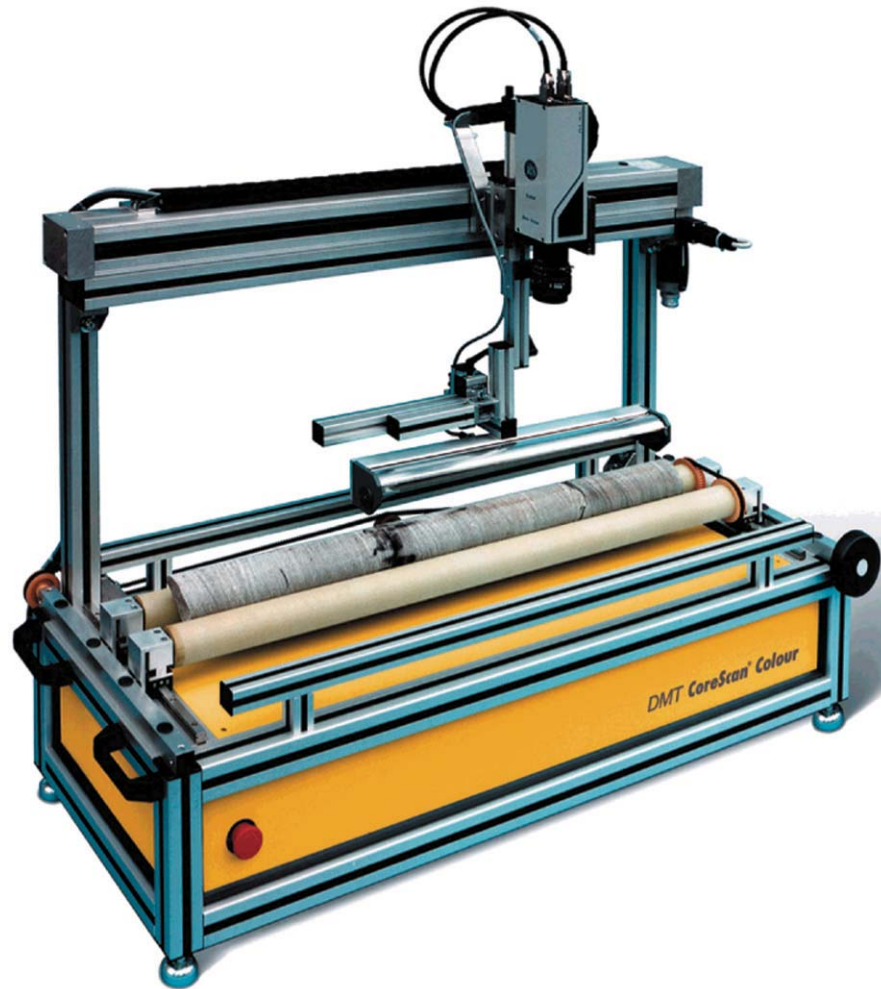


Figure F19. Configuration of the wireline logging tool strings used during Expedition 309/312.

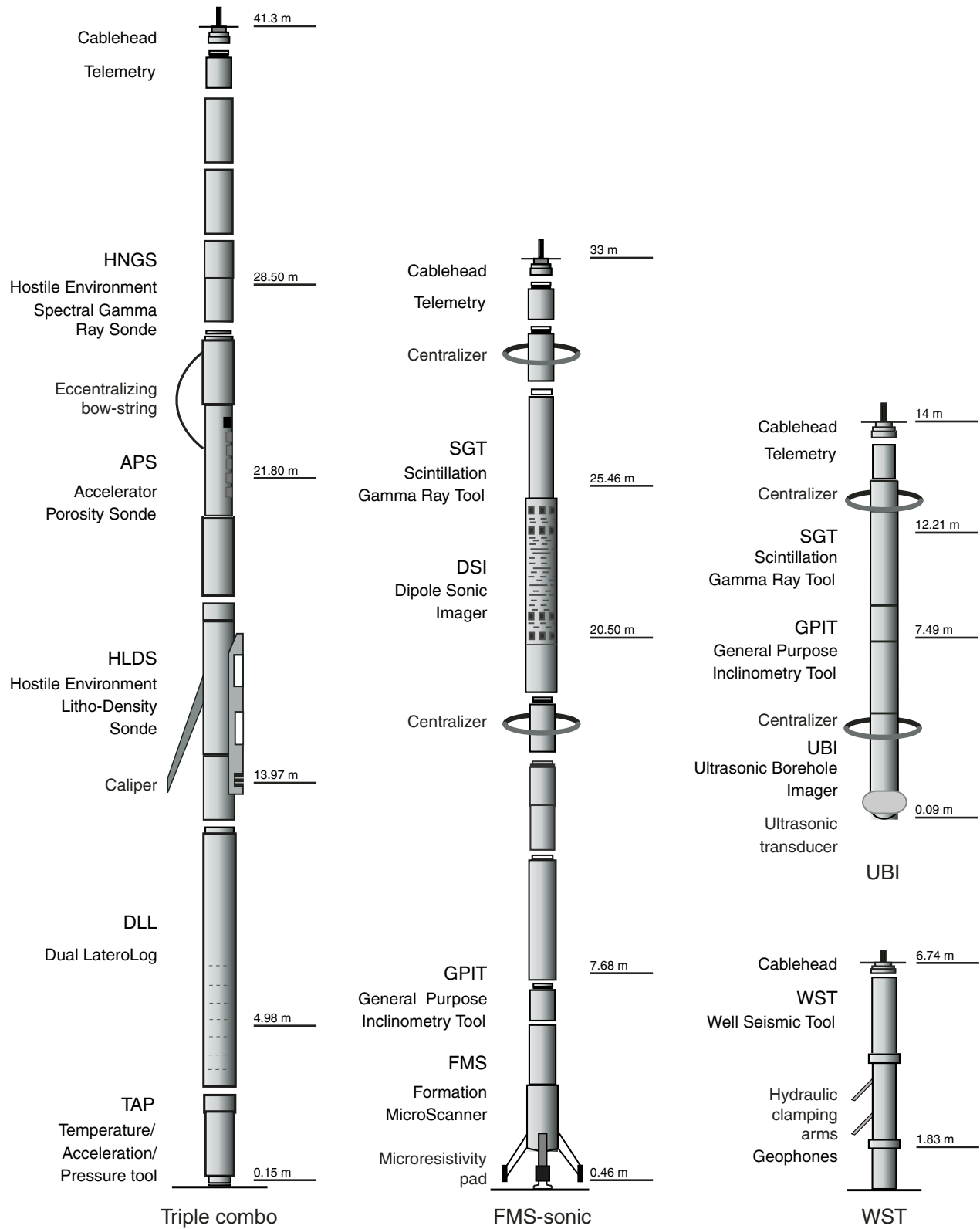


Figure F20. Versatile Seismic Imager used for the vertical seismic profile during Expedition 312.

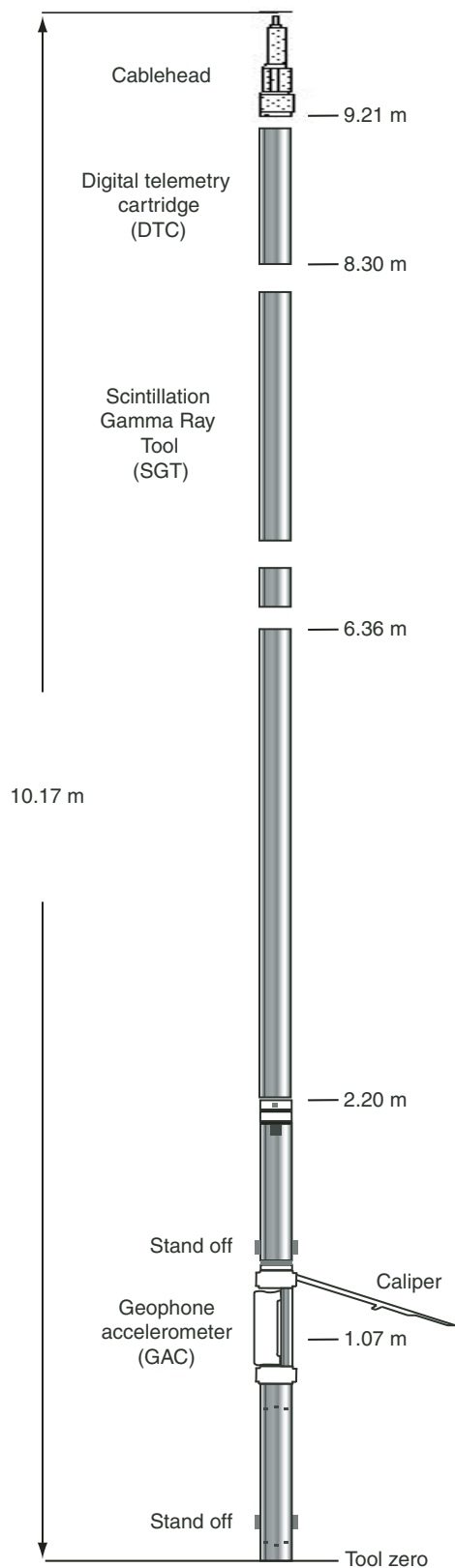


Figure F21. Formation MicroScanner pad.

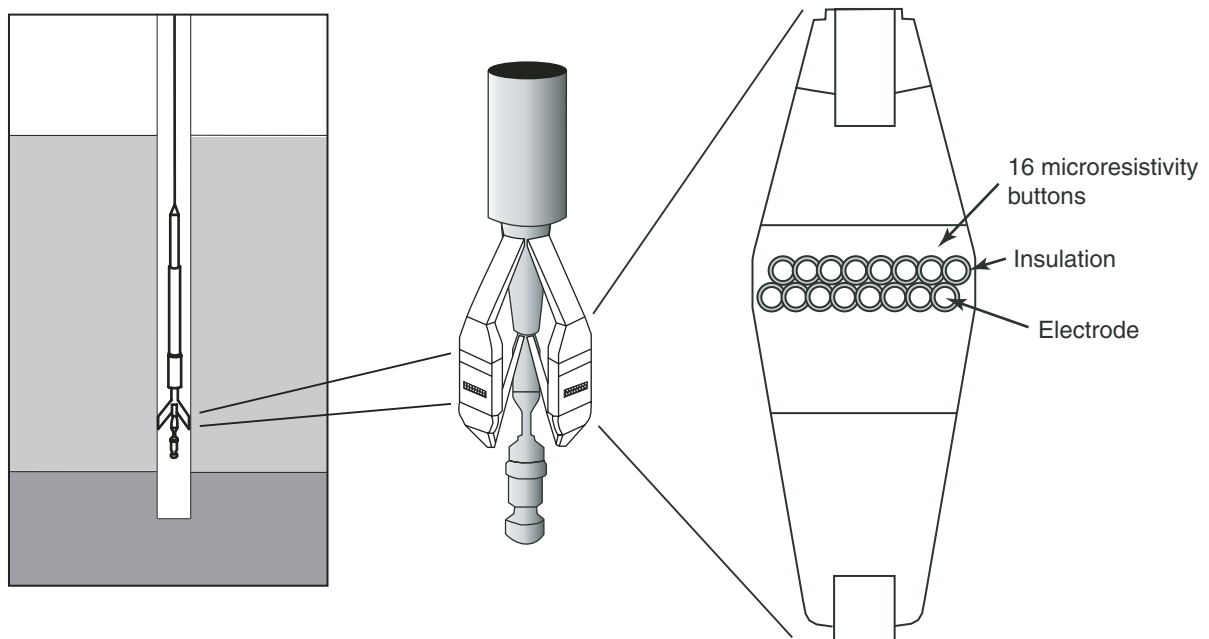


Figure F22. Ultrasonic Borehole Imager.

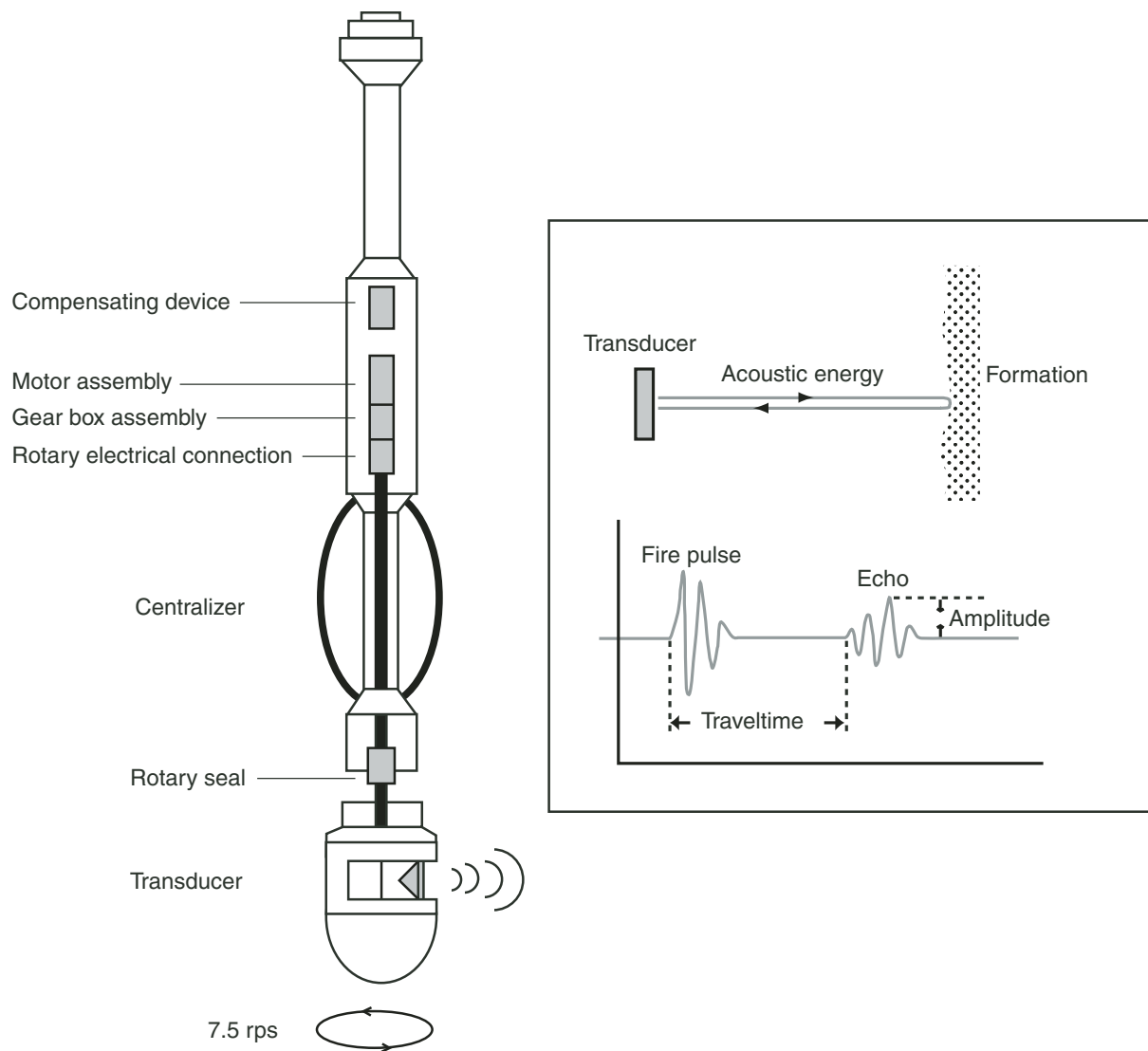
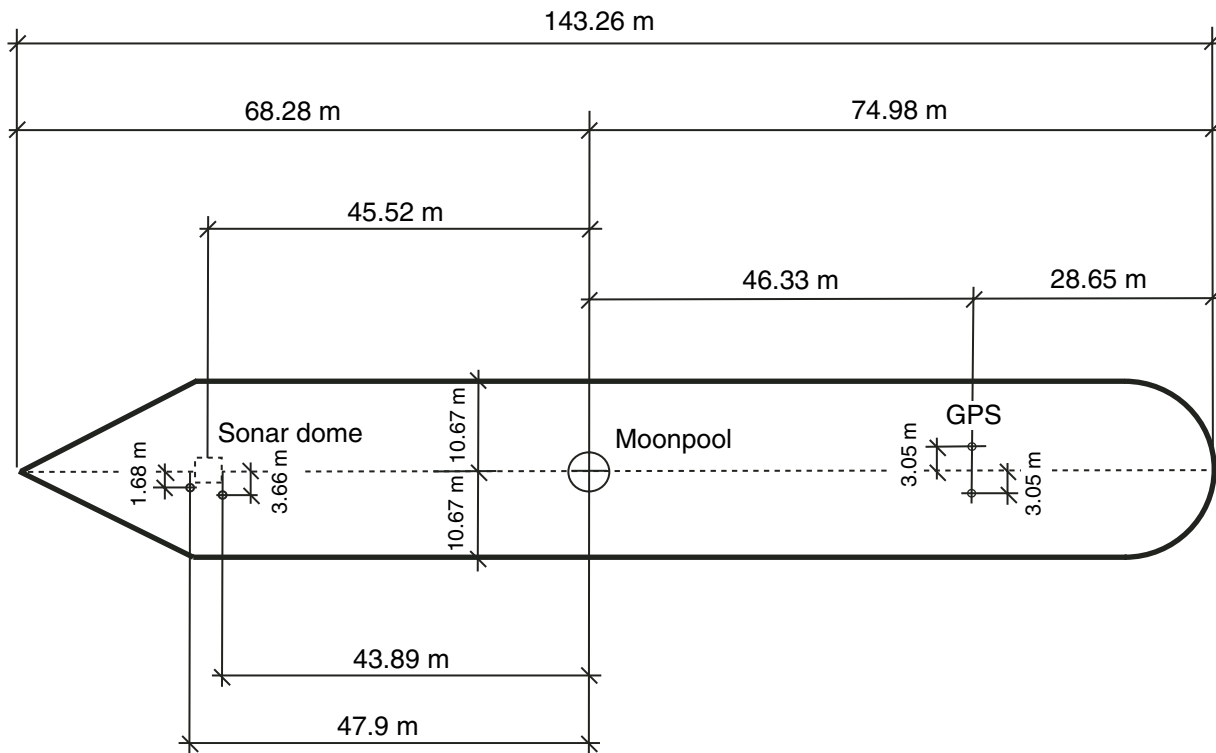


Figure F23. Positions of navigation antennas relative to moonpool datum. GPS = Global Positioning System.



WinFrog ship configuration

Width of bow = 0.5 m
Width of stern = 21.34 m

Origin to bow = 68.28 m
Origin to stern = 74.98 m
Origin to bow curve = 45.52 m
Origin to starboard side = 10.67 m
Origin to port side = -10.67 m

Moonpool width = 5.0 m
Moonpool forward/aft = 0.0 m
Moonpool port/starboard = 0.0 m

GPS antenna offset from origin
Antenna forward/aft = -46.33 m
Antenna (OMNISTAR) port/starboard = 3.05 m
Antenna (Ashtech) port/starboard = -3.05 m

Dynamic positioning GPS antennas

Trimble GPS antenna offset from origin
Antenna forward/aft = 47.9 m
Antenna port/starboard = -1.68 m

Ashtech GPS antenna offset from origin
Antenna forward/aft = 43.89 m
Antenna port/starboard = -3.66 m

Figure F24. Relations between water depth, drilling depth, and sonar depth. DES = dual elevator stool, DP = dynamic positioning, PDR = precision depth recorder (sonar).

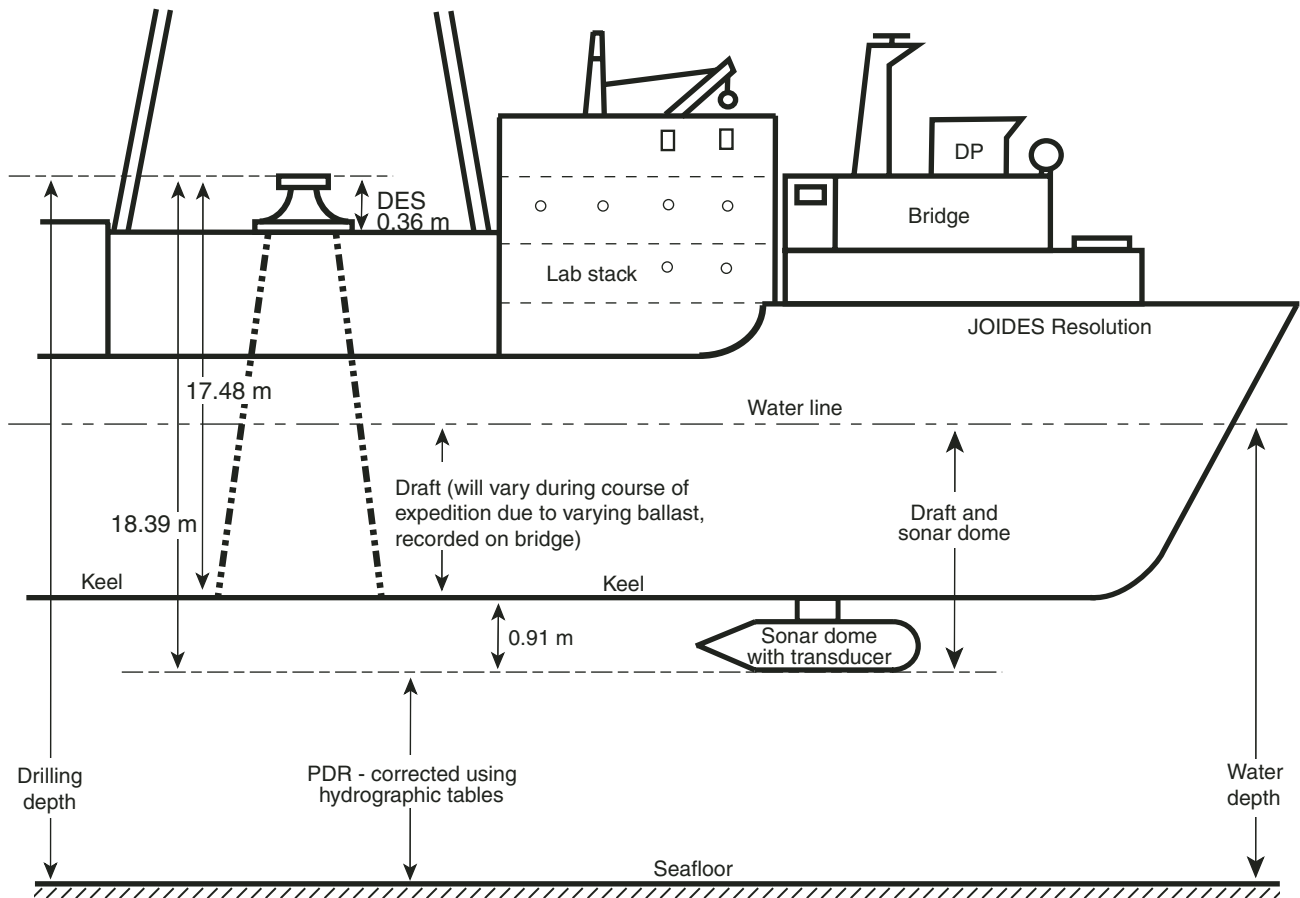


Table T1. Example piece log, Expedition 309/312.

Expedition	Hole	Core	Section	Piece	Top (cm)	Bottom (cm)	Length (cm)	Groundmass grain size	Notes
309	1256D	75R	1	1	1	4	3	cx	Start of Unit 27
309	1256D	75R	1	2	6	10	4	μ x	
309	1256D	75R	1	3	11	14	3	μ x	
309	1256D	75R	1	4	18	20	2	cx	
309	1256D	75R	1	5	23	24	1	cx	
309	1256D	75R	1	6	26	29	3	cx	
309	1256D	75R	1	7	30	44	14	cx	
309	1256D	75R	1	8	45	52	7	fg	Altered chilled margin
309	1256D	75R	1	9	53	54	1	fg	
309	1256D	75R	1	10	56	64	8	fg	

Note: cx = cryptocrystalline, μ x = microcrystalline, fg = fine grained. For the complete piece log, see PIECELOG.XLS in [“Supplementary material.”](#)

Table T2. Example alteration log, Expedition 309/312.

Interval (cm)							Total length (cm)	Depth to core top (mbsf)	Ig. unit	Background alteration (%)			Dark alteration patches (%)	Alteration halos (vein, patch, and amygdale related) (%)						
Exp.	Hole	Core	Section	Piece	Top	Base				Dark gray	Dark green	Green		Brown	Black	Mixed	Light gray	Light green	Dark gray	Pyrite rich
312	1256D	172R	1	1-7	0	26	26	1255.1	66	96									4	
312	1256D	173R	1	1-4	0	25	22	1260.6	66	88									2	
312	1256D	173R	1	5	25	28	2	—	66				95							
312	1256D	173R	1	6	28	32	3	—	66	100										
312	1256D	173R	1	7-8	32	43	9	—	66											
312	1256D	173R	1	9-24	43	136	79	—	66	87				50						
312	1256D	173R	2	1-2	0	24	23	—	66	95				12					1	
312	1256D	174R	1	1-4	0	26	24	1265.4	66	98				5						
312	1256D	174R	1	5-8	26	43	14	—	67	95				2					3	
312	1256D	174R	1	9	43	52	9	—	68	95									5	

Notes: Ig. unit = Igneous unit in Hole 1256D, laum = laumontite, qtz = quartz, ep = epidote, py = pyrite, cp = chalcopyrite, sap = saponite, cel = celadonite, SiO₂ = amorphous silica, FeOx = iron oxyhydroxides, carb = calcium carbonate, anh = anhydrite, chl/sm = chlorite/smectite, chl = chlorite. For the complete alteration logs, see 309ALT.XLS and 312ALT.XLS in "Supplementary material."

Interval (cm)							Amygdules or 100% recrystallized zones		Vesicles		Glass (%)		Comments
Exp.	Hole	Core	Section	Piece	Top	Base	%	Minerals	%	Minerals	Fresh	Altered	
312	1256D	172R	1	1-7	0	26							
312	1256D	173R	1	1-4	0	25							
312	1256D	173R	1	5	25	28	5	Laum, qtz, ep					
312	1256D	173R	1	6	28	32							
312	1256D	173R	1	7-8	32	43	1	Qtz, laum?					
312	1256D	173R	1	9-24	43	136							
312	1256D	173R	2	1-2	0	24							
312	1256D	174R	1	1-4	0	26							
312	1256D	174R	1	5-8	26	43							
312	1256D	174R	1	9	43	52							



Table T5. Checklist for structural geology descriptions. (Continued on next page.)

Term	Explanation
Brittle structures	
Veins (V)	Magmatic/Late magmatic (Vm), Hydrothermal (Vh)
Orientation of vein	
Depth of vein	
Morphology	Planar (Pl), curved (Cv), irregular (Ir), sigmoidal (Sg), stepped (St), T-shaped (T), Y-shaped (Y), splayed (Spl)
Vein array geometry	Conjugate, network, en echelon, anastomosing, riedel
Vein density (N/10 cm)	No vein, slight, moderate, high, complete
Fabric of the filling minerals	Fibrous (Fb), vermicular (Vr), blocky (Bl)
Vein mineralogy	
Average width and length	
Crack and seal structures and number of vein-opening events	
Occurrence of alteration halos	
Crosscutting relationships	
Apparent magnitude of offset	
Apparent sense of shear	
Fracturing and/or shearing of veins	
Joints (J)	
Orientation of joints	
Depth of joints	
Morphology	Planar (Pl), curvilinear (Cv), anastomosing (An), T-shaped (T), Y-shaped (Y), splayed (Spl), stair-stepped (St)
Occurrence of alteration halos	
Crosscutting relationships	
Joint array	Conjugate, network, en echelon
Joint density	
Plumose structures	
Faults (F)	
Orientation of faults	
Depth of faults	
Magnitude of the apparent offset	
Apparent sense of shear	Dextral (dx), sinistral (sx), reversal (r), normal (n)
Slickensides and slickenlines	
Crosscutting relationships	
Average thickness of the fault zone	
Occurrence of alteration halos	
Occurrence and type of fault rocks	
Magmatic and crystal-plastic structures	
Brittle-plastic fabrics (Bp)	
Intensity of fabric	
Orientation of foliation	
Crystal-plastic fabrics (Cpf)	
Intensity of fabric in retrograde assemblage	
Orientation of fabric	Orientation of foliation and lineation
L-, LS-, and S-tectonite	
Shear sense indicators	Block-rotated porphyroclasts, asymmetric augen, SC fabrics, discrete shear bands, mica-fish, tension gash arrays
Sense of shear	Reverse (r), normal (n), dextral (d), sinistral (s)
Mineralogical segregation or banding	
Magmatic fabrics (M)	
Intensity and orientation of magmatic fabric	Orientation of foliations (Mf) and lineations
Minerals that define the shape and/or crystallographic preferred orientations	
Angle between crystallographic and shape fabrics	
Orientation of subfabrics	
Compositional layering (Cl)	
Type of layering	Grain size layering, compositional "modal" layering (Cl)
Thickness of layers	
Orientation and density	
Igneous contacts (Ic)	
Concordant or discordant	
Crosscutting relationships	
Intrusive relationships, relative chronology of the different fabrics	
Angle between compositional layering and magmatic or crystal-plastic fabric	

Table T5 (continued).

Term	Explanation
Breccia (Br)	
Type of breccia	Hydrothermal (Bh), magmatic (Bm), or tectonic (Bc)
Clast features	
Volume percent	Percent clasts vs. bulk rock
Size range	Maximum-minimum average size
Shape	e.g., angular, subangular, subrounded, rounded
Composition	Monomictic, polymictic
Structure	e.g., internal crushing, veining, fracturing; preferred orientation
Alteration	Alteration halos in the clasts
Sorting	Well sorted, moderately sorted, poorly sorted
Matrix features	
Volume percent	Percent matrix vs. bulk rock
Grain size	Coarse, medium, fine
Composition	Lithology and/or mineralogy compared with clasts
Structure	Veining, fracturing, preferred orientation, shearing
Alteration	Alteration in the matrix
Cement features	
Volume percent	Percent cement vs. bulk rock
Composition	Mineralogy (? hydrothermal)
Occurrence of veins network associated with breccia	
Occurrence of contact with the host rock and its orientation	
Crosscutting relationships of veins/fractures with respect to matrix and clasts	

Table T6. Glossary of structural terms.

Term	Definition
Composite vein	Compositionally and texturally zoned vein containing different mineral assemblages that may or may not represent different generations.
Crystal-plastic	Grain-scale plasticity permitted by a deformation mechanism called "dislocation creep" at relatively high temperature. Dislocations are propagated along favored crystallographic planes.
Fabric	Relative orientation of parts of a rock mass. Preferred linear orientation of part of a rock is termed linear fabric, preferred planar orientation is termed planar fabric, and lack of a preferred orientation is referred to as random fabric.
Fault	Fractures with kinematic evidence for shear displacement across the discontinuity or with an associated cataclasis.
Foliation	Any repetitively occurring penetrative planar feature in a rock body.
Joint	Fractures where the two sides show no differential displacement (relative to the naked eye or 10× hand lens) and have no filling material.
Late magmatic vein	Fracture filled with texturally and/or compositionally distinct mineral products of late magmatic fluids, usually cutting the primary features of the basalts.
Shear vein	Obliquely opening veins with minor shear displacement, filled with slickenfibers or overlapping fibers.
Texture	Relative size, shape, and spatial interrelationship between grains and internal features of grains in a rock.
Vein	Extensional or oblique open fractures filled with epigenic minerals.



Table T7. Microstructure of plutonic rocks.

Texture type	Physical state	Plagioclase	Olivine	Pyroxene
1 a b	Magmatic	No or minor crystal-plastic deformation microstructures (e.g., deformation twins, undulose extinction) Random-shape orientation Preferred-shape orientation	No deformation microstructures ± local undulose extinction and/or local subgrain development	No deformation microstructures
2	Crystal-plastic ± magmatic	<30% fine-grained recrystallized matrix; deformation twins and subgrain boundaries may be present	Common subgrain boundaries and undulose extinction	No deformation microstructures ± minor crystal-plastic deformation microstructures
3	Crystal-plastic	>30% recrystallized matrix; deformation twins, subgrain boundaries, and undulose extinction common; moderate shape-preferred orientation; strong crystallographic-preferred orientation	Elongated aggregates of neoblasts	Kinked grains; common to extensive recrystallization
4	Crystal-plastic	Strongly bimodal grain size distribution; localized fine-grained neoblasts, polygonal neoblasts, and sutured neoblasts	Closely spaced subgrain boundaries; pervasive undulose extinction, extensive neoblasts	Bent/Kinked porphyroclasts; localized recrystallization
5	Semibrittle	Common intracrystalline microfractures associated with very fine grained neoblasts; extensive kinked and deformation twinned grains; pervasive undulose extinction; may contain hydrothermal alteration mineral assemblages	Same as plagioclase	Same as plagioclase
6	Brittle/Cataclastic	Intra-/Intercrystalline microfractures and cataclastic bands; extensive kinked and deformation twinned grains; pervasive undulose extinction	Same as plagioclase	Same as plagioclase

Table T8. Sampling and storage protocol for WSTP basement fluid samples.

Lab code	Laboratory	Container	Sample volume	Measurement	Treatment
WSTP overflow (~1 L)					
WSO	Shipboard analysis		Few drops	Salinity, total dissolved solids	
			3 mL	pH, alkalinity	
			50 µL	ICr (SO ₄ , Ca, K, Mg)	
			0.5 mL	ICP (K, Ca, Mg, Na, Li, B, Sr, Ba, Mn, Fe)	
			100 µL	AgNO ₃ titration (Cl)	
			3 mL	Spectrophotometry (SiO ₂ , PO ₄ , NH ₄ ⁺)	
			1.5 mL	TOC-5000A (DIC)	Frozen until analysis
WSOB	Shore-based analysis	Acid washed	100 mL	δD, δ ¹⁸ O, δ ¹³ C _{DIC}	2 mL HgCl ₂
WSOA	Shore-based analysis	Plastic	100 mL	δ ³⁴ S _{SO₄} , δ ³⁴ S _{S₂}	~100 mg Cd acetate
WSOT	Shore-based analysis	Bottles	100 mL	⁸⁷ Sr/ ⁸⁶ Sr, major and trace elements	2 mL concentrated TM HNO ₃
WSTP Ti-coil (~14 mL)					
WST	Shipboard analysis		~100 µL	Salinity, total dissolved solids	
			~100 µL	ICr (SO ₄ , Ca, K, Mg)	
			0.5 mL	ICP (K, Ca, Mg, Na, Li, B, Sr, Ba, Mn, and Fe)	If sample collected >12 mL
WSTB	Shore-based analysis	Glass ampule	5 mL	δD, δ ¹⁸ O, δ ¹³ C _{DIC}	100 µL HgCl ₂
WSTA	Shore-based analysis	Glass ampule	2 mL	δ ³⁴ S _{SO₄} , δ ³⁴ S _{S₂}	10 mg Cd acetate
WSTT	Shore-based analysis	Poly tube	5–6 mL	⁸⁷ Sr/ ⁸⁶ Sr, major and trace elements	100 µL TM HNO ₃

Notes: ICr = ion chromatography, ICP = inductively coupled plasma spectrometry. TM = trace metal grade. TOC = total organic carbon analyzer. DIC = dissolved organic carbon. WSO = water sample overflow, WST = water sampler Ti coil. Suffix for shore-based analysis: B = Banerjee, A = Alt, T = Teagle.

Table T9. Water analyses and corresponding reproducibility.

Parameter (unit)	Method	IAPSO value		Analytical uncertainty	
		Accepted	Measured	1 σ (%)	N
Alkalinity	Gran titration	2.33	2.34	2.2	10
Cl (mM)	Titration with AgCl	559.55	544	0.7	12
H ₄ SiO ₄ (µM)	Spectrophotometry			BDL	
NH ₄ (µM)	Spectrophotometry				
PO ₄ (µM)	Spectrophotometry			BDL	
SO ₄ (mM)	Ion chromatography	28.90	28.9	0.3	6
Mg (mM)	ICP-AES	54.40	10.63	2.1	6
Ca (mM)	ICP-AES	10.54	51.64	2.2	6
K (mM)	ICP-AES	10.46	10.26	4.6	6
Na (mM)	ICP-AES	480.18	465	0.4	6
Sr (µM)	ICP-AES	87.00	90	5.8	6
Ba (µM)	ICP-AES	0.10	70	0.6	6
B (µM)	ICP-AES	426.65	546	2.9	6
Li (µM)	ICP-AES	25.70	21	5.4	6
Mn (µM)	ICP-AES	0.00	0.6	2.6	6
Fe (µM)	ICP-AES	0.00	BDL	BDL	6
DOC (mM)	Gas chromatography			9.6	3

Notes: IAPSO = International Association for the Physical Sciences of the Ocean, standard seawater. BDL = below detection limit. DOC = dissolved organic carbon. ICP-AES = inductively coupled plasma-atomic emission spectroscopy. N = number of replicate analyses.

Table T10. Analyses of grinding contamination and background blank.

Element	Grinding error (N = 3)	Background blank (N = 4)
Major element oxide (wt%):		
SiO ₂	0	0.1
Al ₂ O ₃	BDL	0.01
TiO ₂	BDL	0.01
Fe ₂ O ₃	BDL	0.01
MgO	BDL	0.01
MnO	BDL	BDL
CaO	BDL	0.1
Na ₂ O	BDL	BDL
K ₂ O	0.01	0.01
P ₂ O ₅	BDL	0.02
Trace element (ppm):		
Cr	4.3	19.3
Ni	3.9	3.7
V	BDL	1.7
Sc	BDL	0.9
Ba	BDL	22.2
Sr	BDL	5.8
Y	BDL	1.6
Zr	BDL	9.2
Nb	BDL	BDL

Notes: SiO₂ was subtracted from the grinding error because pure SiO₂ was used to determine grinding contamination. The background blank was determined from drift-corrected intensities and was subtracted from standard and sample analyses. BDL = below detection limit. N = number of analyses.

Table T11. Analytical conditions for hard rock by ICP-AES runs.

Element	Wavelength (nm)	Integration time per calculation point (s)	Voltage (V)	Mode	Increment between points (nm)*
Al	396.152	1	570	Gauss	0.003
Ba	455.403	4	610	Max	0.003
Ca	393.366	1	390	Gauss	0.003
Cr	267.716	4	820	Max	0.003
Fe	259.94	1	570	Gauss	0.003
K	766.49	1	990	Gauss	0.003
Mg	285.213	4	640	Max	0.003
Mn	257.61	4	560	Max	0.003
Na	589.592	1	660	Gauss	0.003
Ni	231.604	4	930	Max	0.002
P	178.229	4	990	Max	0.003
Si	251.611	1	580	Gauss	0.003
Cu	324.754	0.5	670	Gauss	0.002
Zn	213.856	0.5	990	Gauss	0.002
Sr	407.771	1	700	Gauss	0.003
V	292.402	1	890	Gauss	0.003
Y	371.029	4	620	Max	0.003
Zr	343.823	1	640	Gauss	0.003
Ti	334.941	1	620	Gauss	0.003
Nb	269.706	1	550	Gauss	0.003
Sc	361.384	0.5	620	Gauss	0.002
Co	213.856	0.5	625	Gauss	0.002

Note: * = interval between each of the calculation points in Gaussian mode or the calculation window that constitutes the single point in Max mode.

Table T12. Example run sheet for hard rock by ICP-AES run, Hole 1256D.

Analysis number	Cell ID	Hard rock sample	Analysis type
1		Drift 1	Drift
2	1	Blank (1)	Standard analysis
3	2	BIR-1 (1)	Standard analysis
4		Drift 2	Drift
5	3	JA-3 (1)	Standard analysis
6	4	AGV-1 (1)	Standard analysis
7		Drift 3	Drift
8	5	JB-3 (1)	Standard analysis
9	6	Unknown 1 (1)	Sample analysis
10	7	Unknown 2 (1)	Sample analysis
11	8	BHVO-2 (1)	Standard analysis
12		Drift 4	Drift
13	9	BAS-206 (1)	Check standard analysis
14	10	Unknown 3 (1)	Sample analysis
15	11	JGB-1 (1)	Standard analysis
16	12	Unknown 4 (1)	Sample analysis
17		Drift 5	Drift
18	13	BIR-1 (2)	Standard analysis
19	14	Unknown 1 (2)	Sample analysis
20	15	Unknown 2 (2)	Sample analysis
21	16	JA-3 (2)	Standard analysis
22		Drift 6	Drift
23	17	AGV-1 (2)	Standard analysis
24	18	Unknown 3 (2)	Sample analysis
25	19	JB-3 (2)	Standard analysis
26	20	BHVO-2 (2)	Standard analysis
27		Drift 7	Drift
28	21	BAS-206 (2)	Check standard analysis
29	22	JGB-1 (2)	Standard analysis
30	23	Blank (2)	Standard analysis
31	24	Unknown 4 (2)	Sample analysis
32		Drift 8	Drift

Table T13. Precision and accuracy of ICP-AES analyses on the JY-2000, Expedition 309.

Standard:	BAS-206 (N = 18)			BAS-140 (N = 22)		
	Average	RSD (%)	Published value*	Average	RSD (%)	Published value†
Major element oxide (wt%):						
SiO ₂	43.74	3.82	49.53	51.47	2.33	50.5
TiO ₂	1.77	6.66	2.04	1.00	4.22	0.98
Al ₂ O ₃	12.7	1.08	14.22	14.64	1.25	14.6
Fe ₂ O ₃	13.05	2.76	14.30	11.23	1.36	11.1
MgO	0.24	14.45	0.22	0.19	1.43	8.15
MnO	6.00	1.87	6.77	8.21	1.11	0.19
CaO	8.77	1.97	9.70	12.54	1.25	12.4
Na ₂ O	2.48	2.34	2.78	1.80	1.30	1.84
K ₂ O	0.16	15.96	0.18	BDL	111.35	0.01
P ₂ O ₅	0.16	22.50	0.16	0.07	52.05	0.08
Trace element (ppm):						
Zn	103.3	9.4	NR	75.6	11.2	80
Co	48.2	9.0	NR	48.8	9.9	55
Ni	36.4	37.9	53.5	81.4	5.1	85
Sc	41.8	6.8	47	35.3	2.9	43
Cr	72.0	42.4	83.7	182.5	2.7	186
V	407.9	2.4	461	332.8	1.7	NR
Nb	—	—	—	3.0	63.1	1
Cu	60.3	13.5	NR	78.4	3.0	81
Zr	117.3	3.3	127	49.2	2.4	NR
Y	43.8	1.9	43.8	28.3	2.2	24
Sr	101.6	1.6	112	53.0	5.3	44
Ba	41.0	6.5	49.9	2.0	5.8	NR

Notes: Standards analyzed as a check on precision and accuracy. Relative standard deviation (RSD) is calculated as the standard deviation of *N* analyses divided by the average value. For elements with near background concentrations, the relative standard deviation is artificially high (i.e., the actual precision is much better than suggested by the numbers). All values have been normalized to 100% volatile free. * = Leg 206 Shipboard Scientific Party (2003b), † = Sparks and Zuleger (1995). *N* = number of replicated analyses. BDL = below detection limit; NR = not reported, — = not analyzed.

**Table T14.** Precision (reproducibility) of ICP-AES analyses on the JY-2000, Expedition 312.

Standard:	BAS-140 (N = 12)			BAS-148 (N = 13)			BAS-206 (N = 13)			BAS-312 (N = 12)		
	Average	Standard deviation	RSD (%)									
Major element oxide (wt%):												
SiO ₂	50.85	0.33	0.66	50.09	0.32	0.63	49.35	0.27	0.54	49.86	0.35	0.70
TiO ₂	1.00	0.01	1.19	0.90	0.01	1.36	2.09	0.04	1.71	1.33	0.02	1.62
Al ₂ O ₃	14.34	0.08	0.55	15.55	0.08	0.50	13.87	0.05	0.33	15.41	0.10	0.63
Fe ₂ O ₃	11.19	0.09	0.77	9.98	0.05	0.55	14.58	0.09	0.62	10.77	0.06	0.53
MnO	0.19	0.00	0.82	0.17	0.00	1.06	0.26	0.00	0.16	0.18	0.00	1.19
MgO	8.18	0.05	0.66	8.63	0.05	0.61	6.73	0.05	0.67	7.79	0.05	0.63
CaO	12.51	0.11	0.91	12.88	0.09	0.72	9.92	0.03	0.34	11.89	0.10	0.88
Na ₂ O	1.80	0.02	1.10	2.05	0.01	0.58	2.83	0.02	0.79	2.44	0.03	1.22
K ₂ O	0.01	0.00	18.78	0.05	0.00	3.64	0.18	0.00	1.23	0.06	0.00	4.11
P ₂ O ₅	0.08	0.05	61.20	0.07	0.03	49.18	0.19	0.02	12.08	0.09	0.03	27.93
Totals:	100.12	0.36	0.36	100.37	0.44	0.44	100.00	0.28	0.28	99.83	0.44	0.45
Trace element (ppm):												
Ba	BDL	—	—	BDL	—	—	42.75	1.04	2.44	9.54	0.28	2.96
Sr	41.50	1.02	2.47	58.22	0.47	0.81	99.16	0.61	0.61	98.85	1.19	1.20
Zr	45.85	0.61	1.34	44.62	0.52	1.17	111.19	1.02	0.92	71.43	0.86	1.20
Y	23.88	0.22	0.92	22.33	0.13	0.58	34.14	0.05	0.14	24.65	0.22	0.91
Sc	40.17	0.37	0.91	39.40	0.42	1.05	42.59	0.49	1.15	39.99	0.34	0.85
V	307.58	2.12	0.69	264.40	2.21	0.84	421.96	3.29	0.78	295.38	2.07	0.70
Cr	191.81	1.99	1.04	381.61	6.88	1.80	73.28	1.12	1.54	259.03	2.77	1.07
Co	46.31	2.59	5.59	44.88	1.47	3.28	50.78	1.05	2.07	44.27	1.71	3.85
Ni	83.85	3.53	4.21	116.43	2.40	2.06	45.50	1.53	3.35	88.12	3.27	3.71
Cu	67.50	1.07	1.58	75.35	1.14	1.51	52.73	1.44	2.73	74.32	1.07	1.44
Zn	78.57	2.00	2.54	74.30	3.86	5.20	99.29	3.38	3.41	82.75	1.41	1.71

Notes: Relative standard deviation (RSD) is calculated as the standard deviation of *N* analyses divided by the average value. BDL = below detection limit, — = not applicable.

Table T15. Setup parameters used for the cryogenic magnetometer software, Expedition 309.

Parameter	Setting
SQUID configuration:	
SQUID-x response (cm)	6.071
SQUID-y response (cm)	6.208
SQUID-z response (cm)	9.923
SQUID-x calibration (emu)	8.21E-05
SQUID-y calibration (emu)	-8.34E-05
SQUID-z calibration (emu)	4.32E-05
SQUID filter data (x, y, and z) (Hz)	10
SQUID range data (x, y, and z)	1 × range
SQUID slew data (x, y, and z)	Disable fast slew
SQUID feedback data (x, y, and z)	Close feedback loop
Degausser configuration:	
Ramp rate	3
Tracking timeout (s)	40
AF field maximum (mT)	80
AF field minimum (mT)	2
Coil calibration constant (x, y, and z)	1
Character delay	50
Sample handler configuration (right-hand home):	
Home switch type	Limit switch
Home offset (cm)	0
Tray offset (cm)	2.2
Track length (cm)	599.3
Full tray length (cm)	160.3
Scale (steps/cm)	1572
Sample handler positions:	
SQUID (cm)	255.85
Magnetic susceptibility (not applicable)	0
Degauss stage 1 (cm)	190
Degauss stage 2 (cm)	435
IRM stage (not applicable)	0
IRM coil center	0
Background stage 1 (cm)	300
Background stage 2 (cm)	0
Discrete configuration:	
Maximum number of sample positions	4
Center offset (cm)	20
Center separation (cm)	40

Note: SQUID = super-conducting quantum interference device, AF = alternating field, IRM = isothermal remanent magnetization.

Table T16. Measurements made by wireline tool strings.

Tool string	Tool	Measurement	Sampling interval (cm)	Approximate vertical resolution (cm)
Triple combination	HNGS	Spectral gamma ray	15	51
	APS	Porosity	5 and 15	43
	HLDS	Bulk density	2.5 and 15	46
	DLL	Resistivity	15	61
	TAP	Temperature	1 per s	NA
		Tool acceleration	4 per s	NA
		Pressure	1 per s	NA
		Temperature	15	NA
Formation MicroScanner (FMS)-sonic combination	EMS	Resistivity		
	FMS	Microresistivity	0.25	0.5
	GPIT	Tool orientation	0.25 and 15	NA
	SGT	Total gamma ray	15	NA
	DSI	Acoustic velocity	15	107
Ultrasonic Borehole Imager	UBI	Ultrasonic imaging	Variable	0.5–2
	GPIT	Tool orientation	0.25 and 15	NA
	SGT	Total gamma ray	15	
WST	WST	Acoustic arrival time	NA	NA
VSI	VSI	Acoustic arrival time	NA	NA

Notes: All tool and tool string names (except the TAP) are trademarks of Schlumberger. For the complete list of acronyms used in the IODP and for additional information about tool physics and use consult IODP Logging Services at iodp.ldeo.columbia.edu/TOOLS_LABS/tools.html. See Table T17 for explanation of acronyms used to describe tool string and tools. NA = not applicable.

Table T17. Acronyms and units used for wireline logging tools.

Tool	Output	Tool name/Explanation of output	Unit
		Accelerator Porosity Sonde	
	APLC	Near array porosity (limestone calibrated)	%
	SIGF	Formation capture cross section (Σf)	Capture units
APS	STOF	Tool standoff (computed distance from borehole wall)	Inches
		Dual Laterolog	
	LLD	Deep resistivity	Ωm
DLL	LLS	Shallow resistivity	Ωm
		Dipole Sonic Imager	
	DTCO	Compressional wave delay time (Δt)	ms/ft
	DTSM	Shear wave delay time (Δt)	ms/ft
DSI	DTST	Stoneley wave delay time (Δt)	ms/ft
		Environment Measurement Sonde	
	TMP	Fluid temperature	$^{\circ}C$
EMS	REMS	Fluid electrical resistivity	Ωm
		Formation MicroScanner	
	C ₁ , C ₂	Orthogonal hole diameters	Inches
	PIAZ	Pad 1 azimuth	Degrees
FMS		Spatially oriented resistivity images of borehole wall	
		General Purpose Inclinator Tool	
	DEVI	Hole deviation	Degrees
	HAZI	Hole azimuth	Degrees
	F _x , F _y , F _z	Earth's magnetic field (three orthogonal components)	Oersted
GPIT	A _x , A _y , A _z	Acceleration (three orthogonal components)	m/s ²
		Hostile Environment Litho-Density Tool	
	RHOM	Bulk density	g/cm ³
	PEFL	Photoelectric effect	b/e ⁻
	LCAL	Caliper (measure of borehole diameter)	inches
HLDS	DRH	Bulk density correction	g/cm ³
		Hostile Environment Gamma Ray Sonde	
	HSGR	Standard (total) gamma ray	gAPI
	HCGR	Computed gamma ray (HSGR minus uranium contribution)	gAPI
	HFK	Potassium	wt%
	HTHO	Thorium	ppm
HNGS	HURA	Uranium	ppm
		Scintillation Gamma Ray Tool	
SGT	ECGR	Environmentally corrected gamma ray	gAPI
TAP		Temperature/Acceleration/Pressure tool	$^{\circ}C$, m/s ² , psi
		Ultrasonic Borehole Imager	
		Spatially oriented acoustic images of borehole wall	
		Acoustic arrival times and amplitude	ms
		Borehole diameter	Inches
UBI		Borehole azimuth	Degrees
		Versatile Seismic Imager	
		Acoustic arrival times	ms
		Well Seismic Tool	
WST		Acoustic arrival times	ms

Notes: All tool and tool string names (except the TAP) are trademarks of Schlumberger. For the complete list of acronyms used in the IODP and for additional information about tool physics and use consult IODP Logging Services at iodp.ideo.columbia.edu/TOOLS_LABS/tools.html.